UNIVERSITY OF ALBERTA

RELEASE FORM

NAME OF AUTHOR: **Kenneth Bruce Muldrew**

TITLE OF THESIS: **The Osmotic Rupture Hypothesis and its Application to the Cryopreservation of Articular Cartilage**

DEGREE: **Doctor of Philosophy**

YEAR THIS DEGREE GRANTED: **1993**

. . . it is impossible to explain honestly the beauties of the laws of nature in a way that people can feel, without their having some deep understanding of mathematics. I am sorry, but this seems to be the case.

Richard Feynman

UNIVERSITY OF ALBERTA

THE OSMOTIC RUPTURE HYPOTHESIS AND ITS APPLICATION TO THE CRYOPRESERVATION OF ARTICULAR CARTILAGE

BY

Ⓒ

KENNETH BRUCE MULDREW

A thesis submitted to the Faculty of Graduate Studies and Research in partial fulfillment of the requirements for the degree of **Doctor of Philosophy**

IN

MEDICAL SCIENCES

DEPARTMENT OF LABORATORY MEDICINE AND PATHOLOGY

EDMONTON, ALBERTA

FALL 1993

UNIVERSITY OF ALBERTA

FACULTY OF GRADUATE STUDIES AND RESEARCH

The undersigned certify that they have read, and recommend to the Faculty of Graduate Studies and Research for acceptance, a thesis entitled **The Osmotic Rupture Hypothesis and its Application to the Cryopreservation of Articular Cartilage** submitted by **Kenneth Bruce Muldrew** in partial fulfillment of the requirements for the degree of **Doctor of Philosophy** in Medical Sciences (Laboratory Medicine and Pathology).

*This thesis is dedicated to my parents, Gwen and Jim Muldrew, for **everything**; and to my children: Colleen, Jennifer and Nicole, for showing me just how much **everything** is.*

Abstract

The osmotic rupture hypothesis -- the hypothesis that osmotically driven water movement, such as occurs during rapid freezing protocols, leads to pressure being exerted on the plasma membrane (due to the frictional drag of the moving water) which can cause membrane failure if the pressure on the membrane exceeds its tensile properties -- is developed into a biophysical theory describing the genesis of intracellular ice formation. Intracellular ice forms during rapid cooling protocols and is usually associated with a lethal injury to the cell. Equations to describe the pressure that is exerted on the membrane during osmotic water movement and the probability of membrane rupture due to this pressure are developed and tested on cellular systems. This theory is then applied to the problem of cryopreservation of mammalian tissues by using articular cartilage as a model tissue.

The permeability parameters and the parameters which describe membrane rupture are measured for the cells of articular cartilage: the chondrocytes. The kinetics of dimethyl sulfoxide diffusion in articular cartilage are measured and the response of chondrocytes to freezing is measured *in situ*. These data are then combined into a mathematical model of articular cartilage to be used for deriving an optimal cryopreservation protocol. Although the determination of a clinically useful method for cryopreserving articular cartilage is significant, the principal aim of the thesis is to outline an approach for finding cryopreservation protocols for more complex tissues. There has been relatively little progress made in this direction despite decades of effort. Clearly, the systems are too complex for solutions to be found by simple guessing. The present effort connects mathematical modeling of osmotic responses during freezing with a theoretical framework that can be used to predict cell injury, thereby allowing the complexity to be reduced to a manageable level.

Preface

The introductory quotation on the necessity of mathematics in describing the laws of nature does not imply that any deep secrets of nature are about to be revealed in this thesis. Rather, it is meant to convey the pleasure that I have found in developing my hypothesis in a mathematical form and then seeing it supported by the biophysical evidence. To the physicist, I imagine, the lack of a mathematical statement of a hypothesis merely represents fuzzy thinking: an unfinished idea. This is not the case in biology, however, where complexity (and often, a lack of training in mathematics) results is most hypotheses being stated in an ordinary language. The differences are difficult to appreciate for someone who has not tried both. When stating a hypothesis in language, it is relatively easy to rationalize unexpected results that may seem to contradict the hypothesis. In mathematics, any contradiction is final: either the hypothesis is incorrect or there is an error in the experiment. After spending many years developing the ideas that went into the osmotic rupture hypothesis, it was with some trepidation that I applied the equations to the experimental data. There is a tension that develops when faced with the possibility of immediate and unequivocal failure (with no recourse to the relative safety of rationalization). There is a further uncertainty in expressing a hypothesis in mathematical terms: the language of mathematics is not just a language, it is a language plus a collection of logical relationships. When an equation is written, much more is implied than the simple statement; any operation that obeys the laws of mathematics may be done to this equation to alter it. If the equation provides a correct interpretation of the physical phenomenon, then every alteration produced by allowed mathematical operations must also be consistent with physical reality.

Since this thesis is intended for a principally biological audience, I hope that the minimal use of mathematics does not impede the reader's understanding of the material. The mathematics that are used in the development of the hypothesis consist only of basic arithmetic, algebra and probability theory. The only one of these that might provide difficulty to a biologist is probability theory, which should be understood by anyone who uses statistics in their work (this includes most biologists). The model of osmotic water movement uses differential equations to describe water and solute fluxes across the plasma membrane which require the methods of calculus to solve. These equations are central to testing and using the hypothesis, thus I would urge the reader to spend a little time to see what is implied by them.

Finally, I would like to emphasize that the osmotic rupture hypothesis is a *scientific* hypothesis: it has nothing to do with absolute truth. The purpose of scientific theories is to explain the results of controlled experiments. The more experimental results that can be explained by a single theory, the better that theory -- not because it is closer to the truth -- but because it summarizes more knowledge of nature in a form that can be understood by a human mind. It is

very difficult to concentrate on more than a few different facts at a time, thus any framework that allows one to know many facts by simply knowing a single equation is a significant advance in science. The layperson often finds this unsatisfying; they want to have a symbolic mental picture of how things work (and one that will not be proved inadequate in the near future as well). When Sir Isaac Newton was told that his theory of gravitation did not tell one anything about what gravity *is*, he replied "It tells you **how** it moves. That should be enough". The scientist is satisfied with this uncertainty because without it, (s)he is forced to bring preconceived notions of how nature behaves to science -- which can only be counter-productive. The reader should welcome this theory because it allows several aspects of nature to be held in their minds simultaneously, without insisting that nature bow before them in submission.

> *It will be objected that the book deals too much with mere appearances, with the surface of things, and fails to engage and reveal the patterns of unifying relationships which form the true underlying reality of existence. Here I must confess that I know nothing whatever about true underlying reality, having never met any. There are many people who say they have, I know, but they've been luckier than I.*
> *For my own part I am pleased enough with surfaces -- in fact they alone seem to me to be of much importance.*

<div align="right">Edward Abbey</div>

The surfaces presented in this thesis are placed before you so that you may try to prove them to be flawed. There can be no higher compliment to a scientist than this, and I welcome it with gusto!

Quae nocent docent. Fiat bona tempi volvere . . .

<div align="right">

**Ken Muldrew,
Edmonton, Alberta,
June, 1993.**

</div>

Acknowledgments

I wish to express my gratitude and appreciation to the following individuals, without whom this thesis could not have been completed.

To my wife, friend and companion Terry. For her tolerance and patience in the face of what must have seemed an incomprehensible pursuit. Without her love I would be much the poorer.

To Dr. Locksley E. McGann, my supervisor and mentor. I have taken from him much more than I have given in our long and fruitful association. I can only promise to put back what I owe by training others with the same attention and encouragement which he has shown me.

To Dr. Norman S. Shachar for serving as my co-supervisor. His infectious energy and enthusiasm have affected me deeply.

To Dr. Ray Rajotte and Dr. Bob Stinson for serving on my supervisory committee. Their help in defining this project, their guidance and their careful review of this thesis are greatly appreciated.

To Dr. Joan Allalunis-Turner for her insightful review of this thesis.

To Dr. Peter Mazur for devoting many hours to thoroughly reviewing this thesis. The contents are greatly improved due to his efforts.

To Dr. Glen Baker for serving as chairman for my final oral exam and for his careful review of my thesis.

To Chris Studholme for tirelessly critiquing my mathematical reasoning.

Finally, to my children: Colleen, Jennifer and Nicole (Nikki Bok-Chow) for challenging me and reminding me how I got here.

Thank you.

Table of Contents

List of Tables

List of Figures

List of Symbols and Abbreviations

Abbreviations

Å	-	Angstrom
atm	-	Atmosphere
C	-	Celsius
cm	-	Centimeter
DMSO	-	Dimethyl Sulfoxide
DNA	-	Deoxyribonucleic acid
D_2O	-	Deuterium oxide
EB	-	Ethidium Bromide
et al.	-	And others (*et alia*)
FCS	-	Fetal calf serum
FDA	-	Fluorescein diacetate
fig	-	Figure
^1H	-	Proton
H_2O	-	Water
IIF	-	Intracellular Ice Formation
K	-	Kelvin
kcal	-	Kilocalorie
kg	-	Kilogram
L	-	Levorotatory
log	-	Logarithm (base 10)
ln	-	Natural logarithm (base e)
M	-	Molar
m	-	Meter
MEM	-	Minimal Essential Medium
mg	-	Milligram
min	-	Minutes
ml	-	Milliliter
mM	-	Millimolar
mm	-	Millimeter
mol	-	Moles
MW	-	Molecular Weight
N	-	Newton
NaCl	-	Sodium Chloride
nm	-	Nanometer
NMR	-	Nuclear Magnetic Resonance
osmol	-	Osmoles
PBS	-	Phosphate Buffered Saline
ρ	-	Density
ref.	-	Reference
s	-	Seconds

SEM	-	Standard error of the mean
std.	-	Standard
μg	-	Microgram
μl	-	Microliter
μM	-	Micromolar
wt	-	Weight
$[x]$	-	Concentration of species x

Mathematical Symbols

A	-	Surface area of the membrane
α	-	Average rate of occurence of membrane fluctuations
b	-	1.70991/standard deviation
$\overline{C_p}$	-	Mean concentration of permeant solute across membrane
D	-	Diffusion coefficient
D_c	-	Diffusion coefficient in cartilage
D_{H_2O}	-	Diffusion coefficient in water
D_w	-	Diffusion coefficient for water in liquid hydrocarbon
Δx	-	Width of the hydrophobic region of the membrane
dSp/dt	-	Rate of permeant solute movement out of cell
dV/dt	-	Rate of change of cell volume
e	-	Natural exponential function
E_a	-	Arrhenius activation energy
eCi	-	Final concentration of impermeant solute
eCp	-	Extracellular concentration of permeant solute
f	-	Coefficient of friction
F_f	-	Force on the membrane due to the friction of water
H	-	Water content of cartilage
iCi	-	Initial concentration of impermeant solute
∞	-	infinity
J_w	-	Water Flux
k	-	Boltzmann's constant (= 1.38 x 10^{-23} Nm/K)
ℓ	-	Thickness of cartilage
λ	-	Tortuosity factor
lim	-	Limit
L_p	-	Hydraulic conductivity
L_{pg}	-	Hydraulic conductivity at the reference temperature
M_t	-	Amount of solute at a specified time
M_∞	-	Amount of solute at equilibrium
n	-	Number of water molecules moving through the membrane
$\mathcal{P}$	-	Pressure on the membrane due to water flux
$\overline{\mathcal{P}}$	-	Average pressure required for membrane rupture

$\bar{\mathcal{P}}_g$	-	Mean pressure required for failure at a reference temperature
$P(1)$	-	Probability of an event occuring
$P(0)$	-	Probability of no event occuring
P_{IIF}	-	Probability of intracellular ice formation occuring
$P_{rupture}$	-	Probability of a membrane rupture occuring
Ps	-	Permeability to permeant solute
π	-	Pi
π_e	-	Extracellular osmotic pressure
π_i	-	Intracellular osmotic pressure
π_o	-	Initial intracellular osmotic pressure
R	-	Universal gas constant (= 0.082 $m^3 \cdot atm \cdot kmol^{-1} \cdot K^{-1}$)
Sp	-	Moles of intracellular permeant solute
Σ	-	Summation operator
T	-	Absolute temperature
t	-	Time
τ	-	Time constant
$\Delta\tau$	-	Transit time for a water molecule moving through the membrane
T_g	-	Reference temperature
Δt	-	Time interval
v	-	Drift velocity of a water molecule in the membrane
υ	-	Normalized cell volume
υ_d	-	Normalized osmotically incactive cell volume
V_d	-	Osmotically inactive cell volume
Vo	-	Initial intracellular water volume
Vw	-	Intracellular water volume

Chapter 1

Introduction

Introductory Remarks

Cryobiology is the study of life at temperatures too low to support life. On the surface, this statement appears to be a contradiction, however, it must be kept in mind that the study of life cannot be carried out without also studying the loss of life. This is because life is very difficult to define in precise terms; a far simpler task is to define when a living thing has expired. In cryobiology, we study the interface, fuzzy though it may be, between life and death that can be found at low temperatures. For the most part, low temperatures are those below which water freezes. Water, *not* DNA, is the fundamental molecule of life and it is the rare and precious qualities of liquid water that make life possible. Without an environment that contains generous quantities of liquid water, life would not exist. Living in Canada, each winter we see environments in which liquid water does not exist and yet, when spring arrives, life flourishes without any re-population from warmer climes. What is this state that some living things inhabit, where no growth occurs -- to our eyes no time appears to pass -- yet these organisms remain *alive*? This curious phenomenon is the essence of cryobiology.

The environment for life, the surface of the earth, is constantly in flux: from the cosmic time scale in which our sun is becoming hotter to the realm of rapidly changing weather phenomena. Living things must be able to adapt to this changing environment in order to preserve the existence of life itself. It does this by a process of mutation and natural selection. Organisms can undergo random mutations (essentially random errors in chemical processes) which make them slightly different from what they were before. If these differences give them an advantage over other organisms in their environment, then they will thrive, if not, then they will dwindle. One of the paths that has proven successful is the requirement of sexual reproduction in multicellular organisms. In this evolutionary route, two organisms combine their genes (the blueprints for constructing new, identical organisms) to generate mutations at a faster rate than can be achieved with chemical errors. In order for this approach to be successful, however, it is necessary that the organisms die after creating at least two more offspring. If they were to be immortal, then the population would soon rise to a level that could not be supported by the environment (thus preventing the success of any advantageous mutations). This is the boat that we find ourselves in: after a finite time, our organs cease to function, our bodies fail us: we are programmed to die. Although we may pass our genes to our offspring, we cannot pass on our memories or our conscious selves -- those intangible qualities which make us individual entities -- thus it is not easy to accept death knowing that we will cease to be.

Low temperatures provide a means of escaping this fate by suspending the aging process. The processes by which our programmed obsolescence is carried out are chemical in nature, thus the rate at which these reactions occur can be slowed dramatically by lowering the temperature. It might be as simple as this were we not principally composed of liquid water. For when we lower the temperature, water freezes: and this makes all the difference.

All mammalian cells exist in an ionic environment and also maintain a similar concentration of ionic salts in the intracellular space to balance the osmotic pressure. When water freezes to form ice, the crystal is composed only of water molecules which leaves the solutes that were present before freezing to concentrate in whatever fraction of the initial solution remains unfrozen. The temperature at which water freezes is not low enough to bring the rate of chemical processes to a halt, thus the concentrated salt solutions will affect the cells chemically. It is in this temperature region -- between the freezing point of water and the temperature at which the rate of biochemical reactions becomes negligible -- that injury and death occur.

The principal medical application of cryobiology is the benign storage of cells, tissues and organs (some would like to include organisms as well) for use in repairing those parts that no longer function due to disease, injury or aging. The challenge is to take these specimens through the temperature region in which damage can occur and back again without causing irreparable damage. Thus far, this challenge has only been met successfully for cell suspensions and several relatively simple tissue systems.

Modern medicine may be said to have begun with the application of science to the field of medicine. Although medicine is only concerned with the results, the historical accomplishments of the application of the scientific method provides overwhelming support for continuing on this path. This point is often lost on the layperson, who sees basic science as an esoteric extravagance which is performed merely to satisfy the curiosity of the scientist (satisfying curiosity **is** the purpose of basic science; knowledge of natural phenomena, however, is neither esoteric nor extravagant), and it is frequently lost on the cryobiologist who believes that subtle alterations to existing protocols are all that are necessary to achieve success with tissues and organs. Trial and error is not necessarily unscientific. Indeed, guessing is necessary for the scientific method; however, the success of the method relies on building a foundation of guesses that are all supported by the evidence of experiments. In this way, further guesses are supported by the edifice that is the body of scientific knowledge (this is the collection of results of controlled experiments which are summarized by theoretical constructs -- usually mathematical in nature).

There has been little done in the way of summarizing the scientific knowledge of life and death at low temperatures. Without any theoretical construct to guide the cryobiologist, it is unlikely that the problems in medical cryobiology will be solved in the near future. There are far too many experimentally determined facts for a scientist to keep in mind when trying to solve these problems without the unifying construct of theory. It is the purpose

of this thesis to attempt to increase the unification of the facts of cryobiology by proposing a theory which describes the injury that can occur during rapid cooling. This theory will be expressed in the unforgiving language of mathematics -- what the physicist Richard Feynman has called "the logical tight-rope on which we have to walk if we wish to interpret nature" -- where it may be properly (and ruthlessly) tested against experimental facts. The thesis will also attempt to show how this theory may be used to solve the problem of cryopreserving mammalian tissues using articular cartilage as a model system. Although the rate of progress that is implied by following this method (the method of science) may seem slow to those who feel that adding a little more of a certain chemical to their cryobiological elixir will solve the problem, I would ask them to consider the historical record of modern medicine -- in which progress does not seem to have been that slow after all.

The Cellular Environment During Freezing

Mazur introduced the analytical approach to solving cryobiological problems in 1963 (10) through a technique of describing the composition of the extracellular environment and the cell's response to that environment during freezing and thawing. The equations that he developed allowed one to model the biophysical events that occurred during a specified cryopreservation protocol, thereby providing a means of determining how far from equilibrium the cytoplasm was taken during the procedure. From this information, it became possible to make predictions of damaging events, such as intracellular ice formation, and to design protocols to avoid such damage. The power of this approach was demonstrated convincingly by Mazur (11) by applying his equations to systems that had been studied cryomicroscopically. The purpose of this thesis is to build on this framework by providing a detailed theory which is amenable to predicting injury during freezing and thawing.

In the previous section, it was stated that ice crystals are composed solely of water molecules: consequently, any solutes that were present in the solution where an ice crystal has formed become concentrated in the unfrozen fraction of that solution. Following Mazur's original treatment (10), the osmotic pressure of the unfrozen solution will therefore increase upon freezing. If cells are present in this environment, the increase in the extracellular osmotic pressure leads to an osmotic pressure gradient across the plasma membrane. The cell will then lose water (which flows passively down its concentration gradient) until the osmotic pressure of the cytoplasm equals that of the extracellular solution. The rate at which water moves across the plasma membrane is limited by the permeability of the membrane which may be different (and usually is) for different cell types. If the temperature of the extracellular environment continues to drop after ice has formed, then the osmotic pressure of the unfrozen solution will continue to increase as more water is removed in the form of ice. If the cooling rate is rapid enough so that the cell cannot lose water fast enough to maintain osmotic

3

equilibrium between the cytoplasm and the extracellular solution, the cytoplasm will become supercooled (cooled to a temperature below its melting point in the absence of ice). Under these conditions, the cytoplasm can freeze -- an event that is usually associated with a lethal injury to the cell. If intracellular ice formation does not occur (the term *slow cooling* is defined by the avoidance of intracellular ice, *rapid cooling* is the opposite), then the cell will continue to lose water and may become highly dehydrated and shrunken. There is a form of injury that may accompany slow cooling which is usually referred to as *solution effects* (12) injury as it correlates with exposure to high concentrations of solutes. The mechanism by which concentrated solutions cause injury to cells is not yet well understood, although it has been found that cryoprotective compounds (chemicals which reduce the salt concentration during freezing through the colligative properties of the solution) will reduce or eliminate this injury. In fact, this discovery (17) marks the beginning of medical cryobiology. It has also been found that the time of exposure to concentrated solutions correlates strongly with the degree of injury (7). Thus, in general, the cooling should be as rapid as possible to maximize survival. The conventional technique for optimizing cryopreservation protocols for cell suspensions is to find the fastest cooling rates that can be achieved without the formation of intracellular ice. Once cells have been brought down below about -80°C, they can be plunged into liquid nitrogen and stored indefinitely (providing they are shielded from the background radiation). The warming rate at which cells are thawed also is an important variable in the range from -80°C to the melting point.

Intracellular Freezing Injury

The injury associated with intracellular ice formation (IIF) has not been explained in previously proposed hypotheses of the genesis of IIF. Although the implication has been that the presence of ice in the cytoplasm causes the injury, the mechanism by which this might occur remained unexplored until Mazur noticed that rapid warming could reduce the level of this damage in cells that were assumed to have formed IIF (12). This led him to propose that the recrystallization of intracellular ice (recrystallization is the process by which large ice crystals with low surface energy grow at the expense of small ice crystals with higher surface energy) increased the magnitude of the injury. The first plausible hypothesis of the genesis of IIF was Levitt's proposal that IIF results spontaneously when the cytoplasm reaches a critical degree of supercooling (6). His idea was that cells contain efficient nucleation sites which act to cause spontaneous heterogeneous nucleation when the cytoplasm is sufficiently supercooled. Toner et al. (23) have recently put forward a variant of this hypothesis which proposes that the plasma membrane is altered in the presence of ice to form a nucleation site which catalyses IIF. This is a well developed hypothesis in which classical nucleation theory is applied to predict the conditions under which surface catalyzed nucleation might occur during freezing.

Although it has been applied successfully to the prediction of IIF in mouse oocytes (24), the mechanism by which ice alters the plasma membrane to create an efficient nucleation site and the nature of the injury that accompanies IIF has yet to be worked out. Mazur has long held the view that IIF is caused by ice crystals growing through the aqueous pores in the plasma membrane (9). He used the Kelvin equation (which can be used to describe the smallest radius of stable ice crystals at a given temperature) to predict the temperature at which ice crystals would be able to propagate through aqueous pores in the membrane. If the cytoplasm is supercooled at this temperature, then the ice passing through the pores will quickly grow throughout the cytoplasm. Pitt and Steponkus (15) have recently extended the quantitative branch of Mazur's theory. Steponkus and Dowgert (20) proposed that IIF was actually a *result* of damage to the plasma membrane (not its consequence) due to repeated observations of membrane rupture preceding the appearance of ice in the cytoplasm on a cryomicroscope. Steponkus et al. later suggested (21) that the rupture may have been caused by electrical transients at the ice interface but this line of inquiry has not been pursued recently. Muldrew and McGann (13) have explored an alternative mechanism by which the membrane could be ruptured during rapid cooling. The initial proposal was that high osmotic pressure gradients that exist during rapid cooling could be the agents that cause the membrane to fail. The osmotic rupture hypothesis will be extensively developed in this thesis and then applied to the problem of cryopreserving mammalian tissues.

Cryobiology of Tissues and Organs

Although purely empirical approaches have been successful in developing cryopreservation protocols for cell suspensions, this not been the case for complex mammalian tissues; despite prolonged efforts to modify these protocols for this purpose. Attainment of cryopreservation protocols for tissues and organs would have obvious benefits for medicine as they would allow tissues to be banked for transplantation. Banking could eliminate the difficulty in finding suitable tissues and organs for recipients as well as maximizing the use of donated tissues and organs and reducing waste. More importantly, matching of specific anatomical and immunological requirements as well as testing for transmissible diseases could be carried out more extensively due to the extra time that banked tissues could be held in quarantine until needed. Size, shape and anatomical origin can be very important criteria for selecting an appropriate tissue sample to transplant, thus a large inventory is necessary. In a recent review of kidney transplants, Terasaki (22) has found an advantage for those patients who received kidneys which were close tissue type matches. Also, an approach to reduce host versus graft rejection by modulating the host's immune recognition capabilities has been suggested recently (14,16) which may require a significant amount of storage time (while the immune system modulation was

5

being performed); this would be easily and economically achieved with cryopreservation.

Current approaches to tissue and organ cryopreservation use high concentrations of cryoprotective compounds and rapid rates of cooling. Due to the complex set of interacting variables in these approaches, many researchers have turned to mathematical modeling to predict responses and optimize protocols. Current models (18,2,3), which predict the response of the tissue to osmotic events that occur during freezing, are very detailed, but there has not been a theoretical framework in which these models could be used to predict damage to the tissue. The osmotic rupture hypothesis will allow such models to be used to predict the conditions under which injury will occur, and therefore, to predict the conditions whereby this injury can be avoided (if it can be avoided). For conventional cryopreservation (in which crystalline ice does form), the osmotic rupture hypothesis can only be used to predict rapid cooling injury. In order to optimize the protocol using simulations, it will be assumed that optimal cryopreservation will occur (with a cryoprotectant) at the fastest cooling rate at which IIF is avoided. Alternatively, the hypothesis could also be used to design protocols in which the tissue is loaded with cryoprotectants and frozen in such a manner as to achieve vitrification (the vitreous state is an amorphous [non-crystalline] solid state -- see (5) for a brief description of this process). In this approach, the tissue must contain very high concentrations of solutes which usually have a chemical toxicity (4), thus the addition must proceed as rapidly as possible without damaging the tissue. The osmotic rupture hypothesis could be used to optimize solute loading, but this approach will not be pursued in this thesis. In order to demonstrate the utility of the former approach, the osmotic rupture hypothesis will be applied to the problem of developing a cryopreservation protocol for a model tissue. Articular cartilage has been chosen as it is a relatively simple, homogeneous tissue and there is a clinical need for a supply (whole joint or focal replacement of bone-bearing cartilage are current strategies for treating some cases of traumatic injuries, arthritis, osteonecrosis or metaphyseal bone tumors). Although this simplicity means that techniques for cryopreservation could probably be developed using trial-and-error methods, it is only through proving these techniques on simple systems that they can be applied with confidence to more complex tissues and, eventually, whole organs.

Articular Cartilage

Articular cartilage forms the covering of the surfaces of bones which contact other bones in articulating joints. It provides a resilient volume which is responsible for transmitting compressive loads and a smooth surface that, combined with synovial fluid, reduces the friction between the contact areas of the joint. The tissue is composed solely of cells (the chondrocytes) and a matrix: there are no blood vessels, nerves or lymphatic ducts in articular cartilage. The

6

chondrocytes maintain the composition of the matrix, which provides the mechanical properties that define the function of the tissue.

Uncalcified articular cartilage is classified into three morphological zones which are parallel to the joint surface, based on the arrangement of the chondrocytes. Just below the joint surface is the superficial zone. This region consists of the outermost 5-10% of the tissue and has the highest concentration of cells which are slightly flattened. The next 40-50% of the tissue below the superficial zone is the intermediate zone, in which the cells are spherical and evenly distributed. The deep layer consists of the 40-50% of the tissue that is adjacent to the calcified cartilage and bone. The chondrocytes of the deep zone are spherical and arranged in columns which are perpendicular to the bone-cartilage interface. The tissue as a whole is hypo-cellular, meaning that each chondrocyte must maintain a volume of matrix that exceeds the volume of the cell. The maximum volume of matrix that can be supported by a single chondrocyte is not known, but this information will be important for the cryopreservation of articular cartilage if 100% recovery of the chondrocytes cannot be achieved.

The cartilage matrix is responsible for providing the mechanical properties of articular cartilage: primarily resilience (the ability to recover following a deformation) and tensile strength (the ability to distribute a load without breaking). The tensile properties of the matrix are provided by collagen fibrils: extended bundles of cross-linked collagen molecules (principally type II collagen). The orientation of these fibrils goes from being perpendicular to the bone-cartilage interface in the deep zone to being parallel to the joint surface in the superficial zone, forming an arcade arrangement. This was initially thought to provide a spring-like structure in the matrix (1) but is more likely to simply be an arrangement in which the fibers are orthogonal to the principal shear-stresses associated with repetitive loads on the articular surface. The resilient properties of articular cartilage are provided by proteoglycans and their interaction with water (which makes up about 80% of the matrix [8]). The backbone of the proteoglycan molecule is an extended chain of the repeating disaccharide hyaluronic acid. Onto this framework, core proteins are non-covalently bonded at regular intervals. There is also a link protein which stabilizes the bond between the core protein and hyaluronic acid. The core protein serves, itself, as a backbone for small oligosaccharides which bond covalently to it. Many of these oligosaccharides also have either keratan sulfate or chondroitin sulfate molecules bound to them. The sugars of these two repeating disaccharides have negative charges on them, thereby providing an overall electronegativity to the proteoglycan molecule. This array of electric charges serves to order the water of the matrix due to the dipole nature of the water molecule. When a load is applied to the cartilage, the water is removed from the negative charges by hydrostatic pressure. This brings the negative charges of neighboring proteoglycans close together so that eventually, compression is halted due to the

mutual repulsion. Upon release of the load, the water returns to its previous state providing resiliency to the cartilage.

Without the chondrocytes to synthesize collagen and proteoglycans, the cartilage soon loses its biomechanical properties and gives way to degradative enzymes (19). Therefore, any attempt to cryopreserve articular cartilage must be designed to provide optimal recovery of the chondrocytes for the graft to maintain its long term function. It has been demonstrated that chondrocytes in suspension, isolated from the matrix using enzymes, can be cryopreserved with near 100% recovery (19); thus it has been hoped that a similar result could be obtained with intact cartilage. Although some recovery was achieved in early trials, success was sporadic and the results were extremely variable (19). This inconsistency and the uncertainty introduced by uncontrolled variables has made the interpretation of these results difficult. Proceeding on the assumption that the behavior of the matrix could be modelled in a manner similar to solutions of physiological interest, the work in this thesis presents an alternative approach to this problem.

Hypothesis

Osmotically driven water movement, such as occurs during rapid freezing protocols, leads to pressure being exerted on the plasma membrane due to the frictional drag of the moving water. The tensile properties of the plasma membrane can fail (a rupture of the membrane) if this pressure is of a sufficient magnitude, leading to the formation of an aqueous channel connecting the cytoplasm with the extracellular environment.

Objectives and Approach

Initially, the osmotic rupture hypothesis will be developed in a mathematical framework. The tenets of the theory will be tested using a cryomicroscope to measure the kinetics of water loss during freezing. Following this, some data from the literature concerning intracellular ice formation will be used to establish the validity of the hypothesis in its application to predicting the genesis of IIF. Since the application of the osmotic rupture hypothesis requires modeling the responses of cells to osmotic stresses, it is necessary to determine the accuracy with which present models can accomplish this. One of the assumptions that has been previously used in this endeavor -- that the permeability parameters obey an Arrhenius temperature relation -- has recently been challenged. This challenge will be tested experimentally to provide evidence that the model being used gives accurate predictions.

Once the hypothesis and its application to the prediction of IIF in cells in suspension has been developed, the focus will shift to employing this approach to the cryopreservation of articular cartilage. To begin with, the permeability

parameters and their temperature dependence must be measured for chondrocytes so that the osmotic responses of the cells during addition and removal of cryoprotectants, as well as during freezing, can be described. The conditions under which IIF occurs in chondrocytes must also be measured, so that the parameters of the equation which predicts the probability of IIF can be determined. With these parameters, the occurrence of IIF can be predicted for chondrocytes under any conditions for which the composition of the solution can be defined. To predict what happens in intact cartilage, however, more information is necessary. The diffusion coefficient for dimethyl sulfoxide (DMSO) in the cartilage matrix will be measured (DMSO is the most commonly used cryoprotectant for the purpose of reducing solution effects injury) and the recovery of chondrocytes, *in situ*, following various freezing and thawing protocols will be measured to provide insight into the behavior of the matrix solution during cryopreservation. The information thus obtained will then be used in a mathematical model of articular cartilage to be used in simulated cryopreservation protocols. The response of the model can be tested on a computer to optimize the protocol for minimizing the time spent between the freezing point and -80°C and maximizing the number of cells which do not form intracellular ice. It is not expected that the protocol obtained thusly will provide a perfect solution. Indeed, there are some assumptions that have been made which do not have direct experimental verification. However, the result should provide a suitable starting point for empirical optimization, and the dependencies of the variables will be better understood so that a minimum of costly experiments (both in terms of monetary costs and the loss of life that accompanies animal experimentation) must be run in order to establish a clinical protocol.

References

1. Benninghoff, A. 1925. Referenced in: Fulkerson, J., Edwards, C. and Chrisman, O. 1987. Articular Cartilage. in *The Scientific Basis of Orthopaedics*, Albright and Brand, eds., Appleton & Lange, Connecticut, USA. pp. 347-371.

2. Bischof, J. and Rubinsky, B. 1991. Mathematical Models for the Process of Freezing in Tissue. *Cryobiology* **28**: 558.

3. Diller, K., Merchant, F. and Lauchenbruch, C. 1991. Network Thermodynamic Simulation of Combined Osmotic and Mechanical Behavior of Pancreas Islets During Cryopreservation. *Cryobiology* **28**: 587-588.

4. Fahy, G. 1982. Prevention of Toxicity from High concentrations of Cryoprotective Agents. in *Organ Preservation. Basic and Applied Aspects*, Pegg, Jacobsen and Halasz, eds., MTP Press, Boston, MA, USA. pp. 367-369.

5. Fahy, G. and Hirsch, A. 1982. Prospects for Organ Preservation by Vitrification. in *Organ Preservation. Basic and Applied Aspects*, Pegg, Jacobsen and Halasz, eds., MTP Press, Boston, MA, USA. pp. 399-404.

6. Levitt, J. and Scarth, G. 1936. Frost Hardening Studies with Living Cells. II. Permeability in Relation to Frost Resistance and the Seasonal Cycle. *Can. J. Res. C.* **14**: 285-305.

7. Lovelock, J.E. 1953. The Haemolysis of Human Red Blood Cells by Freezing and Thawing. *Biochim. et Biophys. Acta* **10**: 414-426.

8. Maroudas, A. 1979. Physico-chemical Properties of Articular Cartilage, in *Adult Articular Cartilage*, 2nd ed. Pitman Medical. pp. 131-170.

9. Mazur, P. 1960. Physical Factors Implicated in the Death of Micro-organisms at Subzero Temperatures. *Ann. NY Acad. Sci.* **85**: 610-629.

10. Mazur, P. 1963. Kinetics of Water Loss from Cells at Subzero Temperatures and the Likelihood of Intracellular Freezing. *J. Gen. Physiol.* **47**: 347-369.

11. Mazur, P. 1977. The Role of Intracellular Freezing in the Death of Cells Cooled at Supraoptimal Rates. *Cryobiology* **14**: 251-272.

12. Mazur, P., Leibo, S. and Chu, E. 1972. A Two Factor Hypothesis of Freezing Injury. *Exp. Cell Res.* **71**: 345-355.

13. Muldrew, K. and McGann, L.E. 1990. Mechanisms of Intracellular Ice Formation. *Biophys. J.* **57**: 525-532.

14. Odorico, J., Posselt, A., Naji, A., Markmann, J. and Barker, C. 1993. Promotion of Rat cardiac Allograft Survival by Intrathymic Inoculation of Donor Splenocytes. *Transplantation* **5**: 1104-1107.

15. Pitt, R. and Steponkus, P. 1989. Quantitative Analysis of the Probability of Intracellular Ice Formation During Freezing of Isolated Protoplasts. *Cryobiology* **26**: 44-63.

16. Posselt, A., Barker, C., Tomaszewski, J., Markmann, J., Choti, M. and Naji, A. 1990. Induction of Donor-Specific Unresponsiveness by Intrathymic Islet Transplantation. *Science* **249**: 1293-1295.

17. Polge, C., Smith, A.U. and Parkes, A.S. 1949. Revival of Spermatozoa after Vitrification and Dehydration at Low Temperatures. *Nature* **164**: 666.

18. Rubinsky, B. and Pegg, D. 1988. A Mathematical Model for the Freezing Process in Biological Tissue. *Proc. R. Soc. Lond.* **B234**: 343-358.

19. Schachar, N. and McGann, L. 1991. Cryopreservation of Articular Cartilage, in *Bone and Cartilage Allografts: Biology and Clinical Applications*, Friedlaender and Goldberg, editors, American Academy of Orthopaedic Surgeons. pp. 211-230.

20. Steponkus, P. and Dowgert, M. 1981. Phenomenology of Intracellular Ice Nucleation in Isolated Protoplasts. *Plant Physiology* **67**: S-58.

21. Steponkus, P., Stout, D., Wolfe, J. and Lovelace, R. 1984. Freeze Induced Electrical Transients and Cryoinjury. *Cryo-Letters* **5**: 343-348.

22. Terasaki, P. and Cicciarelli, J. 1989. Arguments Against HLA-A, -B, -DR Mismatching in Kidney Transplant Recipients. *Transplantation Proceedings* **21**: 659-660.

23. Toner, M., Karel, M. and Cravalho, E. 1990. Thermodynamics and Kinetics of Intracellular Ice Formation During Freezing of Biological Cells. *J. Appl. Phys.* **67**: 1582-1593.

24. Toner, M., Cravalho, E. and Karel, M. Cellular Response of Mouse Oocytes to Freezing Stress: Prediction of Intracellular Ice Formation. *J. Biomech. Eng.* **115**: 169-174.

Chapter 2

The Osmotic Rupture Hypothesis of Intracellular Freezing Injury[*]

Introduction

There has recently been renewed interest in the phenomenon of intracellular ice formation (the freezing of cytoplasm which is usually associated with lethal injury) in cells exposed to low temperatures. Phenomenological models of intracellular ice formation have been proposed which use statistical information to predict the likelihood of intracellular ice formation during defined freezing protocols (22,30). Mechanistic models have also been proposed, based on two general views: that intracellular ice formation is the *cause* of injury to the cell or that it is a *result* of damage to the plasma membrane. The former approach, most recently applied in a theory proposed by Toner et al. (37), suggests that intracellular ice formation occurs as a result of nucleation within the cell, catalyzed either by the plasma membrane or intracellular particles. An alternate hypothesis, proposed by Muldrew and McGann (29), contends that osmotic stresses which develop during cooling lead to a rupture in the plasma membrane which then allows extracellular ice to propagate into the cytoplasm. Mazur (20), has long held the view that intracellular ice formation is seeded by extracellular ice, although it is not the result of a rupture in the plasma membrane. His hypothesis maintains that when a critical temperature is encountered during cooling, at which the smallest radius of stable ice crystal growth matches the radius of aqueous pores in the plasma membrane, then IIF will occur if there is supercooled water in the cytoplasm.

It is important that the mechanisms of freezing injury be understood if techniques are to be developed which avoid this injury. Although purely empirical approaches have been successful in developing cryopreservation protocols for cell suspensions and a few simple tissue systems, these have not resulted in techniques for cryopreserving complex mammalian tissues. Success in this area would have obvious benefits in medicine as it would allow banking of tissues and organs for transplantation. Current approaches to tissue and organ preservation use high concentrations of cryoprotective compounds and rapid rates of cooling, conditions under which high osmotic stresses and intracellular ice formation are likely to occur. Due to the complex set of interacting variables in these approaches, many researchers have now turned to mathematical modeling of organized tissues at low temperatures to predict responses and optimize protocols. Current models concentrate on describing the response of the tissue to osmotic events that occur during freezing. Although very detailed models have been constructed for several tissue systems (33,2,9), there has not

---

[*] A version of this chapter has been submitted for publication. Muldrew & McGann 1993. *Biophysical Journal.*

been a theoretical foundation of cell damage to allow these models to be used to predict the conditions that could result in lethal injury to the tissue. Hypotheses of freezing injury that relate the mechanism of injury to events which can be modeled during freezing and thawing can be used as tools toward predicting successful protocols in which injury to the tissue is minimized. Mechanistic models have the further advantage of providing physical insight into the systems being studied which may lead to novel solutions which could not have been foreseen from strictly phenomenological models or a purely empirical approach.

The Cellular Environment During Freezing

Mammalian cells necessarily exist in an ionic environment which becomes concentrated during freezing due to the removal of water from the solution in the form of ice. Following Mazur's treatment (21,24), the increased osmotic pressure in the extracellular space creates an osmotic gradient across the cell's plasma membrane which provides a driving force for water efflux from the cell. The rate of water efflux is limited by the membrane's permeability to water, thus it is possible to cool cells under conditions where the rate of water efflux is insufficient to maintain osmotic equilibrium between the cytoplasm and the unfrozen component of the extracellular solution. Under these conditions, the cytoplasm becomes supercooled and can freeze: an event known as intracellular ice formation (IIF) which can be observed microscopically as a sudden darkening (flashing) of the cytoplasm due to the formation of small ice crystals or microscopic gas bubbles which scatter light [35]. Intracellular freezing is almost always associated with a lethal injury to the cell, however, there is continuing debate as to whether this injury is a cause or a result of IIF (37,29).

Recent experimental work has led us to agree with the suggestion that IIF is the result of a rupture in the plasma membrane which allows extracellular ice to propagate into the supercooled cytoplasm (10,36). We have proposed that this rupture is due to osmotic pressure gradients which develop across the plasma membrane during rapid cooling (29). The tentative mechanism of this rupture was proposed to be due to the frictional drag of water, which exceeds the tensile strength of the plasma membrane and leads to structural failure (29). Membrane rupture then allows extracellular ice to rapidly propagate into the supercooled cytoplasm, resulting in the flashing commonly observed.

Frictional Drag of Water During Osmotic Shrinkage

Water movement across the plasma membrane occurs through a combination of diffusion through the lipid bilayer and movement through transmembrane pores which span the bilayer. There are cell types which are known to use pores as the primary route for water movement -- for example, red blood cells and the cells in the renal collecting ducts of the kidney have a water pore protein that has recently been identified (7,31). Extensive screening of the mRNA for this protein in cells from other human tissues has shown that this pore is likely to be unique to these two cell types (42); hence the movement of water through pores which exist specifically for this purpose is not typical of

mammalian cells (14) although there are aqueous pores such as ion channels in all cells which also allow water movement. It has also been shown that pure lipid bilayers can be constructed with water permeabilities which encompass the entire range found in mammalian cells (variation in the composition of the constituent lipids alters the permeability[14]), validating the assumption that diffusion through the bilayer is the primary mode of osmotic water movement across the plasma membrane in most mammalian cells. It is important to note that the theory presented here can be extended to cells in which water flux occurs predominantly through pores. The derivation of the frictional drag would require assumptions about the number, distribution and size of the aqueous pores since this information is not yet well established.

Water movement through lipid bilayers occurs through a solubility-diffusion mechanism (1,14). When a concentration gradient exists, the water enters the bilayer according to its partition coefficient and then moves down this gradient to the opposite side (14). Each water molecule that moves through the bilayer will impart a frictional force on the bilayer due to collisions with the lipid molecules. The partition coefficient for water in liquid hydrocarbon is large enough that water molecules in the membrane act independently of one another (there is insignificant water-water interaction within the bilayer[14]). The frictional force imparted by a single water molecule will therefore be proportional to the velocity of that molecule as it moves through the hydrophobic region of the bilayer. We can define the drift velocity of a water molecule moving through the bilayer as:

$$v = \frac{\Delta x}{\Delta \tau} \tag{1}$$

v = drift velocity of a water molecule in the membrane (m/s)
Δx = width of the hydrophobic region of the membrane (m)
$\Delta \tau$ = average transit time for a water molecule in the membrane (s)

The water flux is defined as the number of water molecules moving through the membrane per unit time.

$$J_w = \frac{n}{\Delta \tau} \tag{2}$$

J_w = water flux (molecules/s)
n = number of water molecules moving through the membrane in time $\Delta \tau$ (molecules)

14

Thus, the drift velocity of a water molecule can be expressed as:

$$v = \frac{J_w \cdot \Delta x}{n}$$

(3)

The frictional force per molecule is proportional to the drift velocity of a water molecule:

$$\frac{F_f}{n} = f \cdot v$$

(4)

F_f = total force on the membrane due to friction of water (N)
f = coefficient of friction (defined by equation 4) (N·s/m)

The frictional force of water in the membrane can therefore be expressed as:

$$F_f = f \cdot J_w \cdot \Delta x$$

(5)

Einstein explained diffusion in terms of friction between molecules (11), and developed an equation relating the microscopic frictional coefficient to the macroscopic diffusion coefficient for the situation in which molecules collide with a sphere which is large compared to the molecules. Levitt has described a more general derivation of this equation (summarized in appendix 1), showing that it is valid for molecules diffusing through a molecular membrane (18):

$$f = \frac{kT}{D_w}$$

(6)

k = Boltzmann's constant (N·m/K)
T = Absolute temperature (K)
D_w = Diffusion coefficient for water in liquid hydrocarbon. (m²/s) For water moving through a cell membrane, the diffusion coefficient of water in liquid hydrocarbon has been shown to describe diffusion of water within the hydrophobic region of the bilayer (14).

Therefore the frictional force on the membrane is:

$$F_f = \frac{kT}{D_w} \cdot J_w \cdot \Delta x$$

(7)

15

The frictional force can be converted to the pressure on the membrane by dividing by the surface area of the cell. The surface area is treated as being constant during osmotic efflux (the lateral compressibility of lipid bilayers is limited (12), thus this assumption is reasonable).

$$\mathcal{P} = \frac{kT}{AD_w} \cdot J_w \cdot \Delta x \qquad (8)$$

$\mathcal{P}$ = Pressure on the membrane due to water flux (N/m^2)

A = Surface area of the cell (m^2)

Prediction of Membrane Rupture Under Water Flux Stress

Equation 8 gives us a means to calculate the pressure that is imparted to the plasma membrane by water moving due to osmotic pressure gradients. The membrane behaves similar to a fluid or plastic material and cannot, therefore, be thought of as a rigid body that suddenly breaks when this pressure exceeds a critical value. If we consider a single cell with a uniform pressure being exerted on the membrane, a local membrane rupture may be viewed as a spontaneous symmetry breakdown, caused by local fluctuations in the tensile strength of the membrane. There will be an average breaking strength for the entire surface of the membrane, however, local variations will occur. The average rate at which a fluctuation of a given magnitude (reflecting a change in the breaking strength) occurs in a specific locality will be constant over long time periods although the occurence of individual events will be random and uncorrelated with the history of this location. Thus we can define a mean rate at which fluctuations (of a given strength) occur :

$$\alpha = \lim_{t \to \infty} \left[\frac{n}{t} \right] \qquad (9)$$

n = the number of fluctuations which occur in time t

t = time interval

α = the average rate of occurence of fluctuations of a given strength

Let us now consider a slightly longer time interval ($t+\Delta t$) in which we make Δt very small so that on average, it is unlikely that a fluctuation will occur in Δt. In this case, the probability of finding a fluctuation in Δt is:

$$P(1, \Delta t) \ll 1 \qquad (10)$$

Probability is defined as the limit that is reached of the number of occurrences per repetition as the number of repetitions becomes infinitely large; thus the

probability of finding at least one occurrence in this very small time interval is related to the average rate of spontaneous fluctuation occurence by:

$$P(1, \Delta t) = \alpha \cdot \Delta t \qquad (11)$$

Therefore, the probability that a fluctuation does not occur in Δt is:

$$P(0, \Delta t) = \left[1 - P(1, \Delta t) \right] \qquad (12)$$

The probability that no fluctuations occur in time t is found by breaking t into $t/\Delta t$ intervals of length Δt. The probability that no fluctuations occur in t is then the product of the probabilities that no fluctuations occur in each of the intervals of length Δt:

$$P(0, t) = \left[P(0, \Delta t) \right]^{t/\Delta t} \qquad (13)$$

Since

$$P(0, \Delta t) = (1 - \alpha \cdot \Delta t) \qquad (14)$$

Then

$$P(0, t) = \lim_{\Delta t \to 0} \left[1 - \alpha \cdot t \left(\frac{\Delta t}{t} \right) \right]^{t/\Delta t} \qquad (15)$$

By definition, the natural exponential function can be expressed as:

$$e^{-x} = \lim_{N \to \infty} \left[1 - \frac{x}{N} \right]^{N} \qquad (16)$$

Therefore, corresponding $t/\Delta t$ to N, we are left with:

$$P(0, t) = e^{-\alpha \cdot t} \qquad (17)$$

The probability that a fluctuation occurs in time t is therefore:

$$P(1, t) = 1 - e^{-\alpha \cdot t} \qquad (18)$$

17

The rate at which fluctuations occur with a given strength is given by a constant:

$$\alpha = c \qquad (19)$$

    c = constant of proportionality

Since c is a rate constant, it can be replaced with the more widely used time constant τ:

$$c = \frac{1}{\tau} \qquad (20)$$

Thus the probability that a fluctuation of a given strength occurs is given by:

$$P(1,t) = 1 - e^{\frac{-t}{\tau}} \qquad (21)$$

There is also a probability of finding a fluctuation of a given strength (the local breaking strength where the fluctuation occurs) at a particular location at one instant in time. The distribution of fluctuations of a given strength over the area of the membrane can be expected to form a normal distribution about some mean value. For a given force being placed on a local area of the membrane, the probability that this pressure will exceed the local breaking strength of the membrane will be given by the integral of the binomial distribution. This can be approximated to a high degree of accuracy by a two parameter logistic equation:

$$P_{\mathcal{P} > \overline{\mathcal{P}}} = \frac{1}{1 + e^{-b(\mathcal{P} - \overline{\mathcal{P}})}} \qquad (22)$$

$P_{\mathcal{P} > \overline{\mathcal{P}}}$ = probability that the force placed on the membrane exceeds the local breaking strength

$\mathcal{P}$ = pressure imparted on the membrane

$\overline{\mathcal{P}}$ = mean strength of the membrane (average pressure required for failure)

b = parameter related to the standard deviation of the membrane strength distribution ($b = 1.70991/\sigma$ where σ = standard deviation)

The probability that a given force (which is constant with time) exceeds the breaking strength of the membrane as a function of time is therefore given by the product of the probability that the force exceeds the breaking strength of the membrane and the probability that a fluctuation of the required strength has occurred:

$$P_{rupture} = \left[\frac{1}{1+e^{-b\left(\mathcal{P}-\overline{\mathcal{P}}\right)}}\right]\left[1-e^{\frac{-t}{\tau}}\right]$$

(23)

The three parameters in equation 23 will have a temperature dependence as they describe a mechanical failure of the lipid bilayer which is stabilized by hydrophobic interactions and Van der Waal's forces (the strengths of which are functions of temperature). This temperature dependence should be adequately described by an Arrhenius relation:

$$\overline{\mathcal{P}}(T) = \overline{\mathcal{P}}_g \cdot e^{\left[\frac{E_a}{R}\left(\frac{1}{T_g}-\frac{1}{T}\right)\right]}$$

(24)

$\overline{\mathcal{P}}_g$ = mean pressure required for failure at the reference temperature

E_a = Arrhenius activation energy

R = Universal gas constant

T = Absolute temperature

T_g = Reference temperature

Experimental estimates of water flux were calculated from the rate of change in cell volume in response to a gradient in osmotic pressure across the plasma membrane. A cryomicroscope was used to experimentally monitor water flux and the incidence of IIF during freezing. The critical water flux resulting in intracellular freezing was used in equation 8 to calculate the pressure imparted on the membrane. This critical pressure was compared to results from other studies in which membrane failure was achieved by hydrostatic pressure gradients. If IIF is a result of a rupture of the plasma membrane, then it is reasonable to expect that the pressure due to water flux (at the magnitude of water flux that correlates with the formation of IIF) should be comparable to the hydrostatic pressure that is required to rupture plasma membranes in situations in which there are no osmotic pressure gradients.

Materials and Methods

The Chinese Hamster fibroblast cells (V79-w, derived from lung tissue) used in this study were grown in tissue culture using minimal essential medium (Gibco, Grand Island, NY) with Hank's salts, 25 mM Hepes buffer (Gibco), 10% fetal calf serum (Gibco), 0.4% sodium bicarbonate, 100 µg/ml penicillin/streptomycin and 2mM L-glutamine. The cells were maintained in

exponential growth phase by harvesting from plastic tissue culture dishes (75 cm^2; Corning Glass Works, Corning, NY) with regular trypsinization (0.25% trypsin [Gibco] for 10 min at 37°C) and resuspension in tissue culture medium.

Microscopic observations of cells at subzero temperatures were made using a computer-controlled convection cryomicroscope stage described previously (29). A 2 μl sample of cell suspension was placed under a cover slip on the cryomicroscope stage and all observations were made within 0.5 mm of the thermocouple junction to minimize the effects of thermal gradients. The stage was cooled to a specified subfreezing temperature and held at that temperature while ice formation was initiated at the edge of the cover slip. Measurements showed that the latent heat of fusion was buffered in less than 1.5 s, which was small compared to the time required for shrinkage. The stage was held at the constant temperature for 1 min following ice formation. Experiments were recorded on video tape for later analysis. The presence of intracellular ice was assayed by observing the sudden darkening of the cytoplasm. Measurements of volume change with time were made by digitizing the images from video tape (TARGA+ digitizing board, Truevision, Inc., Indianapolis, IN) and then using a custom computer program to determine the cross-sectional area of the cell and calculating an equivalent spherical cell volume.

Results

Figure 2.1 shows the dependence of IIF on the temperature of ice nucleation. Intracellular ice begins to appear when the temperature of nucleation is below -4°C. The proportion of cells freezing intracellularly increases rapidly as the nucleation temperature is lowered, with all the cells undergoing IIF at nucleation temperatures below -8°C. The kinetics of cell volume change are shown in figure 2.2 for nucleation temperatures of -2°C and -4°C. There is a wide range of permeabilities within a homogeneous population of cells, so measurement of shrinkage at nucleation temperatures where IIF occurs could be biased by removing the cells which undergo IIF from the population of shrinking cells (i.e. if the cells which lose water slowly are more likely to undergo IIF, then removing these from the sample would bias the average towards a higher permeability). The experimental data in figure 2.2 were fit to equations describing water loss (described in more detail elsewhere [27]) which were adapted from the work of Dick (8). The equations describe the water flux driven by the osmotic pressure gradient which develops during freezing.

$$\frac{dV}{dt} = L_p ART \left(\pi_i - \pi_e \right) \tag{25}$$

dV/dt = Rate of volume change
L_p = Hydraulic conductivity

20

A = Cell surface area
R = Gas constant
T = Temperature
π_e = Osmotic pressure of the suspending medium (calculated from the phase diagram of sodium chloride and water presented in ref. 6)
π_i = Osmotic pressure of the cytoplasm, where the osmotic pressure of the cytoplasm during shrinkage can be expressed in terms of the cell volume using the Boyle-van't Hoff relation applied to the osmotic responses of cells (19).

$$\pi_i = \pi_o \frac{(1 - v_d)}{(v - v_d)} \tag{26}$$

π_o = Isotonic osmotic pressure
v = Normalized cell volume
v_d = Osmotically inactive fraction of cell volume

For hamster fibroblasts, values of the hydraulic conductivity and osmotically inactive fraction, derived by fitting experimental data to equations 25 and 26, are shown in table 2.1. Also shown in this table are values of the permeability parameters for liposomes and oocytes, taken from the literature, which are to be used in the discussion. The values of L_p and v_d thus obtained enable us to use equations 25 and 26 to simulate the kinetics of water loss due to osmotic pressure gradients. The experimental data points and the curves generated using the best-fit values for the parameters are shown in figure 2.2. The magnitude of water flux is maximal immediately upon ice formation as this is when the osmotic pressure gradient is greatest; therefore, the peak rate of water flux can be obtained by taking the initial slope of the curve generated from the fitted parameters. The peak water flux at -2°C was 29 μm^3/s, increasing to 38 μm^3/s at -4°C when IIF begins to occur (as shown in figure 2.1). The hydraulic conductivity of the plasma membrane (and hence the water flux) decreases with decreasing temperature so there is a temperature at which the increase in osmotic stress (due to a decrease in the nucleation temperature) is balanced by the decrease in hydraulic conductivity. At lower temperatures, the water flux will decrease with decreasing nucleation temperature; thus it is important to show that the magnitude of the peak water flux is increasing at temperatures at which IIF begins to occur.

Table 2.1 Permeability Parameters

	V_{iso} (μm^3)	V_d ($\times V_{iso}$)	L_p ($\mu m^3/\mu m^2 \cdot min \cdot atm$)	E_a (kcal/mol)	T_g (K)	Ref.
fibroblasts	885	0.44	0.241		271	
fibroblasts	845	0.42	0.118		269	
oocytes	2.30×10^5	0.018	0.43	13-14.5	295	(16)
oocytes	2.62×10^5	0.214	0.044	13.3	273	(38)
liposomes	4189	0.06	1.82	10.6	295	(4)

V_{iso} = isotonic volume

Discussion

Experimental Measurements of Water Flux

Since the rate of water efflux is still increasing at -4°C, the water flux that occurs in the range over which damage occurs (see figure 2.1) will be greater than the 38 $\mu m^3/s$ that was measured. This value is simply being used to show that the water flux which is associated with IIF generates a frictional drag on the membrane that is within the range of forces that has been shown to cause rupture from hydrostatic pressures. Although the difference between the upper and lower boundaries that were chosen for this study represent a wide range of values, it is important to establish the feasibility of the hypothesis by this method. The precision of estimates of the critical pressure will be significantly enhanced in the discussion when the hypothesis will be used to analyze a published account of the IIF behavior of liposomes. The critical pressure which causes rupture (and hence IIF) in liposomes can be compared directly to the hydrostatic pressure needed to rupture pure lipid bilayers.

Forces Required to Rupture Membranes

Studies of planar lipid bilayers have found that a hydrostatic pressure of 1×10^{-4} atm leads to a rupture of a bilayer spanning a 1 mm diameter circular opening (15). Micropipette suction experiments on red blood cells have found that pressures of 0.1 atm are sufficient to rupture the membrane when it is being suctioned into a 3 μm diameter micropipette (12). We can take these values as the approximate lower and upper limits of hydrostatic pressures needed to rupture a plasma membrane of mammalian cells (a simple lipid bilayer will likely represent the lower limit since there are no structures to add stability; the red cell membrane, with its extensive cytoskeleton, is a reasonable choice for the upper end of the spectrum). These values were used in equation 8 to determine the critical water flux (the water flux which imparts a pressure on the plasma membrane (due to friction) which is sufficient to rupture the membrane). This critical flux will be compared with the experimentally measured water flux at the beginning of the range over which damage occurs (38 $\mu m^3/s$ at -4°C in hamster fibroblasts).

The surface area of the hamster fibroblast cells is assumed to remain constant during swelling and shrinkage and is taken as the surface area of a sphere (isotonic volume = 865 μm^3; therefore surface area = 417 μm^2). The diffusion coefficient for water in liquid hexadecane has been measured at several temperatures (34), giving an Arrhenius activation energy of 3.35 kcal/mol, allowing calculation of the diffusion coefficient at -4°C (2.26 x 10^{-9} m^2/s). The width of the hydrophobic region of the bilayer (Δx) is commonly taken as 50 Å (13), so the critical water flux for hamster fibroblasts can then be calculated using these values in equation 8. The lower limit is 5.6 x 10^{11} molecules/s (or 17.1 μm^3/s) and the upper limit is 5.6 x 10^{14} molecules/s (or 1.71 x 10^4 μm^3/s).

The experimentally measured water flux (at the onset of IIF) is 38 μm^3/s, which is just above the bottom end of the calculated range. The magnitude of the peak water flux will continue to increase as the temperature of ice nucleation is lowered due to the increased osmotic pressure gradients that will be generated. Figure 2.1 shows that the proportion of cells undergoing IIF also increases. This concordance establishes the feasibility of the osmotic rupture hypothesis; however, without detailed measurements of the hydrostatic pressure required to rupture hamster fibroblast membranes, this data cannot be taken any further. To further investigate the implications of the hypothesis, and to subject it to more rigorous testing, we have undertaken to apply it to other systems in which IIF has been studied. By generalizing the approach so that quantities that have been measured for various cell types can be used to predict the onset of IIF, a comparison can be made between predictions of the theory and experimental results.

Application of the Theory

The theory can be used to predict membrane rupture due to osmotic water flux if the conditions under which rupture occurs are known. For the case in which membrane rupture occurs during rapid cooling (indicated by IIF), equation 23 can be readily applied to any cell type for which the permeability parameters and the conditions under which IIF occurs are known. The shrinkage data for the fibroblasts shown in figure 2.2 provided estimates of the hydraulic conductivity and the osmotically inactive volume which can be used with the water flux equations to predict the peak water flux which occurs on nucleation at subfreezing temperatures (the temperature range over which shrinkage measurements were carried out (2°C) is not large enough to determine a reasonable estimate of the Arrhenius activation energy for the hydraulic conductivity, so the value was assumed to be the same as that measured for mouse oocytes, 13.3 kcal/mol, cited by Leibo [16] and Toner et al. [38]). Figure 2.1 shows the measured proportion of cells which undergo IIF on nucleation at several temperatures which can be used with equation 23 to generate estimates of the membrane rupture parameters. This is done by a least squares fit in which the errors to be squared and summed are the

differences between the P_{IIF} from equation 23 and the measured proportion of cells undergoing IIF at each temperature for which a measurement exists. Figure 2.1 shows the results of this fit as a solid line. The estimates of the membrane rupture parameters can then be used to predict rupture under any circumstance in which the osmotic stresses can be defined.

To demonstrate the utility of this approach, two cases from the literature will be discussed. The first system that will be analyzed is that of unilamellar liposomes, as described by Callow and McGrath (4). The behavior of liposomes during freezing is similar to that of cellular systems and they present a simple model system in which the critical pressure is known (this value was presented as the lower boundary for rupture earlier (10^{-4} atm), which was taken from data describing pure lipid bilayers [15]). Thus the critical water flux can be inserted into equation 8 to compare the pressure due to friction which is associated with IIF and the hydrostatic pressure that causes rupture of a lipid bilayer.

IIF in Liposomes

The relevant permeability parameters for the liposomes are summarized in table 2.1. The activation energy is from reference (3) as it is midway between the other two values cited in reference (4). The osmolality of the hypertonic sucrose solution during freezing is taken from the CRC Handbook of Chemistry and Physics (41). The surface area of the liposomes is treated as the surface of a shrinking sphere in the simulations of freezing behavior as this is the assumption that was used to fit the parameters to the original data (4). The equations used to model osmotic water efflux are the same as those used for the fibroblasts discussed earlier. Figure 2.3 shows the water flux as a function of temperature for each of the four cooling rates which define the conditions of IIF for liposomes (4). Using the values of water flux given in figure 2.3, the parameters of equation 23 ($\overline{P}$, b and τ) were fit to minimize the sum of squared errors between the measured and predicted proportion of cells undergoing IIF using an assumed activation energy for these parameters of 5 kcal/mol (-5 kcal/mol for b and τ as they are expected to decrease with temperature -- this has the effect of making the membrane more fragile at lower temperatures). Table 2.2 shows the measured and predicted percentages of cells with IIF as a function of cooling rate. The measured values are taken from ref. (4).

Table 2.2 Intracellular Ice Formation in Liposomes

Cooling Rate (°C/min)	Measured IIF (%)	Predicted IIF (%)
2	0	1
7	34	33
10	70	71
20	100	97

The predicted probability of IIF from equation 23 is shown in figure 2.4 (the predicted values in table 2.2 are the final values in this figure) which can also be used to predict the temperature at which IIF occurs. The mean temperature at which IIF should occur is between -3°C and -5°C which is close to the measured value of -5°C (4). The magnitude of water flux at -4°C which correlates to 5% IIF (57 μm^3/s) can be directly inserted into equation 8 (after converting to molecules/s) to get the pressure due to friction that is associated with this flux.

k = 1.38 x 10^{-23} Nm/K

T = 269 K

A = 1257 μm^2 = 1.257 x 10^{-9} m^2

D_w = 2.26 x 10^{-9} m^2/s

J_w = 57 μm^3/s = 1.9 x 10^{12} molecules/s (1 molecule of water = 3 x 10^{-11} μm^3)

Δx = 5 x 10^{-9} m

Thus, the critical pressure, $\mathcal{P}$ = 12.4 N/m^2 (1.23 x 10^{-4} atm)

The critical pressure which causes damage at the 5% level is 1.23 x 10^{-4} atm, just above the value of 1 x 10^{-4} atm of hydrostatic pressure which causes planar lipid bilayers to rupture (15). Table 2.2 shows that equation 23 is able to describe IIF in liposomes phenomenologically. The strength of the theory, however, is clearly seen when the water flux which is associated with IIF (predicted by fitting to experimental data) is inserted into equation 8 to calculate the pressure that is put on the membrane from this water flux. The pressure due to the frictional drag of water moving osmotically (at the level of water flux that is associated with rupture) is the same as the hydrostatic pressure that causes rupture.

IIF in Mouse Oocytes

Leibo et al. (17) first quantified IIF in mouse oocytes and later, Leibo (16) measured the permeability parameters for these cells. Toner, et al. (39) have recently published very detailed cryomicroscopic studies of IIF in mouse oocytes along with permeability data for these cells (38) which is in agreement with that of Leibo. The relevant permeability parameters are listed in table 2.1. Using the phase diagram for sodium chloride and water (6) to predict the extracellular concentration of solutes as a function of temperature, the water flux during freezing was simulated for the cooling rates which produce IIF (the equations for modeling water movement are the same as in the previous example). Figure 2.5 shows the water flux as a function of temperature for these five cooling rates (predicted from the parameters in table 2.1 applied to the equation for water movement). The parameters for membrane rupture ($\overline{\mathcal{P}}$, b and τ) were fit to these predicted values, minimizing the sum of squared errors between the measured (39) and predicted incidence of IIF (the predicted incidence of IIF is from

equation 23). The values of these parameters that gave the best fit, as well as the percentage of cells undergoing IIF, are presented in table 2.3.

Table 2.3 Intracellular Ice Formation in Mouse Oocytes

Cooling Rate (°C/min)	Measured IIF (%)	Predicted IIF (%)
1	0	21
2	65	81
3.5	88	95
5	100	97
20	100	100

$\overline{P} = 9.0$ N/m^2; $b = 0.90$; $\tau = 30.0$ s

Figure 2.6 shows the predicted probability of IIF for these cooling rates and can be used to predict the mean temperature at which IIF occurs (between -11°C and -13°C) which compares favorably to the measured values between -12°C and -15°C (39).   Rall et al. (32) performed cryomicroscope experiments on mouse embryos and found that the temperature at which IIF occurred was significantly depressed in the presence of cryoprotectants. This phenomenon can be accounted for precisely with the osmotic rupture hypothesis, but because of the potential difficulties introduced by describing multicellular structures such as embryos, the treatment will be left for later chapters. The values of the critical water flux parameters derived from this data can also be used to predict the incidence of IIF for isothermal experiments (these are experiments in which the cells are either cooled extremely rapidly to a specified subzero temperature or supercooled to this temperature and then subjected to freezing followed by a holding period during which the incidence of IIF is observed). Figure 2.7 shows this prediction as well as several points taken from the measured data (39). The fit is very good, showing once again that the theory provides an excellent description of the phenomenology of intracellular ice formation.

Other Phenomena Associated with IIF

There is an effect associated with IIF in which cells that were rapidly frozen can remain viable if the warming rate is also rapid (20,25). This effect is usually ascribed to the lack of time for recrystallization of intracellular ice (recrystallization is the process by which large ice crystals with low surface energy grow at the expense of small ice crystals with high surface energy). In the present theory, IIF results in an ice structure which extends through a hole in the membrane (where the rupture occurred). Therefore, recrystallization could cause this transmembrane extension to enlarge in radius thereby further damaging the membrane (the possibility of small holes resealing is the mechanism by which rapidly warmed cells might survive).

A further implication of this theory is that a cell which has been cooled slowly to some subfreezing temperature could be challenged with high gradients

in osmotic pressure during rewarming which could cause damage. The fact that this is not seen, in fact rapid warming (which would lead to the highest osmotic pressure gradients) is usually beneficial (23). This is due to the fact that the greatest water fluxes occur after ice has melted -- at temperatures high enough to prevent osmotic membrane rupture.

A trend can be seen in the literature in which cells with high values of L_p are able to tolerate faster cooling rates without undergoing IIF (23). From this hypothesis, it must be supposed that a necessary precondition of having a high water permeability, is the possession of a membrane architecture that is able to withstand the stress associated with osmotic water movement. The correlation between high values of L_p and the ability to withstand rapid cooling is, therefore, due to the evolutionary necessity of cells being able to withstand osmotic stresses which would otherwise be lethal. The red blood cell provides an excellent model for comparison to test this idea, however, since the primary route for water movement is through pores (14), this treatment will have to await a further extension of the theory.

Cell injury can be induced by osmotic stresses in the absence of ice which appear to be of the same form as the injury associated with IIF (29). The osmotic stresses required to elicit this injury appear also to be of the magnitude that would be predicted from the osmotic rupture hypothesis (29). In fact, the activation energy for the water flux that causes 50% of the cells to rupture has been measured for hamster fibroblasts and has a value of 22.1 kcal/mol (28). The temperature dependence of plastic flow in red blood cell membranes has an activation energy of 18.6 kcal/mol (40). If we use this value for the activation energy of the critical frictional force in equation 7 (plastic flow is due to a force, not a pressure, so equation 7 is used), the resulting activation energy of the critical water flux is 21 kcal/mol (due to the facts that diffusion of water within the membrane has an activation energy of 3.35 kcal/mol and temperature is also a parameter in the equation). There is currently no other hypothesis of the causes of IIF that can explain this injury; furthermore, with the recent trend to using extremely high concentrations of cryoprotectants to create vitrification solutions, the necessity of predicting osmotic injury at temperatures above freezing has taken on an increased importance. The addition and removal of these cryoprotective compounds is problematic for cell suspensions and very difficult for tissue systems. With the ability to model injury (using the present hypothesis) as a result of osmotic stresses created during addition of high levels of cryoprotectants, it may be possible to optimize protocols without spending excessive time conducting trial and error experiments.

Conclusion

The osmotic rupture hypothesis of cryoinjury was introduced to explain the phenomenon of intracellular freezing due to the failure of prevailing theories to account for several experimental challenges (29). The principal criticism of the

hypothesis, following its introduction, was that the cause of injury was ascribed to osmotic pressure gradients across the plasma membrane. Osmotic pressure is simply a property of a solution; it is not a hydrostatic pressure and critics could not see how it could lead to a rupture in a plasma membrane. This was acknowledged in the initial paper and it was suggested that the water flux that was driven by the osmotic pressure gradient could be the factor by which a physical force was imparted to the membrane during dehydration. In the present report, this idea was formalized and shown to be not only plausible, but, taken with the evidence presented in the initial paper (29), quite likely.

The importance of discovering the mechanisms by which cellular injury occurs during cryopreservation cannot be overstated. With the continuing failure to cryopreserve large mammalian tissues and organs, researchers need a new paradigm. One of the most promising is the use of mathematical models in which cryopreservation protocols can be tested without having to perform lengthy and difficult experiments. Until recently, however, there have not been any theories of cryoinjury in which the onset of damage could be correlated with specific physico-chemical events which occur during freezing and thawing(see [39] for an alternative hypothesis of IIF which is conducive to modeling). The osmotic rupture hypothesis links injury to osmotically driven water flux which is a parameter that can be modeled accurately. There have already been several complex models developed to predict the osmotic responses within tissue and organ systems (2,9), however, these have been restricted by the lack of theories of cryoinjury that could be used within these models. It is hoped that this new hypothesis will be used in such a manner to allow new approaches to cryopreservation to be discovered.

References

1. Bacic, G., Srejic, R. and Ratkovic, S. 1990. Water Transport Through Membranes: A Review of NMR Studies of Model and Biological Systems. *Studia Biophysica* **138**: 95-104.

2. Bischof, J. and Rubinsky, B. 1991. Mathematical Models for the Process of Freezing in Tissue. *Cryobiology* **28**: 558.

3. Blok, M., VanDeenen, L. and DeGier, J. 1977. The Effect of Cholesterol Incorporation on the Temperature Dependence of Water Permeation Through Liposomal Membranes Prepared from Phosphatidylcholines. *Biochim. Biophys. Acta* **464**: 509-518.

4. Callow, R. and McGrath, J. 1985. Thermodynamic Modeling and Cryomicroscopy of Cell-Size, Unilamellar, and Paucilamellar Liposomes. *Cryobiology* **22**: 251-267.

5. Chalmers, B. 1959. How Water Freezes. *Sci. American* **200**(2): 114-122.

6. Cocks, F. and Brower, W. 1974. Phase Diagram Relationships in Cryobiology. *Cryobiology* **11**: 340-358.

7. Denker, B., Smith, B., Kuhajda, F. and Agre, P. 1988. Identification, purification and partial characterization of a novel M_r 28 000 integral membrane protein from erythrocytes and renal tubules. *J. Biol. Chem.* **263**: 15634-15642.

8. Dick, D. 1966. Cell Water. Butterworth, Inc., Washington, D.C. pp. 83-89.

9. Diller, K., Merchant, F. and Lauchenbruch, C. 1991. Network Thermodynamic Simulation of Combined Osmotic and Mechanical Behavior of Pancreas Islets During Cryopreservation. *Cryobiology* **28**: 587-588.

10. Dowgert, M. and Steponkus, P. 1983. Effect of Cold Acclimation on Intracellular Ice Formation in Isolated Protoplasts. *Plant Physiol.* **72**: 978-988.

11. Einstein, A. 1956. Investigations on the Theory of the Brownian Movement (Furth, R., ed.). Dover Publications, Inc.

12. Evans, E. and Skalak, R. 1980. Mechanics and Thermodynamics of Biomembranes. CRC Press, Inc. p. 146.

13. Fettiplace, R., Andrews, D. and Haydon, D. 1971. The Thickness, Composition and Structure of Some Lipid Bilayers and Natural Membranes. *J. Membrane Biol.* **5**: 277-296.

14. Finkelstein, A. 1987. Water Movement Through Lipid Bilayers, Pores, and Plasma Membranes. John Wiley & Sons, Inc.

15. Jain, M. 1972. The Bimolecular Lipid Membrane: A System. Litton Educational Publishing, Inc. p. 54.

16. Leibo, S. 1980. Water Permeability and Its Activation Energy of Fertilized and Unfertilized Mouse Ova. *J. Membrane Biol.* **53**: 179-188.

17. Leibo, S., McGrath, J. and Cravalho, E. 1978. Microscopic Observation of Intracellular Ice Formation in Mouse Ova as a Function of cooling Rate. *Cryobiology* **15**: 257-271.

18. Levitt, D. 1974. A New Theory of Transport for Cell Membranes Pores I. General Theory and Application to Red Cell. *Biochim. et Biophys. Acta* **373**: 115-131.

19. Lucke, B. and McCutcheon, M. 1932. The Living Cell as an Osmotic System and its Permeability to Water. *Physiol. Rev.* **12**: 68-132.

20. Mazur, P. 1960. Physical Factors Implicated in the Death of Micro-organisms at Subzero Temperatures. *Ann. NY Acad. Sci.* **85**: 610-629.

21. Mazur, P. 1963. Kinetics of Water Loss from Cells at Subzero Temperatures and the Likelihood of Intracellular Freezing. *J. Gen. Physiol.* **47**: 347-369.

22. Mazur, P. 1977. The Role of Intracellular Freezing in the Death of Cells Cooled at Supraoptimal Rates. *Cryobiology* **14**: 251-272.

23. Mazur, P. 1984. Freezing of Living Cells: Mechanisms and Implications. *Am. J. Physiol.* **247**: C125-C142.

24. Mazur, P., Rall, W. and Leibo, S. 1984. Kinetics of Water Loss and the Likelihood of Intracellular Freezing in Mouse Ova: Influence of teh Method of Calculating the Temperature Dependence of Water Permeability. *Cell Biophys.* **6**: 197-214.

25. Mazur, P., Leibo, S. and Chu, E. 1972. A Two Factor Hypothesis of Freezing Injury. *Exp. Cell Res.* **71**: 345-355.

26. McGann, L. and Farrant, J. 1976. Survival of Tissue Culture Cells Frozen by a Two-Step Procedure to -196°C. II. Warming Rate and Concentration of Dimethyl sulfoxide. *Cryobiology* **13**: 269-273.

27. McGann, L., Stevenson, M., Muldrew, K. and Schachar, N. 1988. Kinetics of Osmotic Water Movement in Chondrocytes Isolated From Articular Cartilage and Applications to Cryopreservation. *J. Orthop. Res.* **6**: 109-115.

28. McGann, L. and Muldrew, K. 1992. Temperature Dependence of Membrane Sensitivity to Osmotic Stresses. *Cryobiology* **29**: 786-787.

29. Muldrew, K. and McGann, L.E. 1990. Mechanisms of Intracellular Ice Formation. *Biophys. J.* **57**: 525-532.

30. Pitt, R. and Steponkus, P. 1989. Quantitative Analysis of the Probability of Intracellular Ice Formation During Freezing of Isolated Protoplasts. *Cryobiology* **26**: 44-63.

31. Preston, G., Carroll, T., Gugginno, W. and Agre, P. 1992. Appearance of Water Channels in *Xenopus* Oocytes Expressing Red Cell CHIP28 Protein. *Science* **256**: 385-387.

32. Rall, W., Mazur, P. and McGrath, J. 1983. Depression of the Ice-Nucleation Temperature of Rapidly Cooled Mouse Embryos by Glycerol and Dimethyl Sulfoxide. *Biophys. J.* **41**: 1-12.

33. Rubinsky, B. and Pegg, D. 1988. A Mathematical Model for the Freezing Process in Biological Tissue. *Proc. R. Soc. Lond.* **B234**: 343-358.

34. Schatzberg, P. 1965. Diffusion of Water Through Hydrocarbon Liquids. *J. Polymer Sci.* (No. 10,Pt. C): 87-92.

35. Steponkus, P. and Dowgert, M. 1981. Gas Bubble Formation During Intracellular Ice Formation. *Cryo-Lett.* **2**: 42-47.

36. Steponkus, P. and Dowgert, M. 1981. Phenomenology of Intracellular Ice Nucleation in Isolated Protoplasts. *Plant Physiol.* **67**: 58(suppl.)

37. Toner, M., Karel, M. and Cravalho, E. 1990. Thermodynamics and Kinetics of Intracellular Ice Formation During Freezing of Biological Cells. *J. Appl. Phys.* **67**: 1582-1593.

38. Toner, M., Cravalho, E. and Armant, D. 1990. Water Transport and Estimated Transmembrane Potential During Freezing of Mouse Oocytes. *J. Membrane Biol.* **115**: 261-272.

39. Toner, M., Cravalho, E. and Karel, M. Cellular Response of Mouse Oocytes to Freezing Stress: Prediction of Intracellular Ice Formation. *J. Biomech. Eng.* **115**: 169-174.

40. Waugh, R.E. 1982. Temperature Dependence of the yield Shear Resultant and the Plastic Viscosity Coefficient of Erythrocyte Membrane. *Biophys. J.* **39**: 273-278.

41. Weast, R. (editor-in-chief) 1985. CRC Handbook of Chemistry and Physics, 66th edition. CRC Press, Inc., Boca Raton, Florida.

42. Zhang, R., Logee, K. and Verkman, A. 1990. Expression of mRNA coding for kidney and red cell water channels in *Xenopus* oocytes. *J. Biol. Chem.* **265**: 15375-15378.

Intracellular Ice Formation in Hamster Fibroblasts
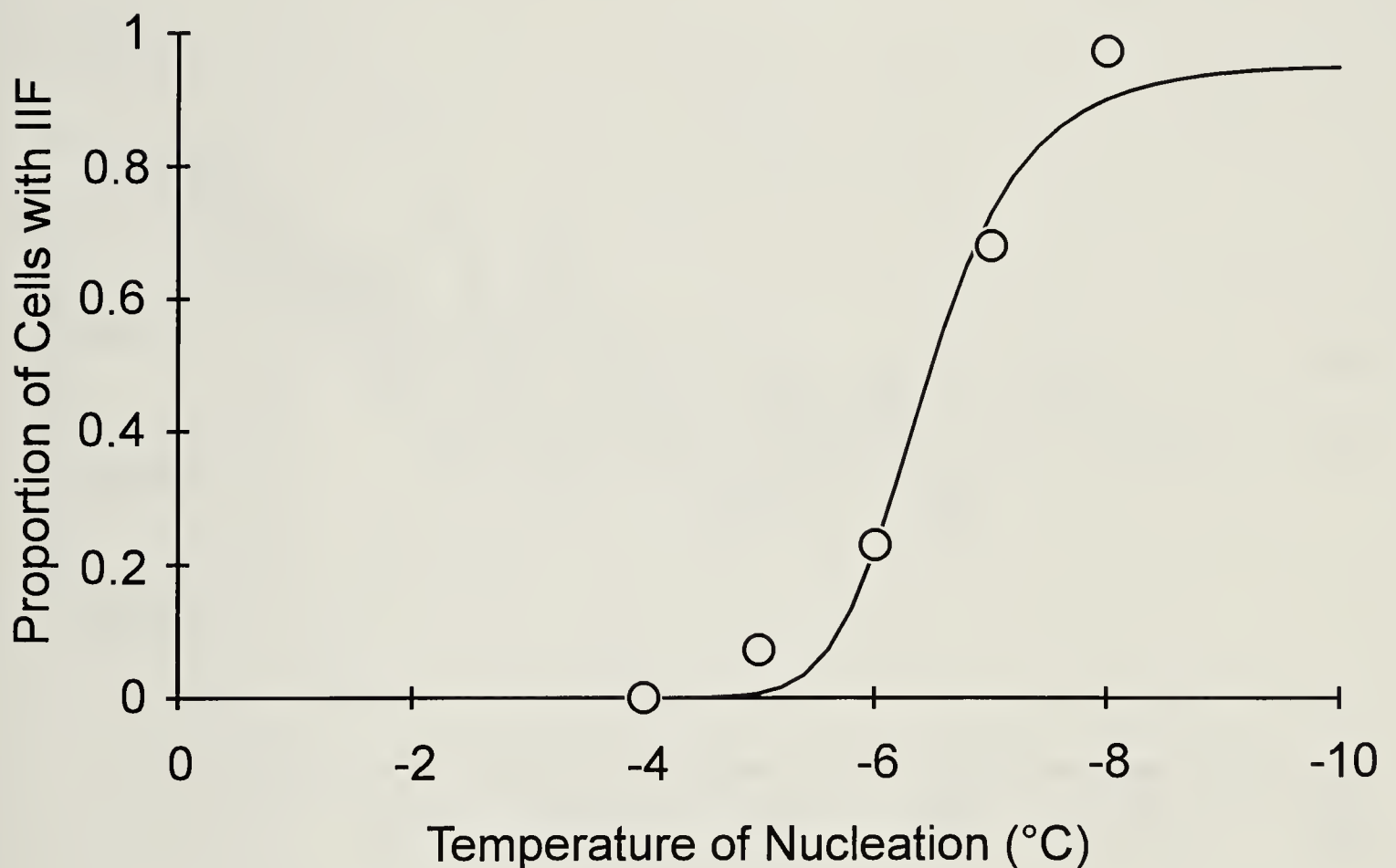
Figure 2.1.
The proportion of cells which "flashed" on ice nucleation at predetermined temperatures. Between 50 and 64 cells were observed for each experimental point. The solid line is a least squares fit of equation 23 with $\bar{\mathcal{P}}$ = 75.6 N/m^2 (activation energy = 18.5 kcal/mol), b = 0.3 (activation energy = -18.5 kcal/mol) and τ = 0.5 s (activation energy = -18.5 kcal/mol) at -4°C.

Figure 2.2.
The closed circles show the average values of cell volume following ice nucleation at -2°C and the open circles represent the average volume following ice nucleation at -4°C. The solid lines show the least squares fit of an equation for osmotic water flux (see text). The fit was accomplished using the simplex method. The initial slope of the line for -2°C is 29 μm^3/s and for -4°C is 38 μm^3/s.

Rate of Water Efflux From Liposomes During Constant Cooling
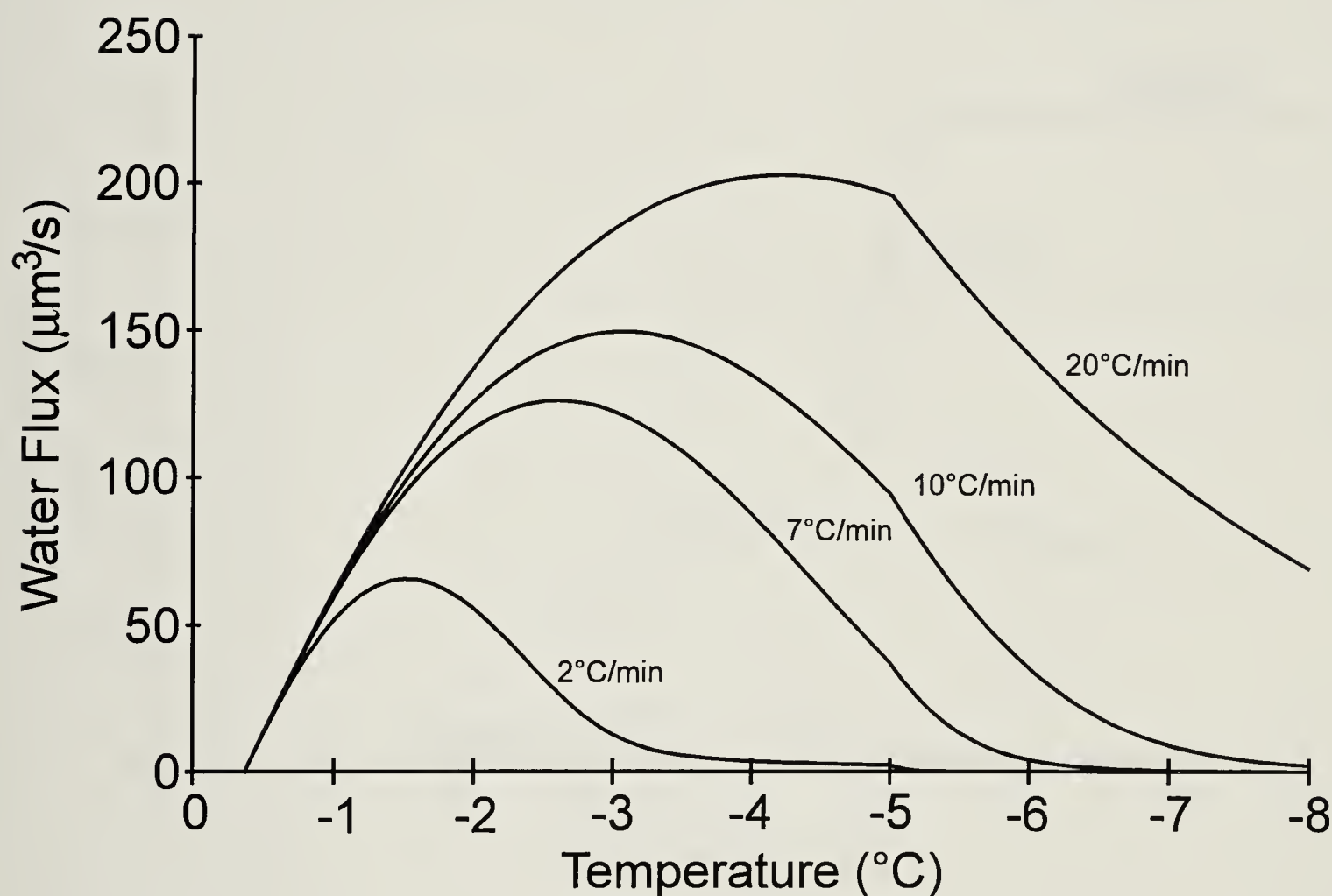
Figure 2.3.
The instantaneous water flux is plotted as a function of temperature for the four different cooling rates (2, 7, 10 and 20°C/min) for liposomes in a 0.2M sucrose solution. The water flux is calculated from the water transport equation in response to the increased osmolality of the unfrozen solution due to ice formation.

Probability of IIF in Liposomes
During Constant Cooling
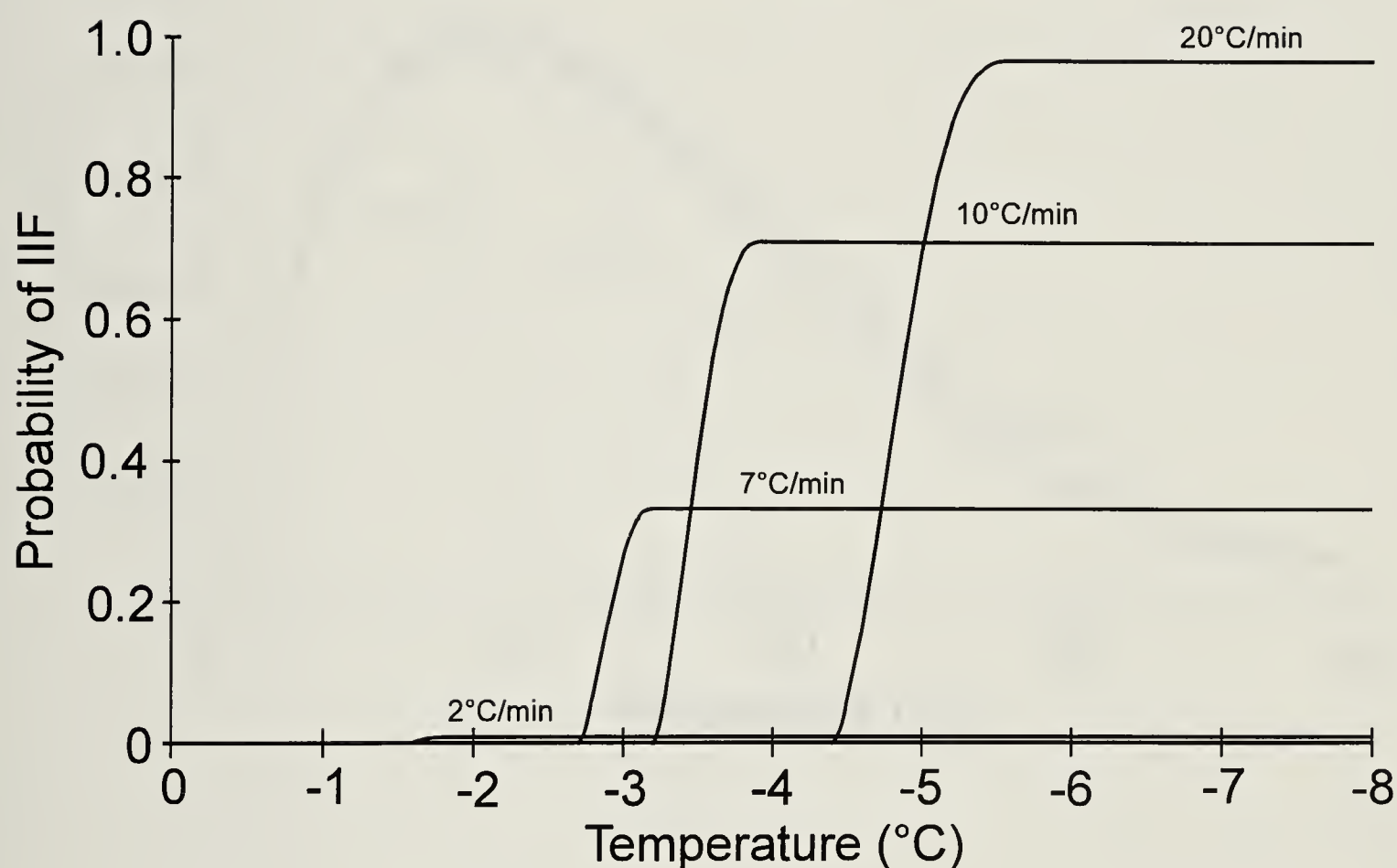
Figure 2.4.

The probability of IIF in liposomes is shown as a function of temperature reached during cooling at four different cooling rates (2, 7, 10 and 20°C/min). The maximum values reached are summarized in Table 2.2. The parameters used to determine these curves are: $\overline{\mathcal{P}}$ = 27.5 N/m^2 (activation energy = 5 kcal/mol), b = 0.30 (activation energy = -5 kcal/mol) and τ = 10 s (activation energy = -5 kcal/mol).

Rate of Water Efflux from Mouse Oocytes During Constant Cooling
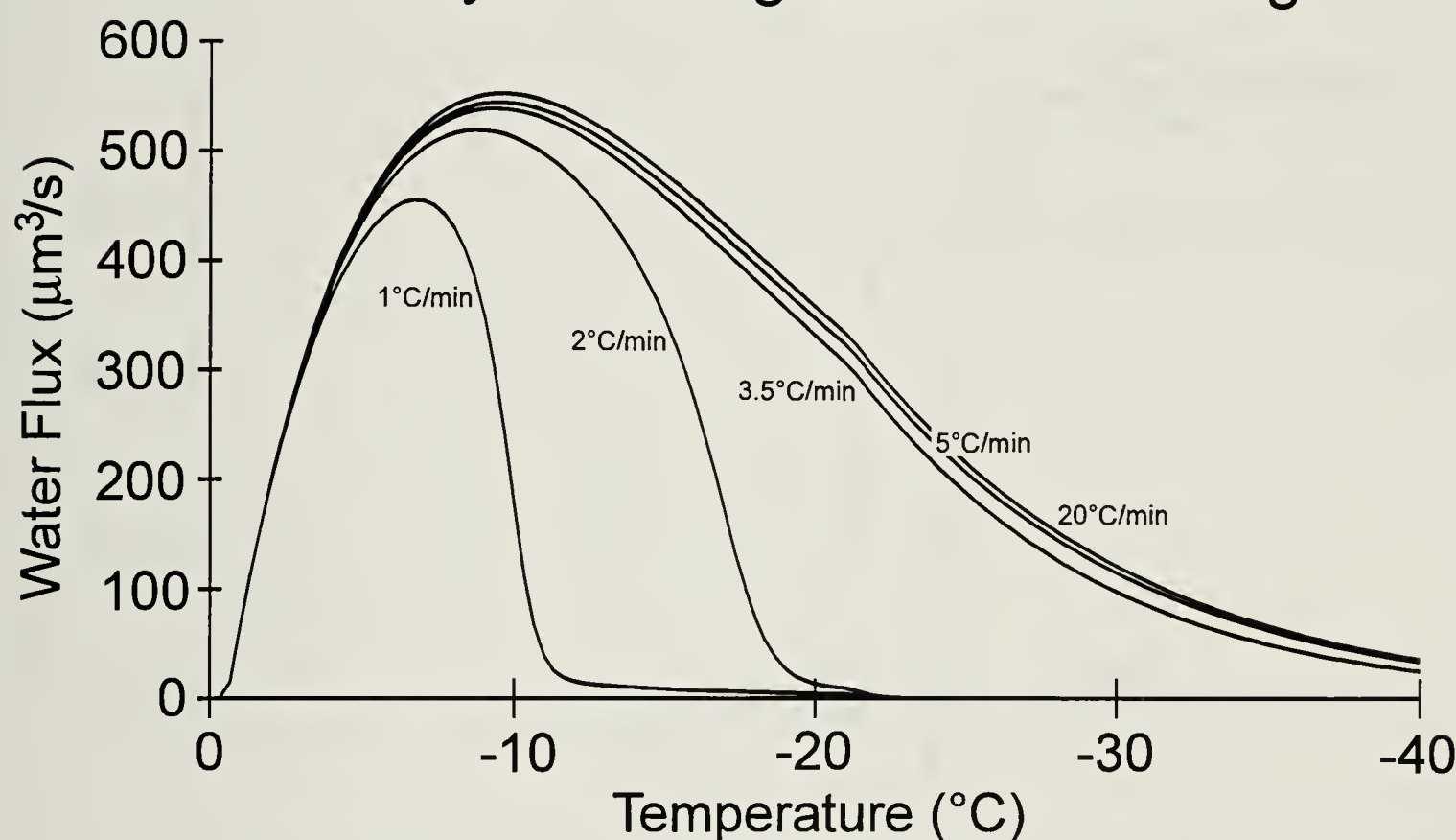
Figure 2.5.
Water flux from mouse oocytes is shown as a function of temperature for five different cooling rates (1, 2, 3.5, 5 and 20°C/min). The permeability parameters used to calculate these fluxes come from ref (32) and are listed in Table 2.1.

Probability of IIF in Mouse Oocytes During Constant Cooling
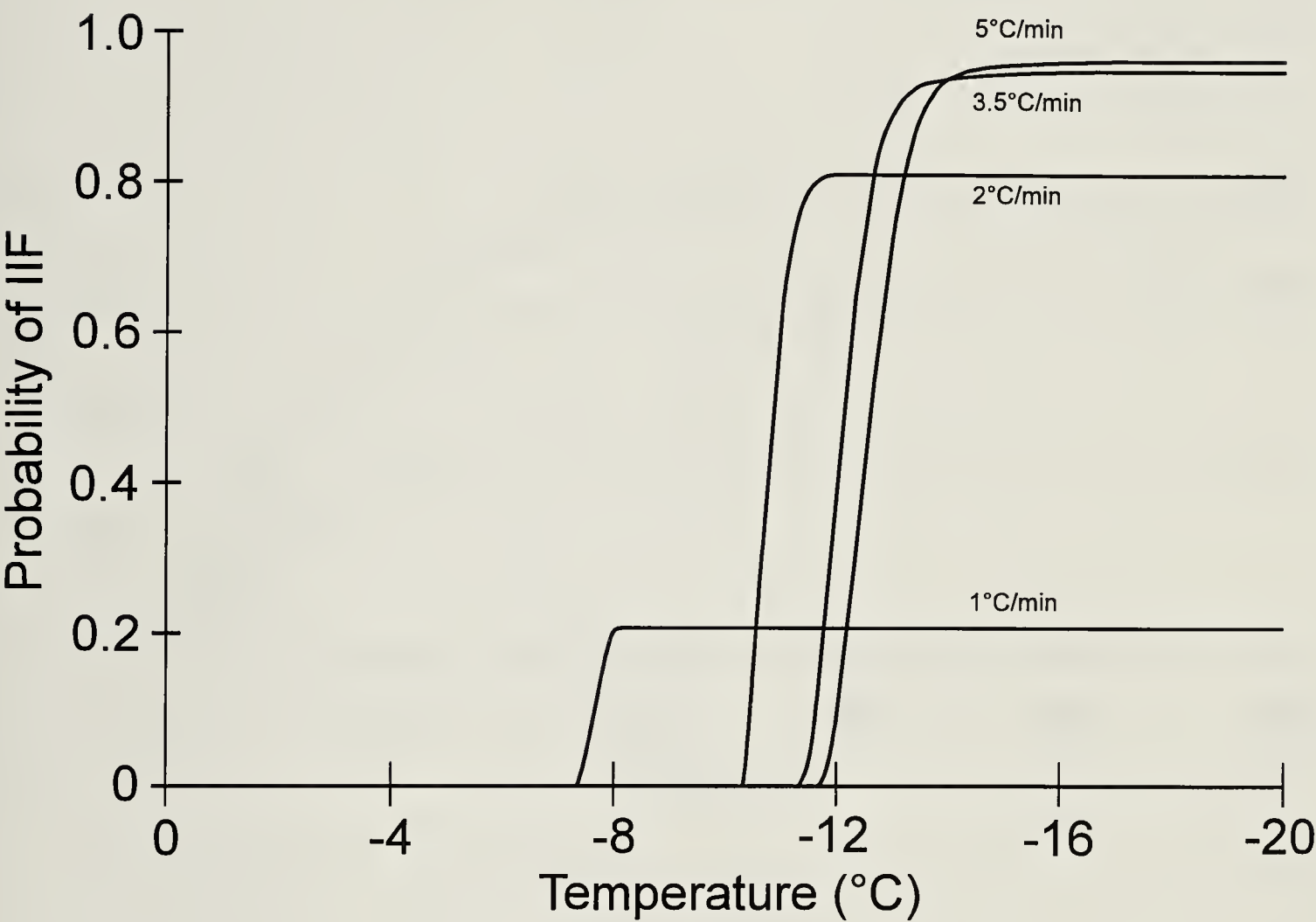
Figure 2.6.

The cumulative probability of IIF in mouse oocytes is plotted as a function of temperature for four cooling rates (1, 2, 3.5 and 5°C/min). The maximum values reached are summarized in Table 2.3. The parameters used to determine these curves are: $\overline{\mathcal{P}}$ = 9.0 N/m^2 (activation energy = 5 kcal/mol), b = 0.90 (activation energy = -5 kcal/mol) and τ = 30 s (activation energy = -5 kcal/mol).

Probability of IIF in Mouse Oocytes During Isothermal Freezing
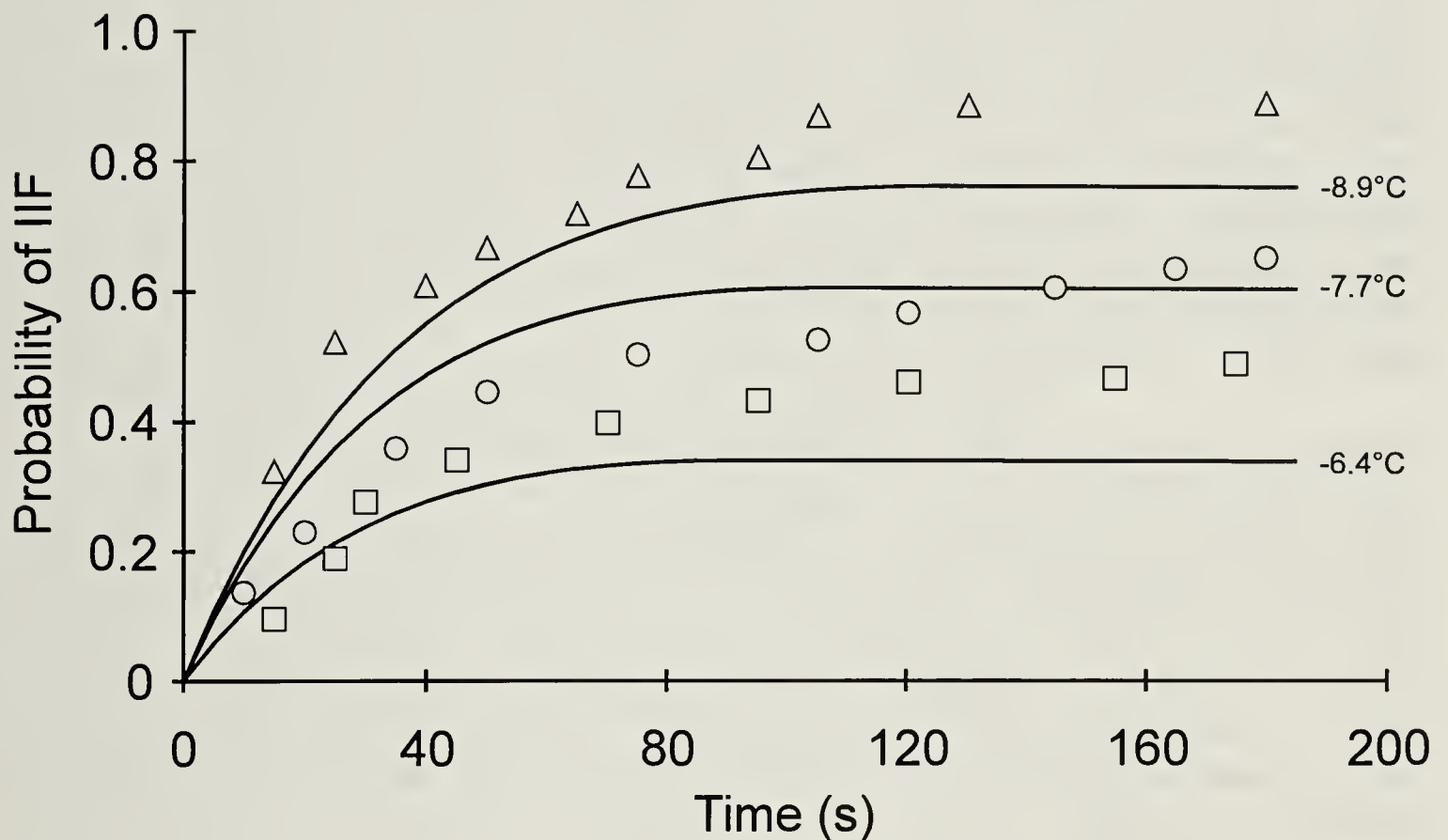
Figure 2.7.

The probability of IIF for mouse oocytes during isothermal experiments (the cells are cooled very rapidly to a specified temperature and then held at that temperature for several min) are plotted as a function of time. The solid lines represent the predicted probability of IIF (using the parameters that were fit to data from the cooling rate experiments modeled in figures 2.6 & 2.7). The shapes are several points taken from the actual data (39) which are representative of the measured response.

Chapter 3

Influence of Ice on the Osmotic Shrinkage of Mammalian Cells

Introduction

Modeling of osmotic responses of cells during freezing and thawing has taken on new importance in efforts to cryopreserve organized tissues and organs. The complex protocols which are now being used in these efforts have too many variables for an individual to correlate mentally. Computer simulations are able to show the interaction of vast numbers of parameters over an infinite range of possible protocols. The danger of using simulations, however, is that the confidence that is placed in their accuracy is often unjustified. Recently, one of the foundations of modeling osmotic responses of cells during freezing and thawing - that cells respond to osmotic pressure gradients independently of the presence or absence of ice in the extracellular environment - has been challenged, thereby suggesting that this modeling is invalid.

The method which has been employed in the past to model the osmotic responses of a particular cell type has been to use permeability parameters obtained by measuring cell volume changes in response to changes in the extracellular osmotic pressure at various temperatures. These data are then fit to a differential equation relating the volume change as a function of time to the osmotic pressure gradient across the cell membrane. The permeability parameters and their temperature dependence can then be determined. These parameters are necessary to model the fate of the cell during freezing and thawing as the formation of ice in a physiological solution results in an increase in the osmotic pressure of the solution (the solutes that are present are excluded from the ice crystal). With the permeability parameters and a knowledge of the osmotic pressure of the solution as a function of temperature, the osmotic behavior of the cell can be predicted during the freezing process.

The temperature dependence of these permeability parameters is usually assumed to be described by an Arrhenius relation (3). Due to the difficulty in measuring cell volume changes below the freezing point, the measurements are usually made in the absence of ice and the Arrhenius relation is assumed to hold in the presence of ice. The suggestion by Toner et al. (7), that the presence of ice can alter the plasma membrane to create an efficient site for surface catalyzed nucleation in the intracellular space prompted them to look for a discontinuity in the Arrhenius extrapolation of the hydraulic conductivity at the freezing point. By measuring the volume change in rat hepatocytes during freezing on a cryomicroscope, they found that extrapolating the parameters thus obtained resulted in a predicted water permeability at room temperature that was 10^6 times greater than what they had actually measured (7). Their methods relied on the measurement of cell cross-sectional area during shrinkage in constant cooling experiments conducted on a cryomicroscope. There are

several aspects of this experiment in which error could have been introduced. Cooling cells to low temperatures without cryoprotectants usually causes damage to the plasma membrane (2) which would affect water permeability. The assumption of spherical geometry which was assumed to extrapolate measurements of cross-sectional area to volume breaks down when cells are highly dehydrated, as occurs when cooling to low temperatures. Measuring cell volume changes as a function of time and temperature adds an extra parameter which must be fit to the permeability equation (the equation used to describe osmotic water movement across cell membranes is a non-linear equation which may have more than one solution which gives a reasonable fit to experimental data - the number of possible solutions usually increases with the number of parameters which must be determined).

These possible sources of error, as well as the importance of establishing confidence in the modeling of osmotic volume changes during freezing and thawing have prompted us to re-address the question of whether the presence of ice causes a significant divergence of the permeability properties of cells. In this study, cell shrinkage as a function of time will be studied both above and below the freezing point. The experiments carried out below the freezing point will be carried out at relatively high temperatures to reduce the departure from spherical geometry and to reduce the possibility of solution effects injury (the membrane damage that occurs due to exposure to hypertonic solutions during freezing). The temperature will also be held constant during the osmotic water loss so that the least number of parameters will have to be fit to the water loss equation.

Materials and Methods

Cells

V79-w hamster fibroblast cells grown in tissue culture were used for all of these experiments. The cells were cultured in minimal essential medium (Gibco, Grand Island, NY) with Hank's salts, 25 mM Hepes buffer (Gibco), 0.4% sodium bicarbonate and 10% fetal calf serum (Gibco). They were harvested from plastic tissue culture dishes (75 cm^2, Corning Glass Works, Corning, NY) by trypsinization (0.25% trypsin [Gibco]) for 10 min at 37°C and resuspended in tissue culture medium. The cells were frequently passaged to maintain the culture in exponential growth phase.

Coulter Volume Measurements

The Coulter volume principle was used to measure cell volumes with a custom interface between a Coulter electronic particle counter (Coulter Electronics, Hialeah, Florida) and an IBM personal computer. As the cells pass through the orifice in the particle counter, the magnitude of the change in electrical conductivity is assumed to be proportional to the cell volume. The computer is programmed to average cell volumes over precisely defined time intervals. A lower threshold for volume measurement was set at about 10% of

the isotonic volume to eliminate any debris from the average volume measurements. The highest measurement channel accumulated any off-scale signals which were also discarded. Cell volumes are averaged over 0.8 s intervals and each determination of volume uses between 1000 and 2000 cells. Plots of relative cell volume with time were converted to absolute volume using a correction factor obtained by measuring the volume of latex microspheres (Coulter Electronics) of known diameter (10.13 µm). Measurements of cell shrinkage were made on three separate occasions for each of the temperatures and each condition was run a minimum of three times on each occasion. The parameters derived from each measurement curve were then averaged.

The hydraulic conductivity and its Arrhenius activation energy were determined at temperatures above 0°C by measuring the average volume change of the cells with time following exposure to various osmotic stresses at several temperatures. The cells were exposed to isotonic phosphate buffered saline (PBS), 3x isotonic PBS (0.9 osmol/kg) and 5x isotonic PBS (1.4 osmol/kg) at 22°C, 14°C and 4°C and the volume recorded until osmotic equilibrium was reached.

Permeability Parameters

The mathematical model of water permeability used in this study is adapted from the work of Dick (1). The rate of water movement across the plasma membrane, dV/dt, is described by the following equation :

$$\frac{dV}{dt} = L_p ART \left(\pi_i - \pi_e \right) \tag{1}$$

where L_p is the hydraulic conductivity of the plasma membrane, A is the cell surface area, R is the universal gas constant, T is the absolute temperature, π_i is the intracellular osmotic pressure and π_e is the extracellular osmotic pressure. The cell surface area is taken as the surface of a sphere and is assumed to remain constant during volume change. This implies that the cell membrane folds or forms microvilli during cell shrinkage and unfolds during swelling: consistent with morphological observations of cell membranes (6). The intracellular osmotic pressure during cell shrinkage can be expressed in terms of the cell volume using the Boyle-van't Hoff relation applied to the osmotic responses of cells (1):

$$\pi_i = \pi_o \left[\frac{1 - v_d}{v - v_d} \right] \tag{2}$$

where π_o is the isotonic osmotic pressure, v is the normalized cell volume (V/V_o) and v_d is the osmotically inactive fraction of cell volume. An Arrhenius relation is

41

used to describe the temperature dependence of L_p in which an activation energy is used to determine L_p at an unknown temperature, given L_p at a known temperature:

$$\ln\left(\frac{L_p}{L_{pg}}\right) = \frac{E_a}{R}\left[\frac{1}{T_g} - \frac{1}{T}\right] \qquad (3)$$

where E_a is the Arrhenius activation energy and L_{pg} is the hydraulic conductivity at absolute temperature T_g.

The experimental data obtained from the Coulter Counter were converted to absolute volume using a correction factor that was determined by measuring the peak height of latex microspheres of known volume. These data were then fit to equation 1 using the Simplex algorithm (5), an efficient least-squares curve fitting routine.

Cryomicroscopy

The experiments used to measure the hydraulic conductivity at subzero temperatures were carried out on a convection cryomicroscope stage (described previously, [4]) which is used to observe cells during precisely defined thermal protocols. In all cases, a 2 μl sample of cell suspension was placed under the cover slip and all observations were made within 0.5 mm of the thermocouple junction (to reduce thermal gradients). The experiments were recorded on video tape with the addition of a time stamp for later analysis.

The stage was cooled to one of three temperatures (-2°C, -3°C or -4°C) and held at that temperature while ice formation was initiated at the edge of the cover slip. Measurements showed that the cooling power of the cryostage was sufficient to remove latent heat of fusion in less that 1.5 s (upon ice formation, the heat released from the phase change warms the stage and a short time delay occurs before the sample is returned to the set temperature). The stage was held at the constant temperature for 1 min following ice formation while cellular osmotic responses were recorded on video tape.

The volume change of the cells was measured by digitizing the video frames using a TARGA+ graphics adaptor (Truevision, Indianapolis, Indiana) and then tracing the perimeter of the cells using a mouse driven cursor. The enclosed area was automatically measured and converted to absolute area using a conversion factor derived from tracing latex microspheres of known volume. Spherical geometry was assumed to convert cross-sectional area to volume.

Thirty cells were measured at various times (cells were only traced when they were in focus) at each of the three experimental temperatures. At each measurement time, the average volume was determined as well as the standard error of the mean. The permeability parameters L_p and v_d were determined by

fitting the data to the model (eq. 1) using a weighting function based on the number of cells averaged at each time. The measurements for each cell were also fit to the equation to yield individual parameters. For error analysis, the curves generated from these parameters were averaged and the area enclosed by this average plus and minus the standard error was used to determine the extreme values L_p of which could fit within this bounding region.

Results

Figure 3.1 shows typical examples of the shrinkage curves for the V79-w cells following exposure to a 3x isotonic PBS solution (0.9 osmol/kg) at 4°C, 14° C and 22°C. The symbols represent the average volume at that time with the solid lines showing the curve generated by the parameters that were obtained by fitting the data to equation 1. Figure 3.2 shows typical examples of the shrinkage curves following exposure to a 5x isotonic PBS solution (1.4 osmol/kg) at 4°C, 14°C and 22°C. The cells shrink in response to the increased osmotic pressure until a new equilibrium value is reached. The final volume is dependent only on the osmotic pressure of the external solution while the rate of shrinkage is strongly dependent on temperature. Table 3.1 shows the values of v_d and L_p that were determined by averaging the parameters that were obtained by fitting data (such as that shown in figures 3.1 and 3.2) to equation 1. The measurements of L_p at the three different temperatures were used to determine the Arrhenius activation energy of L_p as 12.4 kCal/mol.

Table 3.1 Coulter Counter Measurements of Permeability Parameters

Temperature (°C)	v_d +/- std err	L_p +/- std err ($\mu m^3/\mu m^2 \cdot min \cdot atm$)
22	0.428 +/- 0.033	0.837 +/- 0.065
14	0.435 +/- 0.034	0.405 +/- 0.050
4	0.483 +/- 0.025	0.194 +/- 0.014

Figure 3.3 shows the shrinkage curves obtained on the cryomicroscope following nucleation at -2°C, -3°C and -4°C. The symbols show the average volume at each time for which measurements were made. The cells were not traced if they were not in focus over an interval, or the area was not changing. The solid lines show the curve generated from the parameters given by fitting the data to equation 1. The values of v_d and L_p obtained from fitting to this data are shown in table 3.2.

Table 3.2 Cryomicroscopic Measurement of Permeability Parameters

Temperature (°C)	v_d +/- std err	L_p +/- std err ($\mu m^3/\mu m^2 \cdot min \cdot atm$)
-2	0.475 +/- 0.032	0.197 +/- 0.088
-3	0.345 +/- 0.025	0.151 +/- 0.046
-4	0.425 +/- 0.017	0.139 +/- 0.036

Figure 3.4 demonstrates the error calculation for the fitted values of L_p and v_d. The shaded regions represent the mean of the volumes predicted using the parameters for each individual cell plus and minus the standard error of the mean. The solid lines show the curves with the maximum and minimum values of L_p that will fit into the area bounded by the solid curves. These values of L_p represent the range of error of the measurement.

Figure 3.5 shows an Arrhenius plot with all the values of L_p that were measured both above and below the freezing point. The dashed line indicates the activation energy that was determined from the above freezing data while the solid line incorporates all the data.

Discussion

The kinetics of cell shrinkage, as measured on the cryomicroscope in the presence of ice, were almost identical to what had been predicted by extrapolating measurements made above the freezing point. This implies that the presence of ice does not radically alter the permeability of the plasma membrane to water as has been previously suggested (7). Over the range in which it was tested, it appears that the hydraulic conductivity can be described adequately as a temperature-dependent parameter which follows the Arrhenius relation.

This was a critical issue to resolve as the use of mathematical modeling of cellular osmotic responses at low temperatures is becoming increasingly important in cryobiology. The limited success of trial and error methodologies in developing techniques for the cryopreservation of tissues and organs has led many researchers to conclude that an understanding of the biological responses at low temperatures will be necessary to advance this field. One of the principal tools now employed in this venture is the use of mathematical modeling. These models use the permeability properties of cells that are determined at above freezing temperatures and extrapolated to the very low temperatures that are used in cryopreservation. If the presence of ice had some physical effect on the cell membrane which altered its permeability properties, then the models would have been invalidated. It remains to be seen whether the data obtained with rat hepatocytes (7) represent a true non-linearity in the Arrhenius extrapolation or is simply an artifact of the measuring process.

Although the cryomicroscope data revealed the permeability parameters for individual cells, the shrinkage curve of the mean of the sample was used so that the comparison with the data obtained from the Coulter Counter would be valid. The distribution of hydraulic conductivities for individual cells most closely approximates a lognormal distribution as can be seen in figure 3.6, in which the frequency distribution of the 90 cells measured in this study is shown. This means that parameters derived for each cell cannot simply be averaged in order to predict the mean volume of the population as a function of time. Implicit in this method would be the assumption that the distribution of parameters would follow a normal distribution. It should also be noted that when using this data for simulation, the "average" cell that is used cannot be thought of as representing the population. The method of determining the parameters should always be considered in any interpretation of simulations which uses those parameters.

For the parameters which were determined at sub-freezing temperatures, the temperatures that were used are too close together and the error too large to obtain a reliable estimate of the Arrhenius activation energy. However, it is clear from figure 3.5 that there is not a significant departure in the measurement of L_p at the freezing point. If all the measurements of hydraulic conductivity are pooled to determine the activation energy, a value of 10.0 kcal/mol is obtained, which should be regarded as a better estimate than that obtained solely from the Coulter counter measurements.

Although this study has found that the presence of ice has little effect on the Arrhenius extrapolation of the hydraulic conductivity, it does not necessarily justify this extrapolation to very low temperatures (which is often the case in simulations of freeze-thaw protocols). Measurement of cell shrinkage on the cryomicroscope becomes increasingly difficult at temperatures below the freezing point due to excessive ice formation which distorts the image of the cell boundary and a high degree of cell shrinkage which usually invalidates the assumption of spherical geometry.

References

1. Dick, D. 1966. Cell Water. Butterworth, Inc., Washington, D.C. pp. 83-89.

2. Lovelock, J. 1953. The Haemolysis of Human Red Blood-Cells by Freezing and Thawing. *Biochim. et Biophys. Acta* **10**: 414-426.

3. Mazur, P. 1984. Freezing of Living Cells: Mechanisms and Implications. *Am. J. Physiol.* **247**: C125-C142.

4. Muldrew, K. and McGann, L.E. 1990. Mechanisms of Intracellular Ice Formation. *Biophys. J.* **57**:525-532.

5. Nelder, J. and Mead, R. 1965. A Simplex Method for Function Minimization. *Computer J.* **7**: 308-313.

6. Schmid-Schonbein, G., Shih, Y. and Chien, S. 1980. Morphometry of Human Leukocytes. Blood **56**: 866-875.

7. Toner, M., Harris, C., Hubel, A., Sterling, L., Dunn, J., Yarmush, M., Cravalho, E. and Tompkins, R. 1990. Water Permeability Parameters of Isolated Hepatocytes between 0 and -12°C. *Cryobiology* **27**: 632-633.

Osmotic Shrinkage of Hamster Fibroblasts
in 3x Isotonic Saline Solution
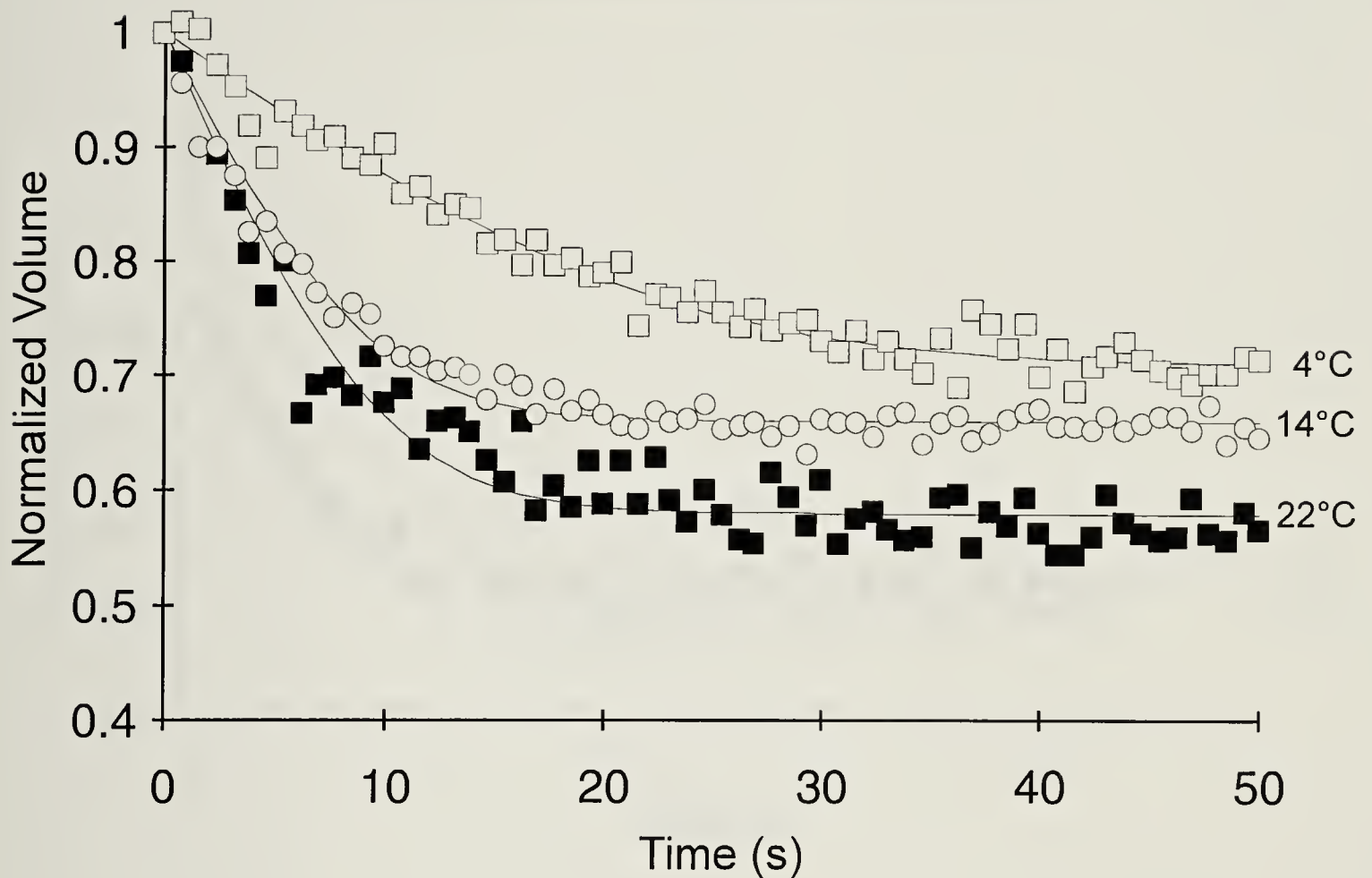
Figure 3.1.
Normalized cell volume is shown as a function of time for cells placed in 0.9 osmol/kg solutions of phosphate buffer saline. Each data point represents the average volume of between 1000 and 2000 cells, taken over a 0.8 s interval. The open squares represent one run at 4°C, the open circles represent one run at 14°C and the close squares represent one run at 22°C. The solid line represents the best fit of the data to equation 1. The initial volume is 800 μm^3.

Osmotic Shrinkage of Hamster Fibroblasts in 5x Isotonic Saline Solution
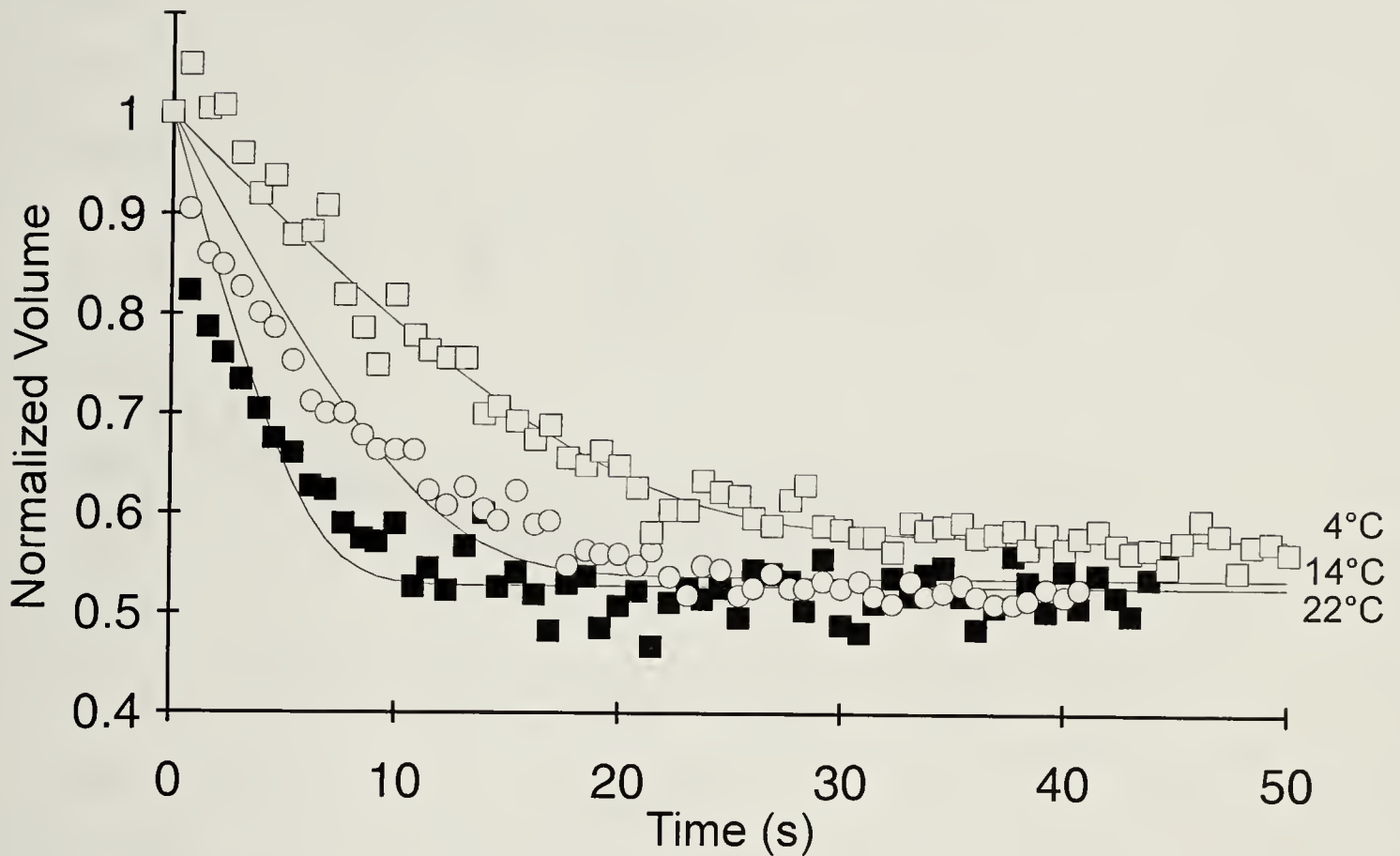
Figure 3.2.
Normalized cell volume is shown as a function of time for cells placed in 1.4 osmol/kg solutions of phosphate buffer saline. Each data point represents the average volume of between 1000 and 2000 cells, taken over a 0.8 s interval. The open squares represent one run at 4°C, the open circles represent one run at 14°C and the close squares represent one run at 22°C. The solid line represents the best fit of the data to equation 1. The initial volume is 800 μm^3.
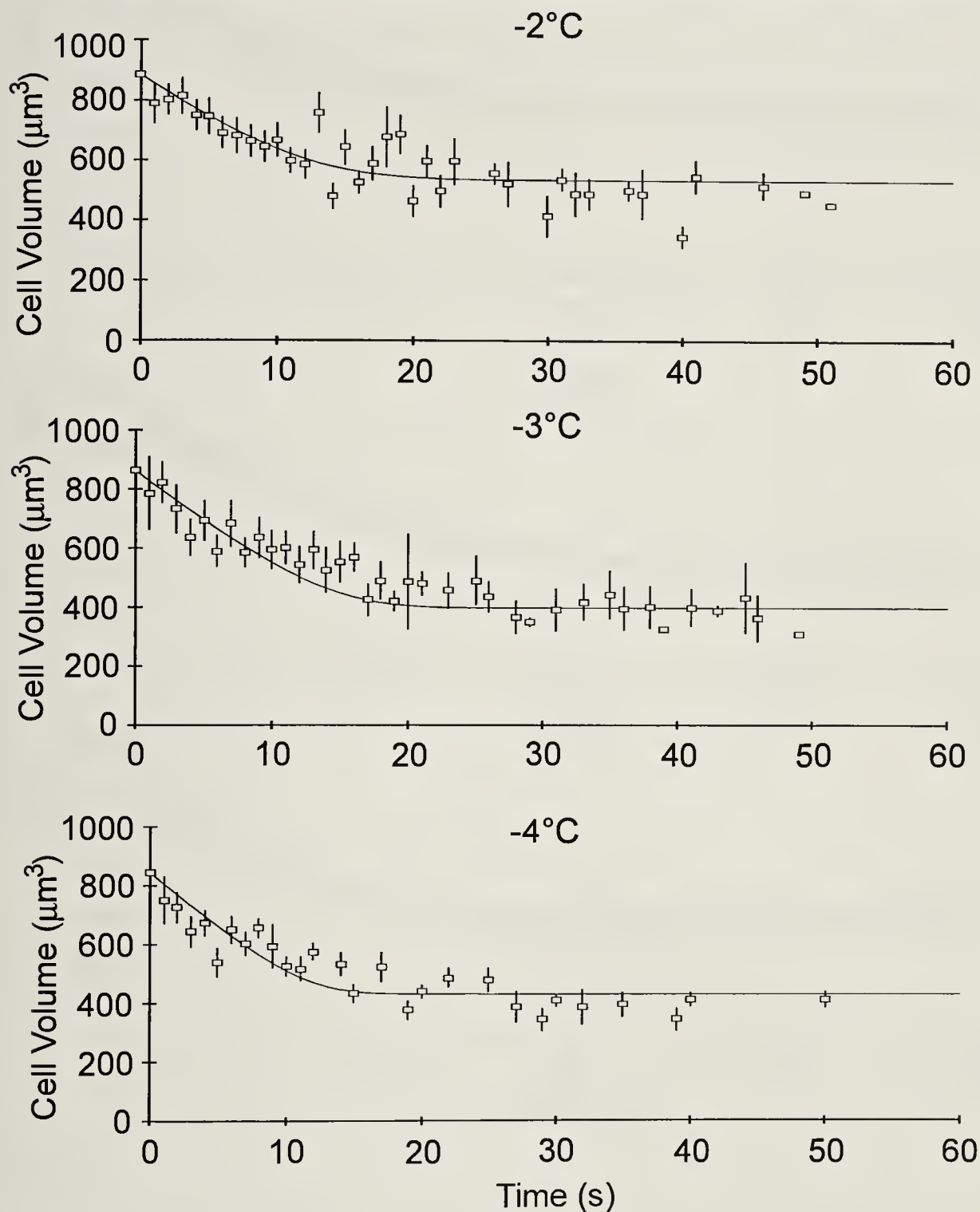
Figure 3.3.

Absolute cell volumes are shown as a function of time for hamster fibroblasts following ice nucleation on a cryomicroscope at subfreezing temperatures. The open squares represent the mean volume at that time and the bars show the standard error of the mean. The solid line represents the best fit of the data, weighted to reflect the number of cells that were measured at each time, to equation 1.

Figure 3.4.
Error analysis of the shrinkage data obtained on the cryomicroscope. The shaded regions show the area bounded by the average volume (determined by averaging the predicted volumes of each cell using the parameters for each cell that give a best fit to equation 1) plus and minus the standard error of this mean. The curves with the minimum and maximum values of L_p that can still fit inside this shaded region are superimposed as solid lines.

Arrhenius Plot of Hydraulic Conductivity Measurements on Hamster Fibroblasts
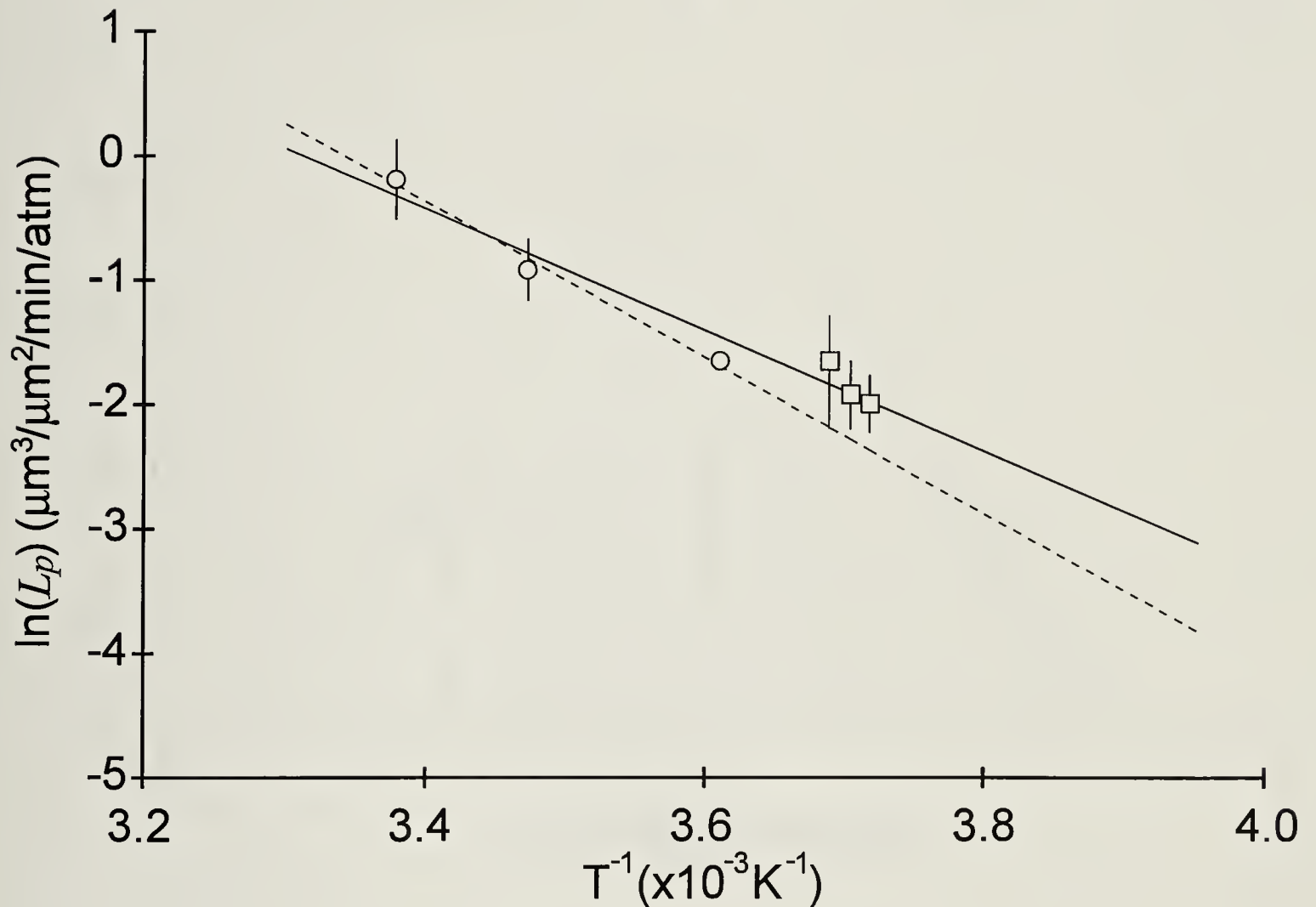
Figure 3.5.
Arrhenius plot of hydraulic conductivity measurements. The open circles represent the measurements of L_p made on the coulter counter and the open squares represent the measurements of L_p made on the crymicroscope. The dashed line shows the best fit line for the Coulter counter data (which gives an activation energy of 12.4 kcal/mol) while the solid line is fitted to all the data (giving an activation energy of 10.0 kcal/mol).

Distribution of Individually Measured Values of the Hydraulic Conductivity of Hamster Fibroblasts
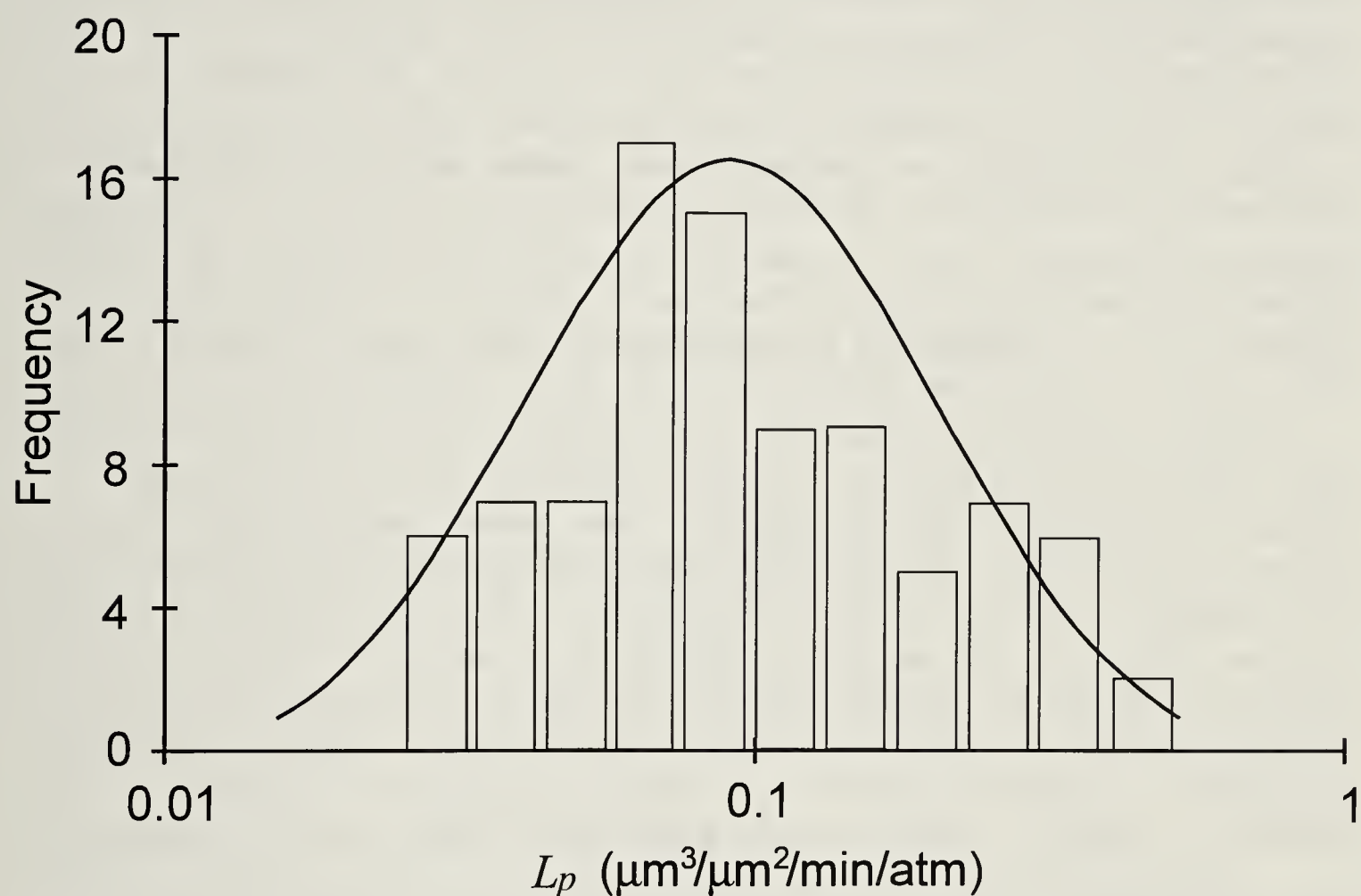
Figure 3.6.
Histogram of the distribution of hydraulic conductivities as measured for each cell. The superimposed lognormal distribution appears to correlates well with the measured distribution.

Chapter 4

Intracellular Freezing During Sinusoidal Temperature Cycling

Introduction

Recently, there has been a renewed interest in understanding the mechanisms which underlie the formation of intracellular ice and the concomitant lethal injury to biological cells which invariably accompanies this phenomenon. This new interest may be due, in part, to the search for new protocols for cryopreserving mammalian tissues and organs spawned by the lack of success in transferring techniques which were effective for cryopreserving cells in suspension. It may also be due to the search for simpler and less expensive methods for cryopreserving cells and tissues for which successful protocols already exist. Given this interest, as well as the urgent clinical need for banking complex tissues and organs for transplantation, it is essential that the underlying mechanisms of intracellular ice formation be elucidated so that the search for successful cryopreservation protocols has a firm basis upon which to expand.

Mazur (7) found that the phenomenon of intracellular ice formation (IIF) can occur when cells are frozen under conditions in which the cytoplasm cannot stay in osmotic equilibrium with the extracellular solution. When a physiological solution is frozen, the salts are excluded from ice crystals, resulting in a concentration of the solutes in the remaining unfrozen portion of the solution. The gradient in osmotic pressure that is created between the cytoplasm and the extracellular unfrozen fraction drives a water efflux from the cell (the rate of which is limited by the plasma membrane's permeability to water). If cooling is fast enough so that water cannot leave the cell quickly enough to maintain osmotic equilibrium with the extracellular unfrozen fraction, IIF may result.

In recent papers (10,11), we have proposed a novel hypothesis of the mechanism of IIF: the osmotic rupture hypothesis. This theory states that intracellular ice forms as a result of damage to the plasma membrane as opposed to the more commonly supposed notion that the injury is a result of IIF. The damage is in the form of a rupture which is caused by the frictional drag of the water flux (driven by the high osmotic pressure gradient) exceeding the tensile properties of the membrane. Once ruptured, external ice rapidly propagates through the hole in the membrane into the supercooled cytoplasm (the cytoplasm is supercooled because it is in thermal equilibrium but not in osmotic equilibrium with the extracellular solution).

In our first paper (10), we tested this conjecture along with three other hypotheses of IIF. Although the osmotic rupture hypothesis was the only one supported by all the data, Levitt's hypothesis (5) that IIF is a result of critical supercooling of the cytoplasm could only be discounted by indirect argument. This hypothesis states that cells contain efficient nucleating agents that will allow ice to spontaneously nucleate heterogeneously when the cytoplasm has reached

a state of critical supercooling. Using step cooling experiments and freezing cells at constant cooling rates, the change in supercooling is directly proportional to the change in osmotic pressure gradient. The two arguments that were used to differentiate the two are the following: 1.) The magnitude of supercooling and osmotic pressure gradients required to achieve 50% IIF in the step cooling experiments was found to be temperature dependent. This could only be rationalized for the membrane rupture hypothesis in which the increased fragility of the membrane at lower temperatures could account for the same degree of damage with comparatively less force. 2.) Extrapolation of this temperature dependence to 0°C showed that the osmotic pressure gradient that caused 50% intracellular freezing matched that required to produce 50% damage to cells exposed to high osmotic pressure gradients in the absence of ice. Recently, there have been further refinements in hypotheses which correlate IIF to the degree of supercooling (13,17).

Mazur's hypothesis (6) that IIF is a result of ice growth through aqueous pores in the plasma membrane, was discounted on the basis of an incomplete understanding of the mechanism that was actually proposed by Mazur. We argued that the geometry of growing ice crystals would be dependent on the cooling rate, which did not correlate with the incidence of IIF. Mazur's idea was that IIF will occur under conditions in which the smallest radius of stable ice crystals (given by the Kelvin equation) matches the radius of aqueous pores in the membrane. This radius will only be dependent on the temperature, thus the criticism based on cooling rates was inappropriate.

The present study was designed to further refine our understanding of the mechanisms of IIF by uncoupling the effects of supercooling from those of osmotic pressure gradients. This was accomplished using sinusoidal temperature cycling which allows the creation of large gradients in osmotic pressure in the absence of deep supercooling. By observing the onset of IIF under these conditions using a cryomicroscope, a comparison can be made with the maximum occurrences of the relevant parameters, as predicted by mathematical modeling, to see which best coincides with the incidence of IIF.

Modeling Osmotic Responses

The transport of water across cell membranes in response to osmotic pressure gradients can be modeled by a relatively simple differential equation (9). However, when freezing cells, cryoprotective compounds are invariably required to reduce injury. These compounds are usually able to permeate cell membranes, which complicates the description of mass transfer during freezing. Mazur (7,8) has made the assumption that only water movement need be described during freezing as it permeates much faster than cryoprotective solutes. Kedem and Katchalsky were the first to apply the principles of irreversible thermodynamics to this problem (4) and their equations were rewritten in a simpler form by Johnson and Wilson (3). These equations

54

describe the instantaneous water and solute fluxes generated by imbalances in the concentrations of impermeant and permeant solutes (adapted from [3]):

$$\frac{dVw}{dt} = LpART\left[\frac{iCi \cdot Vo + \sigma \cdot Sp}{Vw} - \sigma \cdot eCp - eCi\right]$$

(1)

$$\frac{dSp}{dt} = PsA\left[eCp - \frac{Sp}{Vw}\right] + (1-\sigma)\overline{Cp}\frac{dVw}{dt}$$

(2)

Lp	= Hydraulic Conductivity ($\mu m^3/\mu m^2 \cdot min \cdot atm$)
A	= Cell Surface Area (assumed to remain constant during shrinkage and equal to the surface area of a sphere with the isotonic volume) (μm^2)
R	= Universal Gas Constant ($L \cdot atm/mol \cdot K$)
T	= Absolute Temperature (K)
iCi	= Initial concentration of impermeant solute (osm/kg)
eCi	= Final concentration of impermeant solute (osm/kg)
eCp	= Extracellular concentration of permeant solute (osm/kg)
Sp	= Moles of intracellular permeant solute (mol)
Vw	= Osmotically active cell volume (μm^3)
Vo	= Initial osmotically active cell volume (μm^3)
Ps	= Permeability to permeant solute ($\mu m/min$)
σ	= Reflection coefficient
$\overline{Cp}$	= Mean concentration of permeant solute across membrane

$$= 0.5\left[eCp + \frac{Sp}{Vw}\right] \text{ (osm/kg)}$$

These equations can be combined with a mathematical description of the frozen state of a solution, such as Pegg has described (15) based on the phase diagram of the ternary solution DMSO/NaCl/H$_2$O, to give a model of the osmotic excursions that occur during a prescribed freezing and thawing protocol. Implicit in this model are the assumptions that the cytoplasm behaves as an ideal dilute solution and that the equilibrium between ice and water is maintained in the extracellular environment.

In a more recent formulation of the osmotic rupture hypothesis (11), we proposed an equation for calculating the probability of IIF as a function of the pressure exerted on the membrane due to water flux. By using measurements of IIF under controlled conditions to determine the values of the coefficients, this equation can be used to predict the probability of IIF under any other circumstances if the magnitude of the water flux is known or can be predicted from the transport equations. The equation to calculate the pressure exerted for a given magnitude of water flux is:

$$\mathcal{P} = \frac{kT}{AD_w} \cdot J_w \cdot \Delta x \tag{3}$$

$\mathcal{P}$ = Pressure on the membrane due to water flux (N/m^2)

k = Boltzmann's constant ($N \cdot m/K$)

T = Absolute temperature (K)

A = Surface area of the cell (μm^2)

D_w = Diffusion coefficient for water in the hydrophobic region of the bilayer (m^2/s)

This pressure can then be used to calculate the probability of IIF using:

$$P_{IIF} = \left[\frac{1}{1 + e^{-b(\mathcal{P} - \overline{\mathcal{P}})}} \right] \left[1 - e^{\frac{-t}{\tau}} \right] \tag{4}$$

$\overline{\mathcal{P}}$ = mean strength of the membrane (average pressure required for failure) (N/m^2)

b = parameter related to the standard deviation of the membrane strength distribution (b = 1.70991/standard deviation)

τ = time constant (s)

Materials and Methods

Cell Culture Technique

The Chinese hamster fibroblast cells (V79-w) used in this study were grown in tissue culture using minimal essential medium (Gibco, Grand Island, NY) with Hank's salts, 25 mM Hepes buffer (Gibco), 10% fetal calf serum (Gibco), 0.4% sodium bicarbonate, 100μg/ml penicillin/streptomycin and 2mM L-glutamine. The cells were maintained in exponential growth phase by harvesting from plastic tissue culture dishes ($25cm^2$; Corning Glass Works, Corning, NY) with regular trypsinization (0.25% trypsin [Gibco] for 10 min. at 37°C) and resuspension in tissue culture medium. The cells were maintained in suspension by gentle shaking at 22°C before use in the experiments.

Measurement of Permeability Parameters

The hydraulic conductivity, DMSO permeability (and their respective Arrhenius activation energies) and the DMSO reflection coefficient were determined by measuring the average volume change of the cells with time following exposure to various osmotic stresses at several temperatures and then fitting these data to equations 1 & 2. The cells were exposed to solutions of 1M, 2M and 3M DMSO in isotonic phosphate buffered saline at 23°C, 14°C and 4°C

and the resulting volume changes were recorded on a Coulter Counter. The data obtained from the Coulter Counter was converted to absolute volume using a correction factor that was determined by measuring the response due to latex microspheres of known volume (10.13 μm, Coulter Electronics, Hialeah, Florida). The volume versus time data for the cells was fit to equations 1 & 2 using the Simplex algorithm (14), an efficient least squares fitting routine which allows parameters to be optimized for any non-linear equation. Following determination of values of L_p, P_s and σ which gave the best fit at each temperature, the values of σ were averaged to determine that parameters value (the reflection coefficient is not a rate and should not have a temperature dependence). The values of L_p and P_s were then determined anew while holding σ constant.

Cryomicroscopy

Microscopic observations of cells at subzero temperatures were made using a computer-controlled convection cryomicroscope described previously (10). A 2 μl sample of cell suspension was placed on the stage under a cover slip. All observations were made within 0.5 mm of the thermocouple junction to minimize the effects of thermal gradients on the stage. Experiments were recorded on video tape with a time stamp superimposed for subsequent analysis. The formation of intracellular ice is easily observed under the light microscope, since the cytoplasm is in a supercooled state when intracellular ice forms. This results in the formation of small ice crystals and microscopic gas bubbles which scatter light. The event is characterized by a rapid transition of the cytoplasm from transparent to opaque, commonly referred to as "flashing". In the experimental conditions in which DMSO was added to the cell suspension, this was accomplished at 22°C by adding half of the DMSO, waiting for 2 min, adding the balance of DMSO (for a final concentration of 1M) and then waiting a minimum of 5 min before beginning the experiment (no cells were exposed to DMSO for more than 30 min).

The step freezing protocol consists of placing the sample of the cryostage at 22°C and then cooling at 20°C/min to a pre-determined temperature between -4°C and -8°C for the cells without cryoprotectant and -7°C to -12°C for the cells in 1M DMSO. Upon reaching this temperature in the absence of extracellular ice, nucleation was artificially nucleated by holding a copper wire cooled in liquid nitrogen just above the edge of the cover slip. Measurements indicated that the latent heat of fusion was buffered within 1.5 s of ice formation. The sample was held at the same temperature for 30 s following ice formation, at which time the experiment was terminated.

The sinusoidal thermal cycling protocol consists of cells in tissue culture medium being placed on the stage and then cooled at -20°C/min to -1°C for cells without cryoprotectant or -5°C for cells in 1M DMSO. Ice formation was initiated in the extracellular solution by holding a copper wire cooled in liquid nitrogen

above the edge of the cover slip. The stage was held at this temperature for 1 min after ice had formed to allow the cells to equilibrate osmotically. The stage was then cooled at -20°C/min to one of 3 temperatures: -5°C, -6°C or -7°C for the cells without cryoprotectant and -12°C, -13°C or -14°C for the cells in 1M DMSO. This cooling rate was "slow" for these cells meaning that they were able to remain at (or close to) osmotic equilibrium during cooling. The stage was then held at the set temperature for an additional 30 s to ensure that osmotic equilibrium had been achieved. At this point, the temperature of the stage is then cycled following a sine function at an amplitude that would allow the maximum temperature reached to be equal to the melting point of the solution(-0.5°C for no cryoprotectant, -2.7°C for 1M DMSO). Four periods of oscillation were used for each condition (15, 20, 25 & 30 s) and each condition was allowed to run for 5 complete cycles before terminating the experiment.

Results

The permeability parameters for these cells have been determined previously for the case in which no cryoprotectant is present (12). The hydraulic conductivity must be measured again with DMSO present as there is some interaction between DMSO movement and water movement. The average values of the two temperature dependent parameters, L_p are P_s are shown in table 4.1 along with the standard error of the mean. The parameters were determined using a minimum for three runs per day on each of three different days (for each experimental condition) and then taking the average.

Table 4.1 Permeability Parameters in the Presence of DMSO

Temperature (°C)	L_p (permeant) $\mu m^3/\mu m^2 \cdot min \cdot atm$	P_s $\mu m/min$
22	0.634 ± 0.050	14.8 ± 1.2
14	0.425 ± 0.038	4.28 ± 0.38
4	0.188 ± 0.006	1.00 ± 0.03
E_a (kcal/mol)	9.14	20.1

E_a = Arrhenius activation energy

Summary of V79-w permeability parameters

V_o = 800 μm^3

V_d = 359 μm^3 (0.449 · V_o) (12)

T_g = 273 K (0°C)

L_{pg} = 0.183 μm^3/μm^2·min·atm (impermeant) E_a = 10.0 kcal/mol (12)

L_{pg} = 0.145 μm^3/μm^2·min·atm (permeant) E_a = 9.14 kcal/mol

P_{sg} = 0.512 μm/min E_a = 20.1 kcal/mol

σ = 0.9

Reference values (denoted by a subscripted g) are determined from the regression line of an Arrhenius plot.

Figure 4.1 shows the proportion of cells which were observed to "flash" (indicating the presence of IIF) in the step freezing experiment on the cryomicroscope. The cells without cryoprotectant begin to form IIF upon nucleation at -5°C and the incidence rises sharply so that virtually all the cells form IIF when the solution is nucleated below -8°C. The cells in 1M DMSO begin to form IIF when nucleated at -6°C and all the cells are freezing internally when the solution is nucleated below -12°C. This data was combined with the predicted water flux that would occur after nucleation at these temperatures (by inserting the permeability parameters into equations 1 & 2, the water flux can be determined) and fit to equation 4 to determine the parameters which describe IIF (although independent measurement of these parameters should be possible, they are treated here as adjustable parameters). This process gave values of 93 N/m^2 for the value of $\overline{\mathcal{P}}$ at the reference temperature of 0°C (E_a = 35 kcal/mol), 0.075 for the value of b at the same reference temperature (E_a = -24 kcal/mol) and 0.06 s for τ (E_a = -24 kcal/mol). The solid lines show the incidence of IIF that would be predicted from these parameters for the experimental conditions.

The total incidence (after 5 complete cycles) of IIF in the sinusoidal cycling experiments without cryoprotectant is shown in figure 4.2. The fraction of cells with IIF increases with decreasing mean temperature (and increasing amplitude) but is relatively independent of the period of oscillation over the range tested. The fraction of cells flashing in each cycle (the experiments were continued for 5 complete cycles) is shown by the shapes in figure 4.3. In all cases, if a cell was observed to flash in one cycle, it also flashed in each subsequent cycle although the temperature at which this subsequent "flash" occurred increased with the number of cycles that elapsed. In many cases, the advancing ice front simple propagated into the cytoplasm unobstructed. For the situation in which a subsequent "flash" occurred, there would have to have been a resealing event following the melting of intracellular ice. It can be seen from the figure that the incidence of IIF tapers off toward the fifth cycle. The temperature at which each cell flashes is averaged (only the first flashing event is recorded, the temperature of flashing on subsequent cycles is ignored) and shown in figure 4.4. Under these conditions, IIF occurs at very high subzero temperatures. Because each temperature is seen twice in each cycle, it is

important to establish the point in the cycle at which IIF occurs. Figure 4.5 shows that IIF occurs at, or slightly in advance of, 180° in the temperature cycle, independent of the mean temperature and the period of oscillation.

For the cells suspended in 1M DMSO, the incidence of IIF is shown in figure 4.6. The pattern is similar to that in figure 4.3 (no DMSO) except for the slight difference between this case and that without DMSO in that the largest number of IIF events occur in the first cycle with DMSO while without DMSO they occur in the second cycle. The phase angle at which IIF occurs with 1M DMSO is shown in figure 4.7. It can be seen that the formation of intracellular ice is somewhat retarded by the presence of DMSO. It occurs mainly between 200 and 240° in the cycle although it appears to be independent of mean temperature and period of oscillation as was the case for cells without cryoprotectant.

Discussion

The values for the permeability parameters obtained from the Coulter Counter data can be used with a description of the composition of the solutions used in these experiments to predict the magnitude of the water flux at each point in the sinusoidal temperature cycle. The phase diagram for sodium chloride and water has been described (2) and Pegg has generated an equation to calculate the composition of solutions of DMSO, sodium chloride and water at a given sub-freezing temperature (15). The solute concentrations in solutions without DMSO have been calculated as *osmolalities* while those in solutions with DMSO have been calculated as *osmolarities* as has been suggested by Pegg (16). The results of these simulations can be seen in figure 4.8 for the solutions without DMSO and in figure 4.9 with 1M DMSO. In both cases, the peak water flux occurs at 180° in the cycle. The water flux values can be inserted into equation 3 to get the probability of IIF as a function of position in the cycle (for water influx - which are treated as negative here - the water flux is rectified to give it a positive value so that the signs come out properly). When this is done for the case with no DMSO, the predicted incidence of IIF is shown as solid lines in figure 4.3 for each of the mean temperatures which were experimentally tested. The agreement with the measured incidence of IIF is excellent. The probability of IIF can also be used to determine the point in the cycle at which 50% of the cells which are predicted to flash will have already formed IIF. Figure 4.10 shows the predicted incidence of IIF for the case in which the mean temperature is -6°C. It can be seen that the formation of IIF is expected to occur over a narrow range from 160° to 200° with the mean occuring at 185°. If the equation is applied to the other two conditions, then the mean values come out to 176° for a mean temperature of -7°C and 185° for a mean temperature of -5° C, in agreement with the measured values shown in figure 4.5. When the predicted water flux for the case with 1M DMSO is inserted into equations 3 & 4, then the incidence of IIF is expected to be >96% for all the cases tested. It is not

known where the source of this disagreement lies, however, several assumptions have gone into the simulations of the cellular behavior in the solution containing DMSO which do not have experimental justification. If, for instance, the activation energy of the hydraulic conductivity is increased by a factor of 2, then the calculated water flux gives the same prediction of IIF as was observed as shown for the case in which the mean temperature is 13°C in figure 4.10. These curves can then be used to find the average point in the cycle at which IIF should occur: 220°, which does agree with the observations in figure 4.7.

Thus the osmotic rupture hypothesis is supported qualitatively for the experiment with 1M DMSO but not quantitatively. This may indicate a serious flaw in the hypothesis or it may simply be a reflection of the assumptions made in predicting the water flux that occurs during freezing in a solution of water, DMSO and NaCl. The solution is expected to behave as an ideal dilute solution which may be a gross simplification at low temperatures where most of the water is removed to form ice. So far, there has been no experimental confirmation of the accuracy of the equations used here to model water and solute flux (equations 1 & 2) in the frozen environment (especially at the relatively high temperatures used in this study where solute flux can be considerable). Therefore, it cannot yet be determined whether the osmotic rupture hypothesis or the description of osmotic processes during freezing has been invalidated.

The data presented here do provide an opportunity to critically evaluate Levitt's critical supercooling hypthosis. As can be seen from figure 4.4, IIF occurs under some conditions at supercoolings of less than 3°C. The argument of spontaneous heterogeneous nucleation is very weak in light of this as it is unlikely that there are nucleating agents (other than crystals of ice itself) which could initiate ice formation on a time scale of less than a few seconds at these high temperatures. Since only the osmotic rupture hypothesis and Mazur's Kelvin hypothesis (6) invoke ice as the agent of nucleation, these must be considered as the most likely candidates to explain this result.

Recently, Toner et al. have proposed a novel mechanism of IIF which holds that the plasma membrane interacts with extracellular ice to form a surface which catalyzes intracellular heterogeneous nucleation (17). Again, this hypothesis seems unlikely since it must be supposed that this nucleation site resembles almost exactly an ice crystal so that it can cause nucleation at such low supercoolings. Also, this hypothesis does not explain the effect that is observed in which a cell, once undergoing IIF, always undergoes IIF in each subsequent cycle in the sinusoidal thermal protocols. Indeed, the point in the cycle at which these repeat IIF events occurs seems to advance with repeated cycles and, in some cases, there is an obvious hole in the membrane through which ice passes by the fifth cycle.

References

1. Chalmers, B. 1959. How Water Freezes. *Sci. American* **200**(2): 114-122.

2. Cocks, F. and Brower, W. 1974. Phase Diagram Relationships in Cryobiology. *Cryobiology* **11**: 340-358.

3. Johnson, J. and Wilson, T. 1967. Osmotic Volume Changes Induced by a Permaeble Solute. *J. Theoret. Biol.* **17**: 304-311.

4. Kedem, O. and Katchalsky, A. 1958. Thermodynamic Analysis of the Permeability of Biological Membranes to Non-Electrolytes. *Biochim. et Biophys. Acta* **27**: 229-246.

5. Levitt, J. and Scarth, G. 1936. Frost Hardening Studies with Living Cells. II. Permeability in Relation to Frost Resistance and the Seasonal Cycle. *Can. J. Res. Sect. C Bot. Sci.* **14**: 285-305.

6. Mazur, P. 1960. Physical Factors Implicated in the Death of Micro-organisms at Subzero Temperatures. *Ann. NY Acad. Sci.* **85**: 610-629.

7. Mazur, P. 1963. Kinetics of Water Loss from Cells at Subzero Temperatures and the Likelihood of Intracellular Freezing. *J. Gen. Physiol.* **47**: 347-369.

8. Mazur, P., Rall, W. and Leibo, S. 1984. Kinetics of Water Loss and the Likelihood of Intracellular Freezing in Mouse Ova: Influence of teh Method of Calculating the Temperature Dependence of Water Permeability. *Cell Biophys.* **6**: 197-214.

9. McGann, L., Stevenson, M., Muldrew, K. and Schachar, N. 1988. Kinetics of Osmotic Water Movement in Chondrocytes Isolated from Articular Cartilage and Applications to Cryopreservation. *J. Orthop. Res.* **6**: 109-115.

10. Muldrew, K. and McGann, L.E. 1990. Mechanisms of Intracellular Ice Formation. *Biophys. J.* **57**: 525-532.

11. Muldrew, K. and McGann, L.E. 1993. The Osmotic Rupture Hypothesis of Intracellular Freezing Injury. Submitted to the Biophysical Journal.

12. Chapter 3 of this thesis.

13. Pitt, R. and Steponkus, P. 1989. Quantitative Analysis of the Probability of Intracellular Ice Formation During Freezing of Isolated Protoplasts. *Cryobiology* **26**: 44-63.

14. Nelder, J. and Mead, R. 1965. A Simplex Method for Function Minimization. *Computer J.* **7**: 308-313.

15. Pegg, D. 1986. Equations for Obtaining Melting Points and Eutectic Temperatures for the Ternary System Dimethyl Sulphoxide/Sodium Chloride/Water. *Cryo-Letters* **7**: 387-394.

16. Pegg, D. 1984. Red Cell Volume in Glycerol/Sodium Chloride/Water Mixtures. *Cryobiology* **21**: 234-239.

17. Toner, M., Karel, M. and Cravalho, E. 1990. Thermodynamics and Kinetics of Intracellular Ice Formation During Freezing of Biological Cells. *J. Appl. Phys.* **67**(3): 1582-1593.

Intracellular Ice Formation in Hamster Fibroblasts
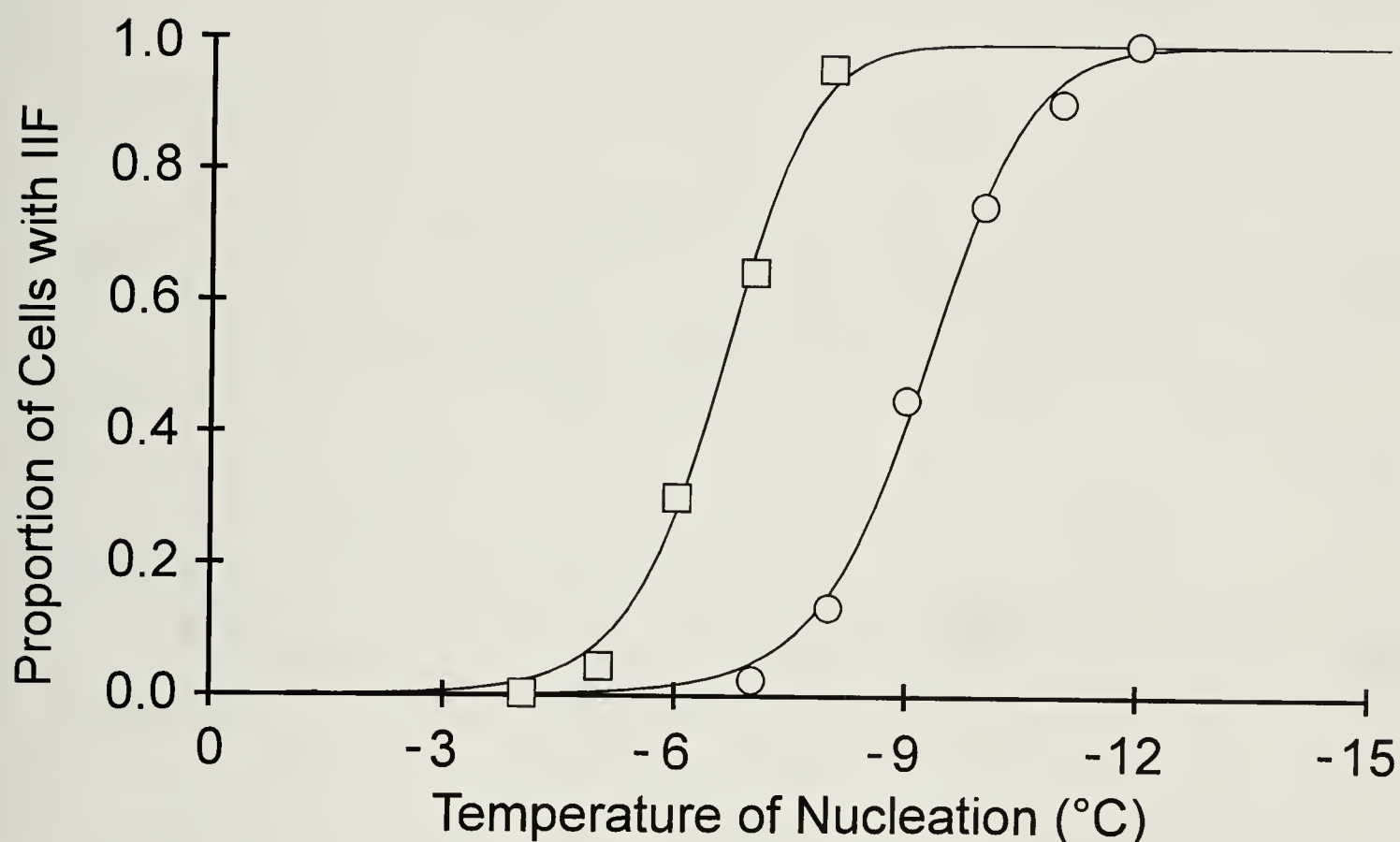
Figure 4.1.
Intracellular ice formation in hamster fibroblasts upon ice nucleation at supercooled temperatures (a minimum of 100 cells are used for each data point). The shapes represent the proportion of cells undergoing IIF following ice nucleation at the temperatures indicated on the abscissa. The open squares are for cells suspended in isotonic tissue culture medium, the open circles for cells suspended in isotonic medium with 1M DMSO added. The solid lines represent the best fit of equation 3 to this data, yielding the following values for the coefficients at 0°C: $\overline{P}$ = 93N/m^2 (E_a = 35 kcal/mol), b = 0.075 (E_a = -24 kcal/mol) and τ = 0.06 s (E_a = -24 kcal/mol).

Total Incidence of IIF as a Function of Oscillation Period With No Cryoprotectant

Figure 4.2.

The incidence of IIF in all the sinusoidal protocols tested for cells suspended in isotonic media without cryoprotectant is shown. The closed squares represent cycling with a mean temperature of -5°C and an amplitude of 9°C, the open circles represent cycling with a mean temperature of -6°C and an amplitude of 11 °C and the open squares represent cycling with a mean temperature of -7°C and an amplitude of 13°C.
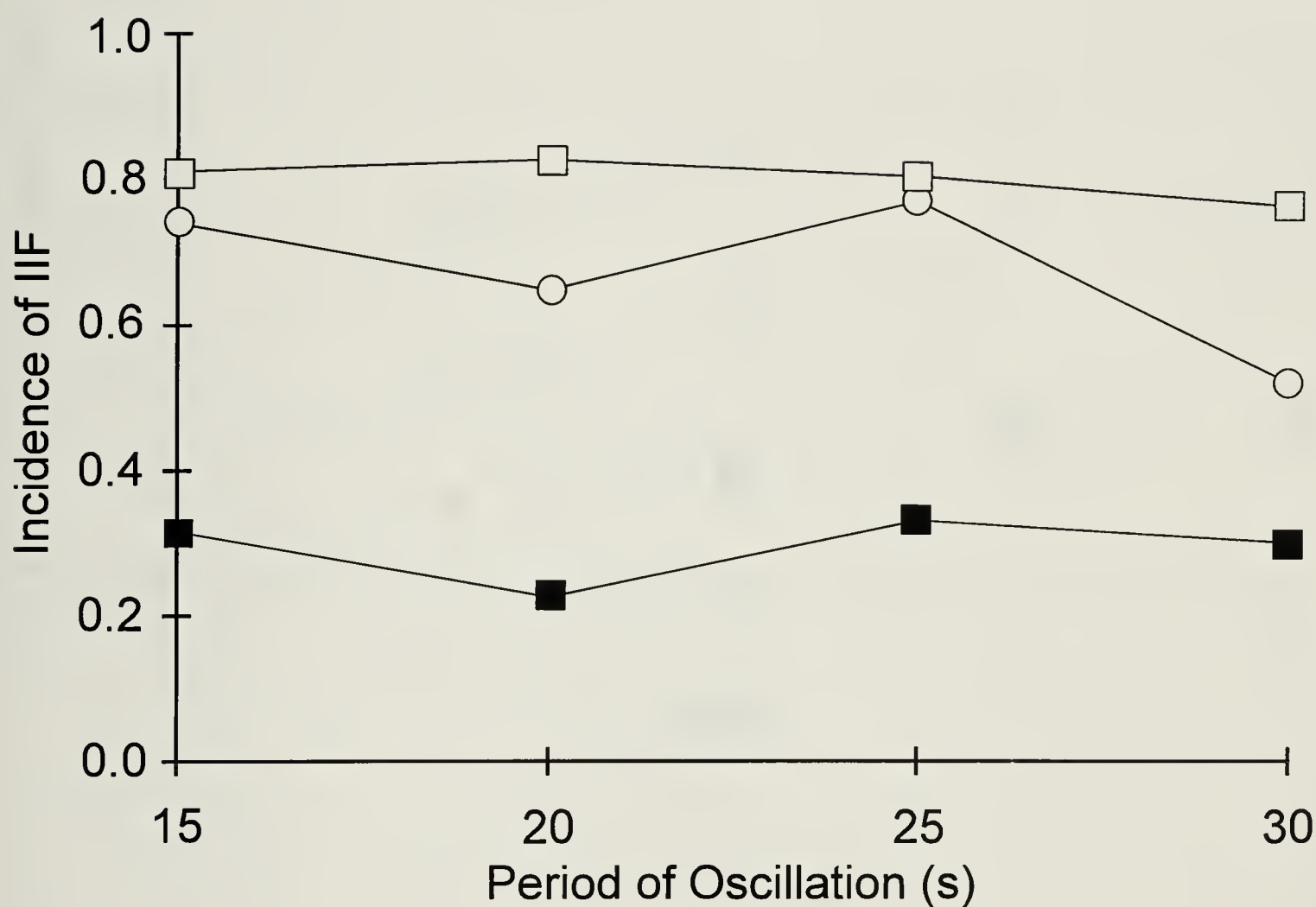
Incidence of IIF as a Function of Oscillation Cycle with no Cryoprotectant
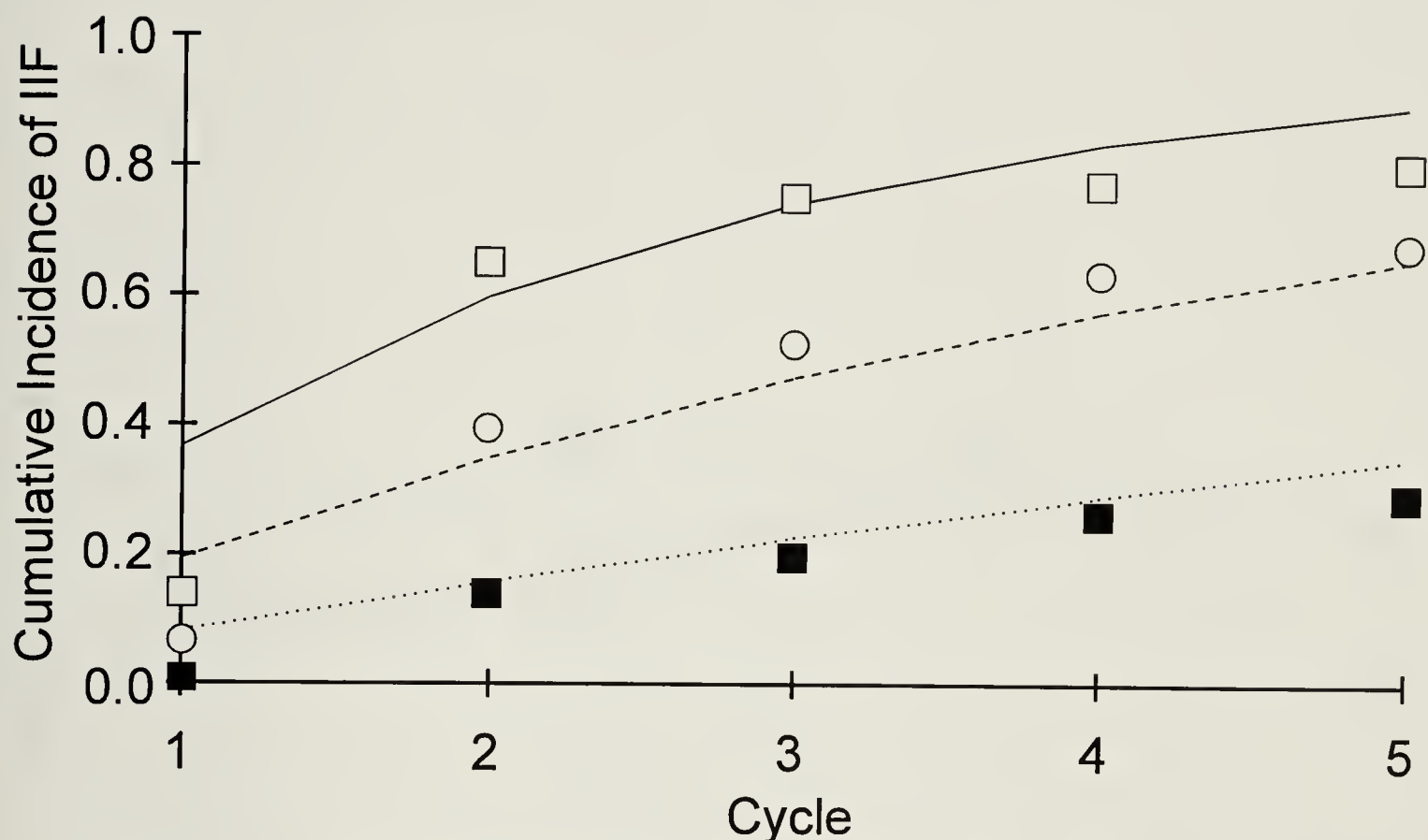
Figure 4.3.
The cumulative fraction of cells undergoing IIF is shown as a function of the number of complete sinusoidal thermal cycles which have occurred. The closed squares represent cycling with a mean temperature of -5°C and an amplitude of 9°C and the dotted line is the predicted fraction of cells undergoing IIF (under the same conditions) using the parameters calculated from figure 4.1 in equation 3. The open circles represent cycling with a mean temperature of -6°C and an amplitude of 11°C and the dashed line is the predicted incidence of IIF for this regime. The open squares represent fraction of cells undergoing IIF for the condition in which the mean temperature is -7°C and the amplitude is 13°C and the solid line is the predicted incidence of IIF for this protocol.

Average Temperature of IIF
With No Cryoprotectant

Figure 4.4.

The average temperature at which IIF occurs is shown as a function of the period of oscillation for the cycling protocols in which the cells were suspended in isotonic media without cryoprotectant. The closed squares represent the protocol in which the mean temperature is -5°C and the amplitude is 9°C, the open circles represent the protocol in which the mean temperature is -6° and the amplitude is 11°C and the open squares represent the protocol in which the mean temperature is -7°C and the amplitude is 13°C. The bars represent the standard error of the mean (they are not shown for the cases in which they are smaller than the symbols).

Average Phase Angle at which IIF occurs with no Cryoprotectant

Figure 4.5.

The average phase angle of the sinusoidal cycle at which IIF occurs is shown as a function of the period of oscillation for the cycling protocols in which the cells were suspended in isotonic media without cryoprotectant. The closed squares represent the protocol in which the mean temperature is -5°C and the amplitude is 9°C, the open circles represent the protocol in which the mean temperature is -6° and the amplitude is 11°C and the open squares represent the protocol in which the mean temperature is -7°C and the amplitude is 13°C. The bars represent the standard error of the mean (they are not shown for the cases in which they are smaller than the symbols).

Incidence of IIF as a Function of
Oscillation Cycle with 1M DMSO
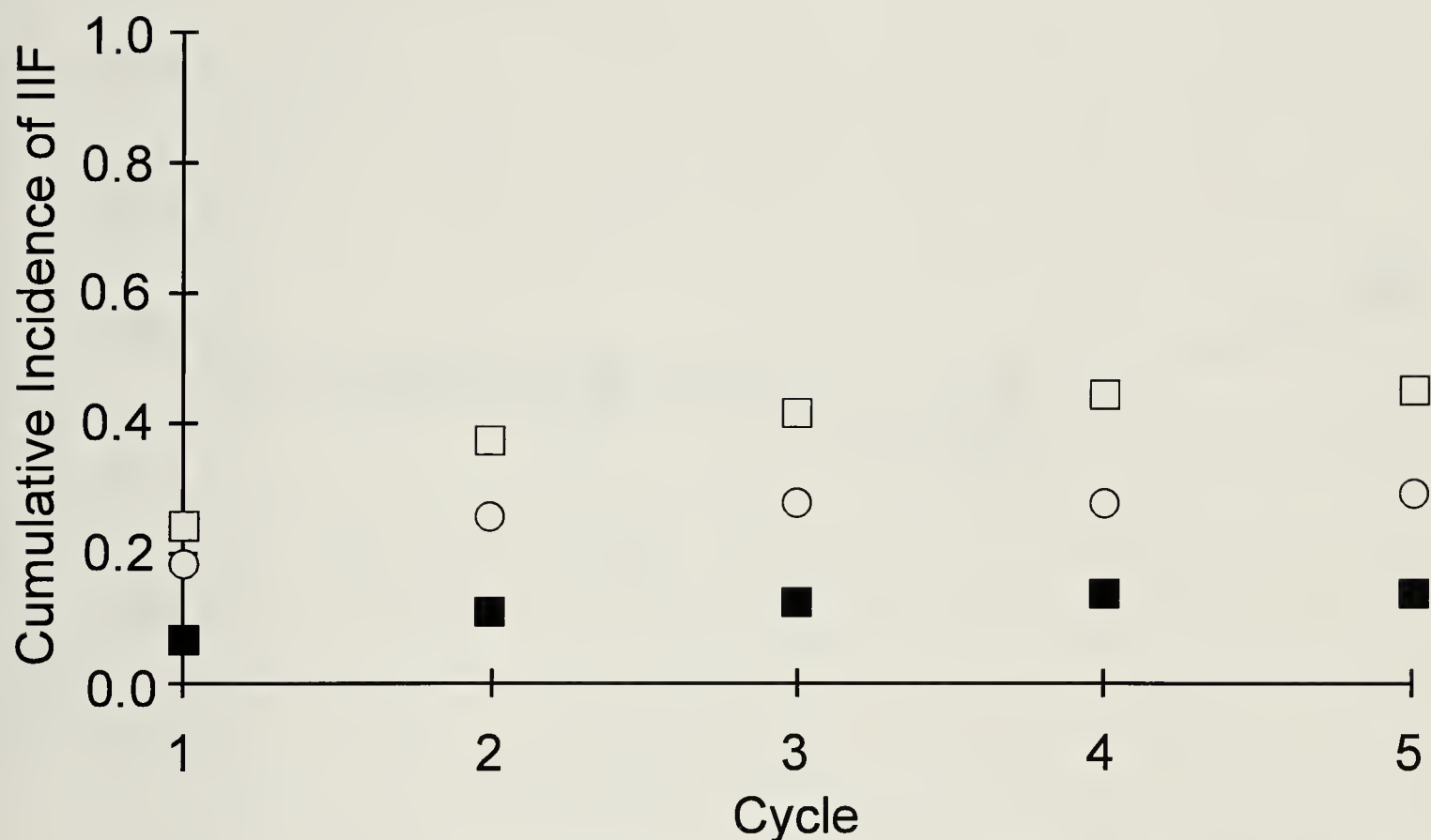
Figure 4.6.
The cumulative fraction of cells undergoing IIF is shown as a function of the number of complete sinusoidal thermal cycles which have occurred. The closed squares represent cycling with a mean temperature of -12°C and an amplitude of 17°C. The open circles represent cycling with a mean temperature of -13°C and an amplitude of 19°C. The open squares represent fraction of cells undergoing IIF for the condition in which the mean temperature is -14°C and the amplitude is 21°C.

Average Phase Angle at which IIF occurs with 1M DMSO
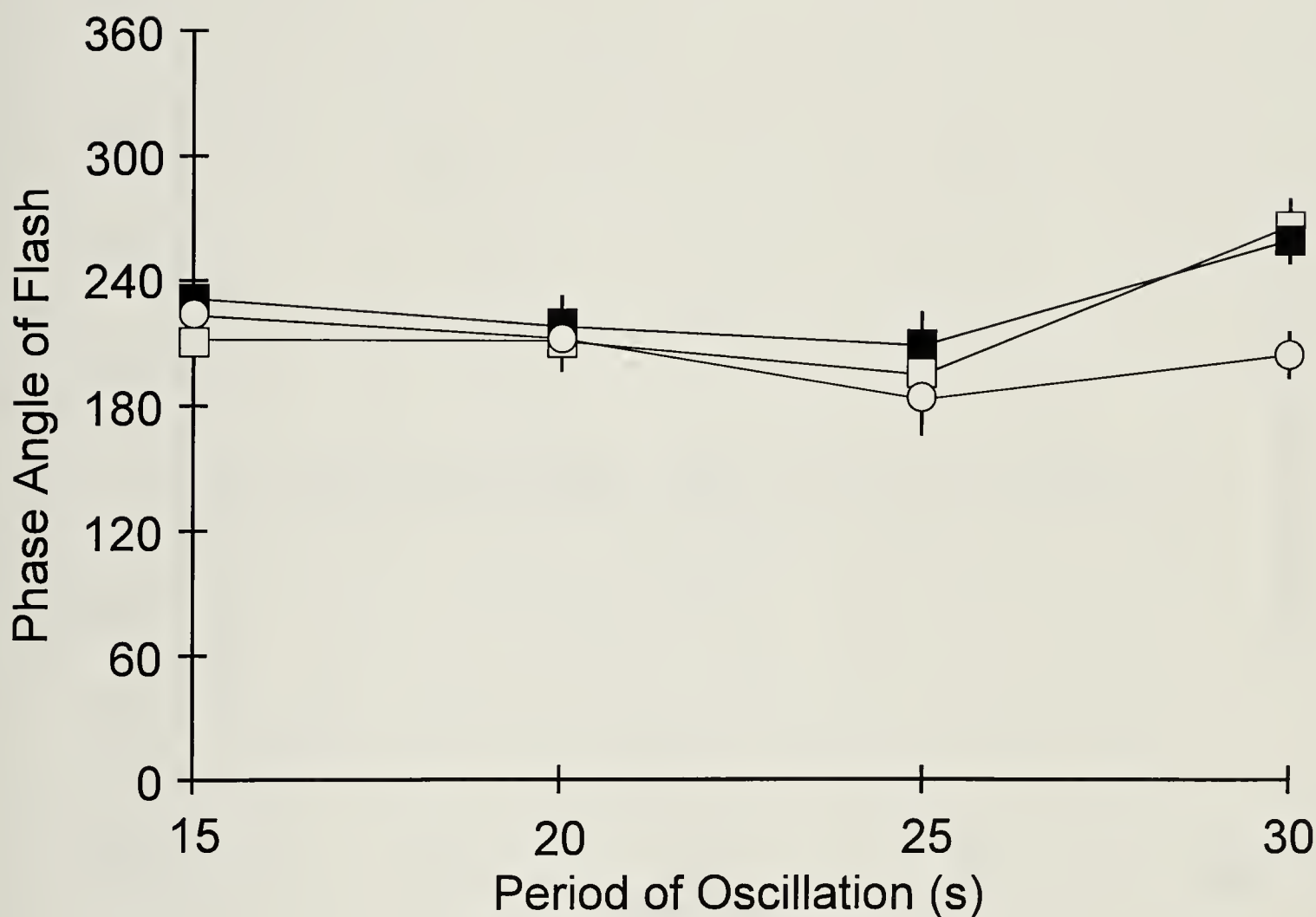
Figure 4.7.

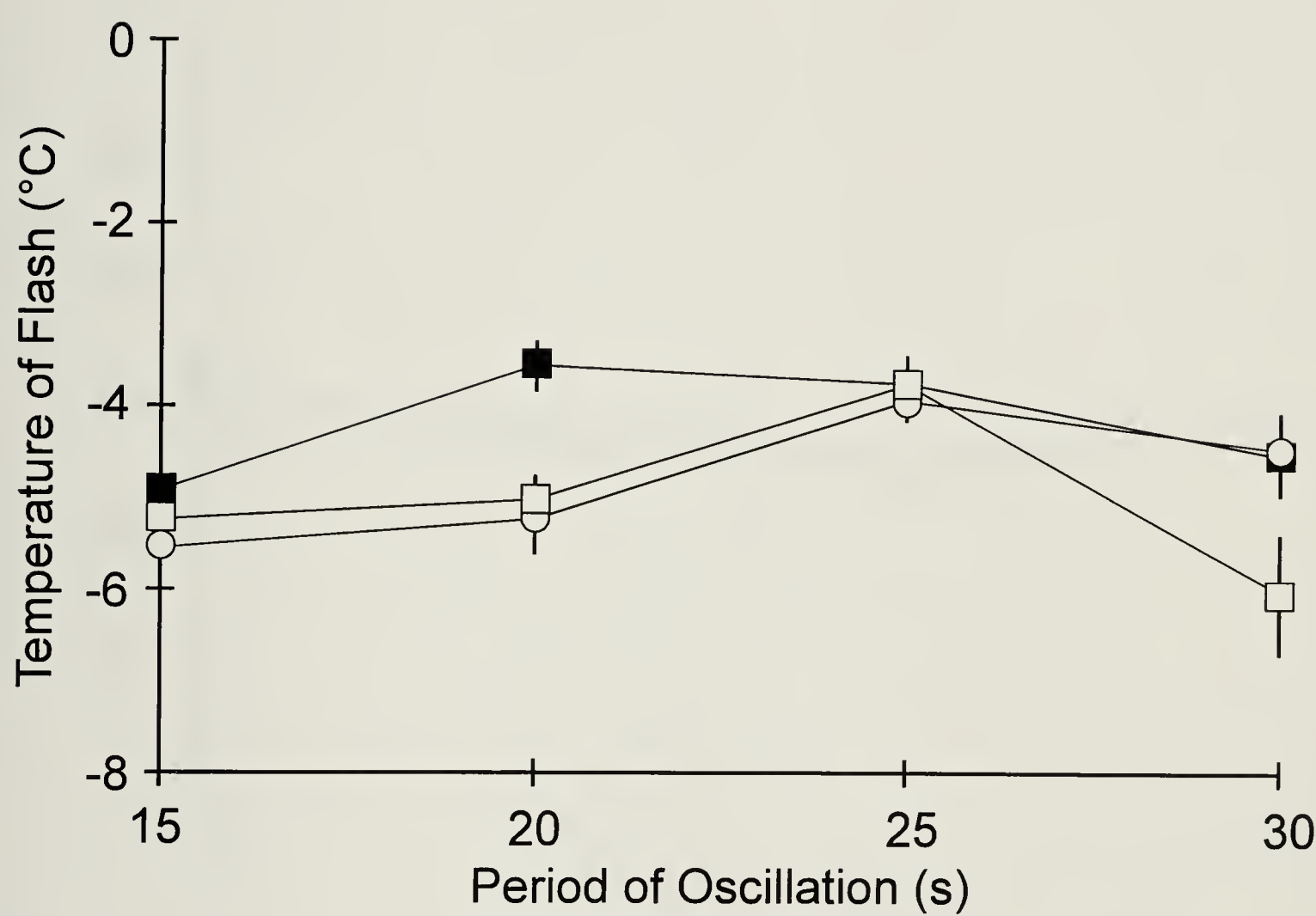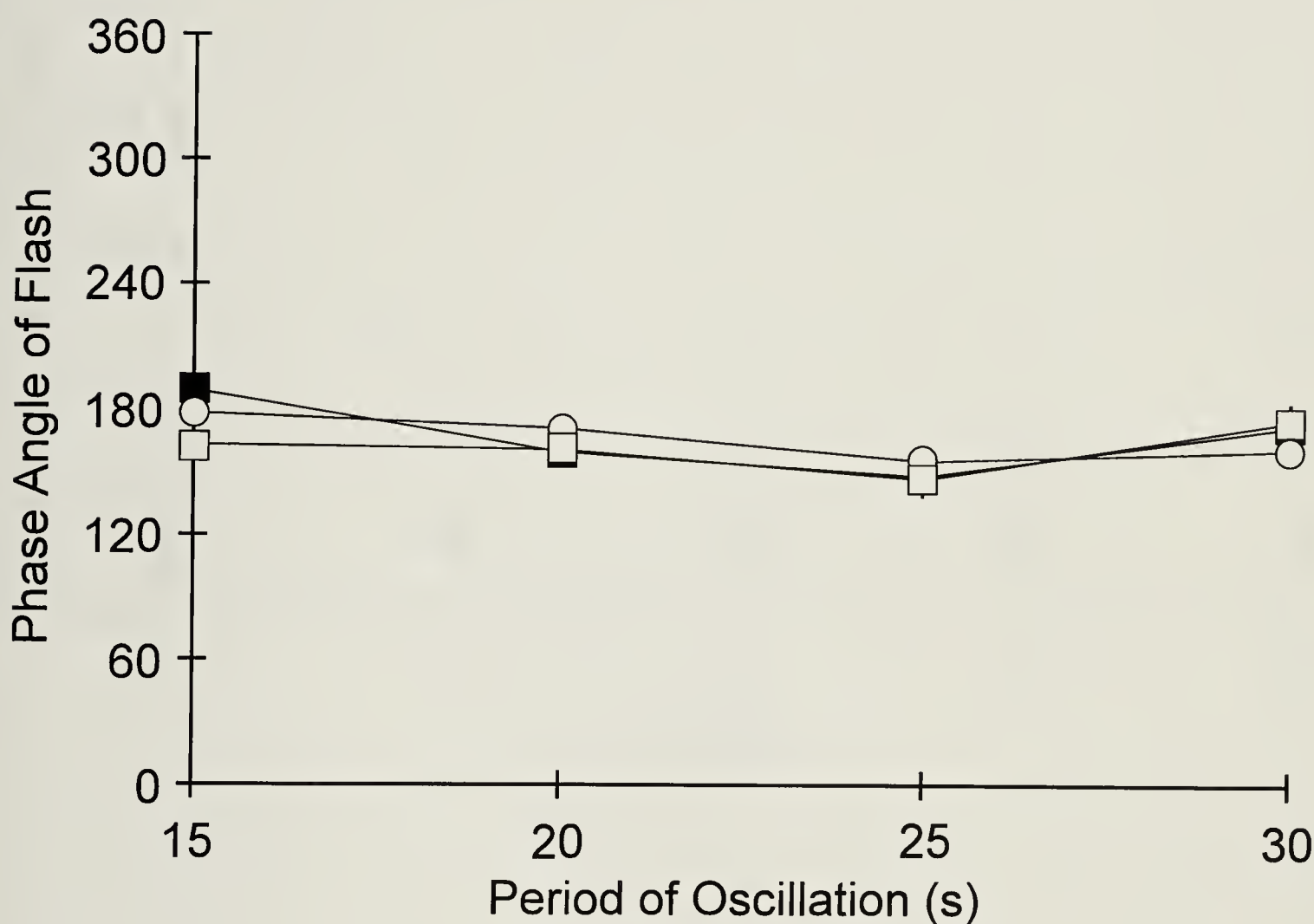The average phase angle of the sinusoidal cycle at which IIF occurs is shown as a function of the period of oscillation for the cycling protocols in which the cells were suspended in isotonic media with 1M DMSO. The closed squares represent the protocol in which the mean temperature is -12°C and the amplitude is 17°C, the open circles represent the protocol in which the mean temperature is -13°C and the amplitude is 19°C and the open squares represent the protocol in which the mean temperature is -14°C and the amplitude is 21°C. The bars represent the standard error of the mean (they are not shown for the cases in which they are smaller than the symbols).

Water Flux During Sinusoidal Thermal Cycling With No Cryoprotectant
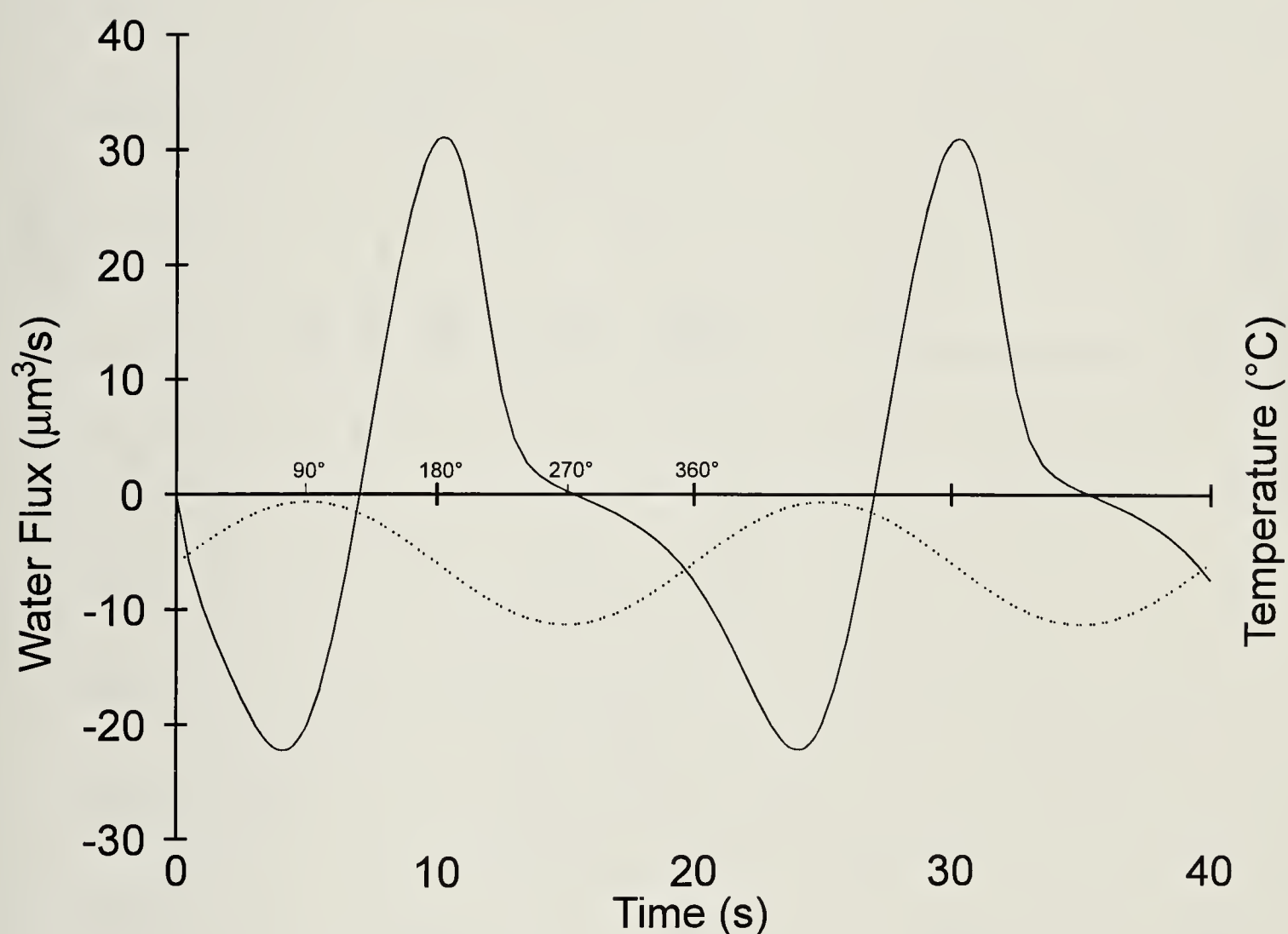
Figure 4.8.
The water flux that occurs during sinusoidal thermal cycling (two complete cycles are shown) for cells in isotonic media without cryoprotectant, as predicted by equation 1, is shown by the solid line. The dotted line indicates the temperature (the ordinate scale is the same for both plots). The specific simulation shown has a mean temperature of -6°C, a period of 20 s and an amplitude of 11°C.

Water Flux During Sinusoidal Thermal Cycling With 1M DMSO
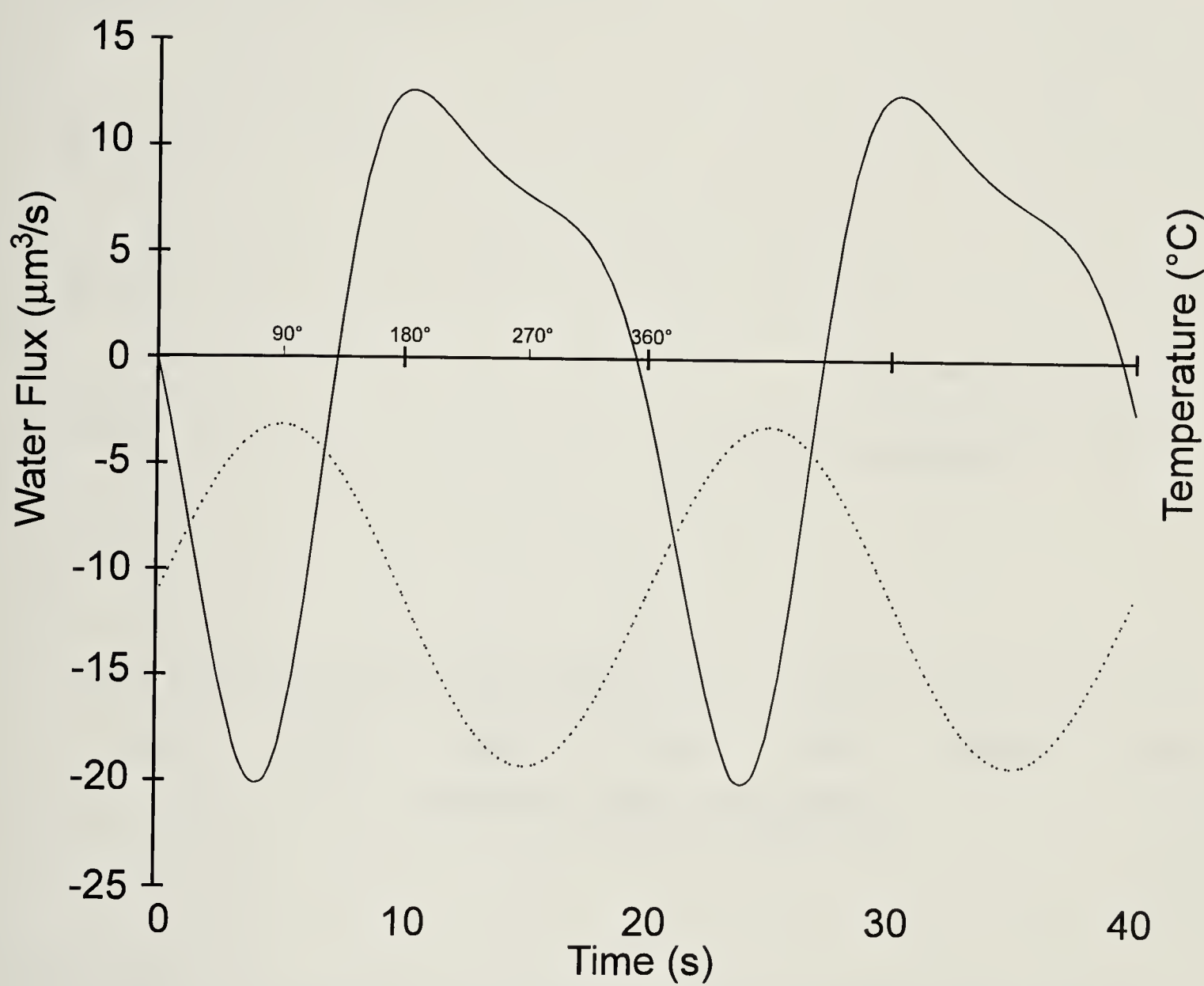
Figure 4.9.

The water flux that occurs during sinusoidal thermal cycling (two complete cycles are shown) for cells in isotonic media with 1M DMSO, as predicted by equations 1 & 2, is shown by the solid line. The dotted line indicates the temperature (the ordinate scale is the same for both plots). The specific simulation shown has a mean temperature of -13°C, a period of 20 s and an amplitude of 19°C.

Probability of IIF During Sinusoidal Thermal Cycling
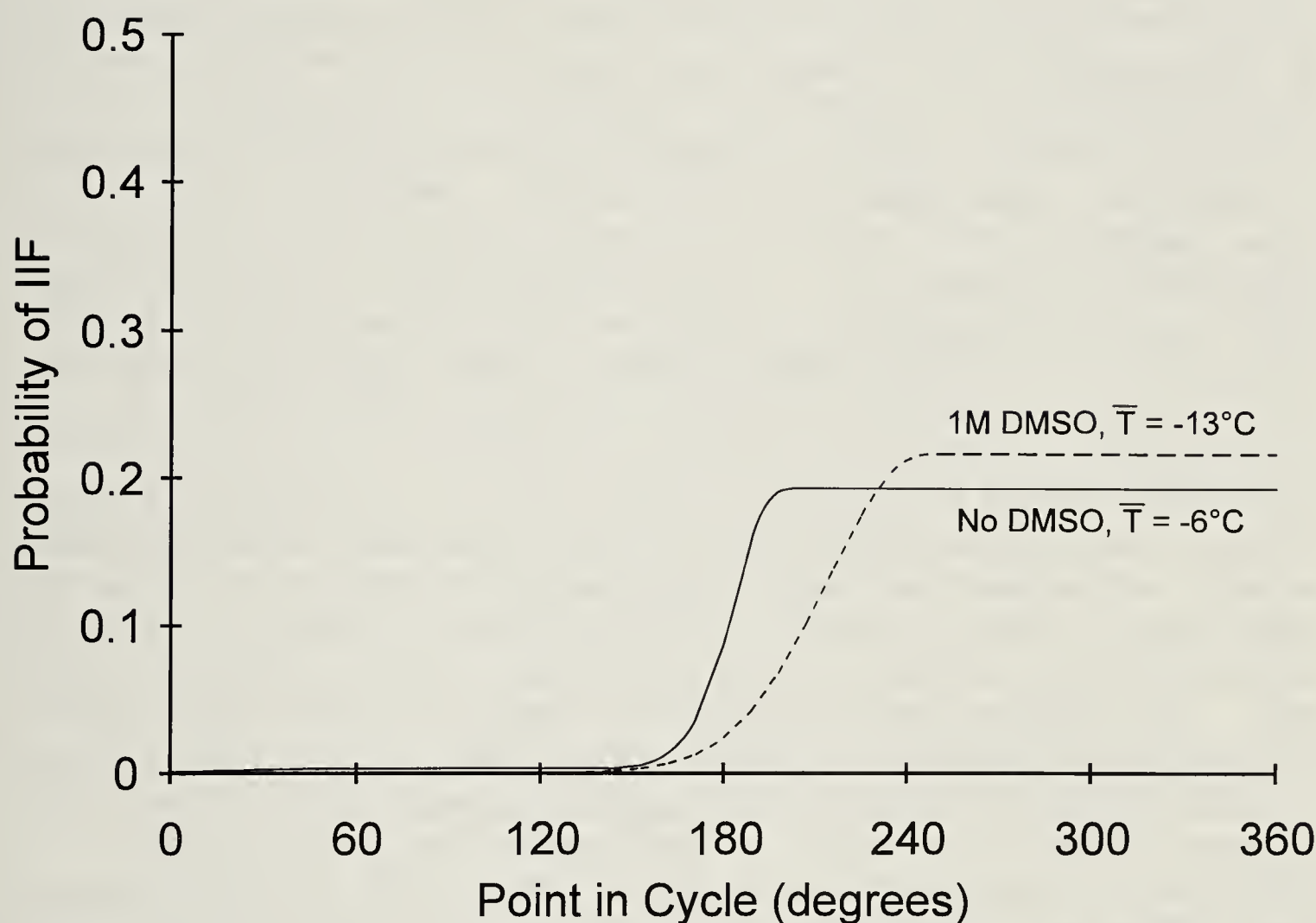
Figure 4.10.
The solution to equation 3 for sinusoidal thermal cycling with a period of oscillation of 20 s. The solid line shows the probability of IIF for one cycle with a mean temperature of -6°C and an amplitude of 11°C using equation 1 to calculate the water flux. The dashed line shows the probability of IIF for one cycle with a mean temperature of -13°C and an amplitude of 19°C. The water flux was calculated from equations 1 & 2; however, the activation energy of the hydraulic conductivity was increased to 17.5 kcal/mol to bring the predicted incidence of IIF in line with the observed incidence (this modification predicts accurately the magnitude of IIF for the three mean temperatures tested with 1M DMSO).

Chapter 5

Permeability and Cryobiology of Bovine Chondrocytes

Introduction

While the use of empirical approaches for the cryopreservation of cell suspensions has been the most useful method in the past, this approach has not met with the same level of success when applied to the cryopreservation of tissue and organ systems. This is largely due to the lack of understanding of the responses of individual cells at low temperatures. Without definite knowledge of how the many interacting variables that are present when attempting to cryopreserve organized tissues relate to the survival of the constituent cells, there is little hope of finding optimal solutions. The correlation of mathematical modeling of the physical environment with the physiological responses which occur during freezing and thawing, initiated by Mazur (6) in 1963, is emerging as an essential tool which can provide information on cellular behavior at low temperatures as well as providing a mechanism for the practical optimization of protocols for routine use. In this study, an extension of Mazur's model (6,8) describing osmotic responses of cells has been combined with phase diagram information of solutions of cryobiological interest to describe the physical parameters of various experimental protocols. Since the advent of microscope stages with precise thermal control (2), it has been possible to test theoretical models against direct experimental observations during freezing (3,7). This approach will be applied here, thereby allowing a correlation of physiological responses with physico-chemical changes during prescribed freezing protocols.

During freezing and thawing, cells are subjected to osmotic pressure gradients caused by the separation of pure water from solution when ice forms. Virtually all successful cryopreservation protocols also rely on the addition (and subsequent removal) of cryoprotective compounds, thus providing further osmotic stresses to the cell. In response to osmotic pressure gradients, cells will shrink or swell, with the rate being determined by several factors: the permeability of the membrane to water or to any permeant solutes which might be present, the osmotic pressure gradient, gradients in concentration of permeant solutes and the temperature. Although the microscopic structure of the plasma membrane is not yet known well enough to predict permeability from first principles, mathematical models which employ the above mentioned factors have been derived from the theory of irreversible thermodynamics which describe the macroscopic behavior of the plasma membrane. Once the various parameters for a given membrane have been determined under controlled circumstances, the model may be used to predict behavior under conditions which are less amenable to careful study, such as the conditions under which cryopreservation is carried out.

Kedem and Katchalsky were the first to apply the principles of irreversible thermodynamics to the problem of describing the kinetics of transport across biological membranes (5). These equations were rewritten in a simpler form by Johnson and Wilson with the additional assumptions of a negligible specific volume of permeating solute and the absence of a hydrostatic pressure gradient across the membrane (4). We have modified these equations so that concentration of solutes is expressed in osmoles to reflect the osmotic pressure of the solutions.

$$\frac{dVw}{dt} = LpART\left[\frac{iCi \cdot Vo + \sigma \cdot Sp}{Vw} - \sigma \cdot eCp - eCi\right] \tag{1}$$

$$\frac{dSp}{dt} = PsA\left[eCp - \frac{Sp}{Vw}\right] + (1-\sigma)\overline{Cp}\frac{dVw}{dt} \tag{2}$$

Lp = Hydraulic Conductivity ($\mu m^3/\mu m^2 \cdot min \cdot atm$)

A = Cell Surface Area (assumed to remain constant during shrinkage and equal to the surface area of a sphere with the isotonic volume) (μm^2)

R = Universal Gas Constant (L·atm/mol·K)

T = Absolute Temperature (K)

iCi = Initial concentration of impermeant solute (osm/kg)

eCi = Final concentration of impermeant solute (osm/kg)

eCp = Extracellular concentration of permeant solute (osm/kg)

Sp = Moles of intracellular permeant solute (mol)

Vw = Osmotically active cell volume (μm^3)

Vo = Initial osmotically active cell volume (μm^3)

Ps = Permeability to permeant solute ($\mu m/min$)

σ = Reflection coefficient

$\overline{Cp}$ = Mean concentration of permeant solute across membrane

$$= 0.5\left[eCp + \frac{Sp}{Vw}\right] \text{ (osm/kg)}$$

These equations can be combined with a mathematical description of the frozen state of a solution, such as Pegg has described (12) based on the phase diagram of a solution of DMSO/NaCl/H_2O, to give a model of the osmotic excursions that occur during a prescribed freezing and thawing protocol. The cytoplasm is assumed to behave as an ideal dilute solution in this model and the extracellular environment is assumed to follow the phase diagram (ie. ice and water are in equilibrium during freezing).

75

solution. By measuring the parameters which describe the permeability and susceptibility to IIF of the chondrocytes, the conditions under which injury will occur can be modeled, thereby reducing the number of experiments that must be carried out to optimize a given protocol.

Materials and Methods

Chondrocyte Isolation

Fresh, intact bovine radial carpal joints were harvested from 12-16 month old steers at the slaughterhouse. The joints were opened under aseptic conditions and full thickness cartilage was removed from both faces of the joint and placed in sterile minimal essential medium (MEM, Gibco, Grand Island, NY, USA). The cartilage was then diced into pieces smaller than 1 mm^3 in a glass petri dish using two scalpels. The pieces were then incubated in a shaking water bath at 37°C in a 2 mg/ml solution of clostridial collagenase (Sigma, St. Louis, MO, USA) in MEM with penicillin and streptomycin added (100 µg/ml) for 5 hours. The suspension was filtered through a single thickness of sterile Nitex nylon gauze (40 µm pore size, B & SH Thompson, Scarborough, Ontario, Canada) to remove any undigested cartilage. The suspension was then washed twice in MEM + 10% fetal calf serum (FCS, Gibco) and finally suspended in MEM + 10% FCS at a concentration of 1 x 10^6 cells/ml. This suspension was incubated at 37°C with gentle shaking for 12 hours to allow recovery from the isolation procedure. Prior to use, the cell suspension was concentrated to 1 x 10^7 cells/ml and a sample was assayed for viability using fluorescent dyes. Fluorescein diacetate (10µM) and ethidium bromide (10µM) were added to the sample which was incubated for 10 min at 37°C before viewing on a Zeiss fluorescent microscope under ultraviolet illumination of 440-480 nm. In all cases, greater than 90% of the cells stained green, indicating esterase enzyme activity and an intact plasma membrane which was able to exclude ethidium bromide.

Coulter Volume Measurements

Cell volumes were measured using a Coulter electronic particle counter interfaced to an IBM Personal Computer. A custom program allowed the measurement of average cell volumes as a function of time. A lower threshold for volume measurement was set at about 10% of the average chondrocyte volume to remove any small debris from the measurement process. Clumps of cells produced off-scale signals which accumulated in the highest measurement channel and were eliminated from the averaging procedure. Microscopic visual assessment of the samples revealed little evidence of cell-sized debris or clumped cells.

Cell volumes were averaged over 0.2 s intervals, including an average of about 200 cells in each determination. The conversion of relative volume to absolute volume was accomplished by measuring the volume of calibrated microspheres (Coulter Electronics) of known diameter (10µm) as standards.

Chondrocytes in suspension are spherical in shape, so this method of calibration should provide reasonable results.

Permeability Parameters

The mathematical modeling of cellular osmotic responses used in this study is based on the Johnson and Wilson implementation (4) of the Kedem and Katchalsky equations (5) of membrane permeability. An Arrhenius relation was used to describe the temperature dependence of the cellular permeability parameters. The composition of the extracellular compartment during freezing was described by equations published by Pegg (12) which describe the phase diagram for the ternary system of water, sodium chloride and dimethyl sulfoxide (DMSO).

The hydraulic conductivity, DMSO permeability and DMSO reflection coefficient and their respective Arrhenius activation energies were determined by measuring the average volume change of the cells with time following exposure to various osmotic stresses at several temperatures. The cells were exposed to isotonic phosphate buffered saline (PBS), 3x isotonic PBS, 5x isotonic PBS, 1M DMSO in 1x PBS, 2M DMSO in 1x PBS and 3M DMSO in 1x PBS at 22°C, 14°C and 4°C and then the volume was recorded until equilibrium was reached. The osmotic pressure of each solution was measured using a freezing point depression osmometer (Precision Systems, Sudbury, MA, USA).

The experimental data obtained from the Coulter Counter were converted to absolute volume using a correction factor that was determined by measuring the peak height of latex microspheres of known volume (10.9 μm diameter, Coulter Electronics, Hialeah, Florida, USA). These data were then fit to the mathematical model using the Simplex algorithm (11). This is a least squares fitting routine which allows data to be fit to any non-linear equation.

Cryomicroscopy

Determination of the conditions under which intracellular freezing occurred in chondrocytes was carried out on a convection cryomicroscope stage (described previously, [9]). In all cases, a 2μl sample of cell suspension was placed under the cover slip and all observations were made within 0.5mm of the thermocouple junction to insure that the measured temperature corresponded to the physical environment under observation. The experiments were recorded on video tape with the addition of a time stamp for later analysis. The occurrence of intracellular freezing was assayed by observing a "flash" (a sudden darkening of the cytoplasm due to light scattering that accompanies ice formation in supercooled solutions). In the cases in which DMSO was added to the cells, this was accomplished by step-wise addition of DMSO at 22°C over 5 min. For a final concentration of 0.5M DMSO, a single step was used; for a final concentration of 1M DMSO, two steps were used; and for a final concentration of 2M DMSO, four addition steps were used with 5 min separating each step.

For the step cooling protocol, the sample was placed on the stage at 22°C and then cooled at 20°C/min to a pre-determined temperature between -4°C and -16°C. Upon reaching this temperature in the absence of extracellular ice, nucleation was artificially initiated by holding a copper wire cooled in liquid nitrogen just above the edge of the cover slip. Measurements indicated that the latent heat of fusion was buffered within 1.5 s of ice formation. The sample was held at the same temperature for 30 s following ice formation whereupon the experiment was terminated.

Constant cooling protocols were also run in which the sample was placed on the stage at 22°C and then cooled at 20°C/min to a temperature just below the freezing point of the solution (-1.5°C for 0M DMSO, -4°C for 0.5M DMSO, -6°C for 1M DMSO and -8.5°C for 2M DMSO) where nucleation was initiated as in the step cooling protocol (the samples must be cooled to a temperature below their melting points in order to make the artificial nucleation process more efficient). The samples were then held at this temperature for 2 min to allow osmotic equlibrium to be reached and were then cooled at one of five rates (20°C/min, 30°C/min, 40°C/min, 50°C/min, or 100°C/min) to a final temperature of -50°C. A time stamp was superimposed on the video record so that flashing events could be correlated with temperature.

Results

Figures 5.1 and 5.2 show examples of the measurement of volume changes in response to osmotic changes using the Coulter Counter. In figure 5.1, chondrocytes at 22°C have been removed from an isotonic solution and placed in a 3x isotonic solution at time zero. The average volume is recorded 5 times per second until equilibrium is established. These data are then fit to the equations describing osmotic water flux to determine the values of the parameters which give the best fit. The solid line in the figure indicates the solution to the equations using these values of the parameters. Figure 5.2 shows an example of chondrocytes being transferred from isotonic media into a solution with isotonic salts and 1M DMSO at 22°C. The cells initially lose water in response to the increased concentration of extracellular solutes but then regain their isotonic volume as DMSO (to which the plasma membrane is permeable) enters the cells to establish an equilibrium. By using several concentrations of impermeant salts and permeant DMSO, repeating the experiments at several temperatures and averaging the results of several runs (using chondrocytes from different donors for different runs), the parameters were determined and are presented in table 5.1 (the errors represent the standard error of the mean). The osmotically inactive volume is significantly higher than that measured by Dick (1) for fibroblasts derived from chick heart. There are also different values for the hydraulic conductivity (Lp) for the cases in which a permeant solute is present or absent due to the interaction between

water and solute. The temperature dependence of these parameters is assumed to follow an Arrhenius relation which is given as an activation energy in the table. Figure 5.3 shows a plot of the logarithm of the permeability parameters as a function of the inverse temperature. The slopes of the regression lines for each case give the activation energy.

Table 5.1. Permeability Parameters for Bovine Chondrocytes

Temperature (°C)	L_p (impermeant) $\mu m^3/\mu m^2 \cdot min \cdot atm$ +/- SEM	L_p (permeant) $\mu m^3/\mu m^2 \cdot min \cdot atm$ +/- SEM	P_s $\mu m/s$ +/- SEM
22	0.430 ± 0.051	0.313 ± 0.060	8.03 ± 1.03
14	0.225 ± 0.009	0.143 ± 0.018	3.00 ± 0.25
4	0.0600 ± 0.011	0.0610 ± 0.005	0.679 ± 0.117
E_a (kcal/mol)	14.8	12.2	18.5

The following parameters were used for all the simulations in this study:

V_0 = 1000 μm^3
V_d = 430 μm^3
A = 484 μm^2
T_g = 287 K (14°C)
L_{pg} = 0.189 $\mu m^3/\mu m^2/min/atm$ (impermeant) E_a = 14.8 kcal/mol
L_{pg} = 0.146 $\mu m^3/\mu m^2/min/atm$ (permeant) E_a = 12.2 kcal/mol
P_{sg} = 2.70 $\mu m/min$ E_a = 18.5 kcal/mol
σ = 0.95

Figures 5.4 through 5.6 show the solutions for the permeability equations using the parameters of table 5.1. In figure 5.4, the effect of temperature on water efflux is seen for the three temperatures used in this experiment. The rate of water loss can be seen to be strongly dependent on temperature, with the fastest rates occurring at higher temperatures. Figure 5.5 shows the effects of increasing the concentration of impermeant solute from 3x isotonic to 5x isotonic. Both the rate of water loss and the final equilibrium volume are affected. Figure 5.6 shows the shrinkage and subsequent re-swelling of cells placed in various concentrations of DMSO. The rate of water loss is more strongly dependent on the concentration gradient than is the rate of DMSO influx. It can also be seen that it takes substantially longer for cells to regain their isotonic volume when they are placed in higher concentrations of permeant solutes.

Figure 5.7 shows the tendency of chondrocytes to form IIF when they are subjected to ice formation at supercooled temperatures on the cryomicroscope stage. As the temperature of ice nucleation is lowered, the proportion of cells undergoing IIF increases rapidly until a point is reached in which all the cells will "flash" upon ice seeding. The effect of cryoprotectant on the temperature at which IIF occurs has been observed before (14) and follows directly from the

osmotic rupture theory. Figure 5.8 shows the proportion of cells which freeze intracellularly during constant cooling. These cells are cooled in the presence of ice, thus the rate of water efflux is dependent on the cooling rate. The average temperatures at which these IIF events occur are shown in figure 5.9.

Discussion

The values of the permeability parameters that are presented in table 5.1 can be used with the permeability equations to predict the osmotic events which occur during a specified freezing and thawing protocol if the physico-chemical environment of the bathing solution can be described during freezing. Since the formation of ice removes pure water from the solution, the solutes that are present become concentrated in the unfrozen compartment. It is this concentration of solutes that provides the osmotic stress which causes cells to shrink during freezing. With the trend to using high concentrations of several different solutes (in the attempt to achieve vitrification - an amorphous solid state that does not contain any ice crystals), a full description of the phase separation during freezing becomes harder to obtain. Pegg has published equations (12,13) which can be used to calculate the phase behavior of the ternary systems water/NaCl/glycerol and water/NaCl/DMSO which are the most widely used cryoprotective solutions. The equations for the water/sodium chloride/DMSO system have been employed in this study to correlate the magnitude of the osmotic water flux during freezing with the observation of IIF on the cryomicroscope. This has allowed us to measure parameters which can be used to predict the conditions under which IIF occurs for bovine chondrocytes.

The three parameters which describe the osmotic behavior of a specific cell type (in the presence of a permeating solute) are the hydraulic conductivity, the permeability of the solute which can move across the plasma membrane and the reflection coefficient of this solute. The two permeability parameters are temperature dependent and therefore require measurement of their respective activation energies before osmotic behavior can be predicted during conditions in which the temperature changes with time. Since we are interested in predicting osmotic responses at temperatures within the frozen domain, it would be best if we could make our permeability measurements in this same region. This is difficult, however, due to the presence of ice and the high solute concentrations which attend its formation. Practically, it is far simpler (and the measurements are more accurate) to make these measurements at temperatures above the freezing point and then use the activation energy to extrapolate to the subfreezing domain. The accuracy of this extrapolation has been questioned recently (15), so it is a possible source of error in this investigation.

The utility of these parameters is demonstrated in the application of predicting the water flux that accompanies IIF. We have recently proposed a mechanism of intracellular ice formation (9,10) which indicts water flux as the agent of injury. During osmotic shrinkage, the frictional drag of the water efflux

can exceed the tensile strength of the membrane, resulting in mechanical failure which manifests itself as a rupture in the membrane. Since the cytoplasm is supercooled during rapid cooling (although cooling is too rapid to allow the cell to remain in osmotic equilibrium, it is not rapid enough to prevent the cell from remaining in thermal equilibrium with its environment), the extracellular ice quickly propagates into the cytoplasm, causing the cell to appear to "flash" when viewed microscopically.

By simulating the water flux for the freezing protocols that were carried out on the cryostage, the pressure that is exerted on the membrane can be calculated as a function of time and temperature using equation 3. Figure 5.10 shows the calculated water flux pressure that is exerted on the membrane during constant cooling in 1M DMSO and figure 5.12 shows the water flux pressure for the step cooling protocol in 1M DMSO. The observed incidence of IIF can then be used with equation 4 to determine the three parameters of that equation (b, $\overline{\mathcal{P}}$ and τ) and their activation energies. The lines in figures 5.7 and 5.8 show the predictions of equation 4 when the parameters are optimized to minimize the errors in both the step cooling and constant cooling experiments. Figure 5.11 shows the predicted incidence of IIF during constant cooling for the case of 1M DMSO. This figure can also be used to predict the temperature of IIF, which should occur between -12°C and -30°C. The measured temperatures of IIF for 1M DMSO (from figure 5.9) are between -20°C and -45°C. This pattern of predicting a higher temperature of IIF than was actually measured is consistent for each of the solutions that were tested in this study. These discrepancies are probably indicative of the sensitive dependence on the starting conditions that are present in the constant cooling experiments. The temperature at which ice is seeded and the time that is allowed for equilibration at this temperature are critical parameters in determining the cell volume and the subsequent levels of water flux when constant cooling is initiated. Because we are assuming that an average cell can describe the behavior of the population, the assumption that all the permeability parameters are normally distributed is also made. If this is not true, then considerable error could be introduced by having some cells far from osmotic equilibrium when cooling is initiated. The average behavior of the population will not follow the behavior of an average cell in this case and a relatively small sample size could lead to an even greater departure from the predicted behavior. For this reason, the step cooling experiments are favored for determining the parameters of equation 5. The volume of the cells upon ice nucleation is unaffected by the temperature of nucleation; thus the behavior of the cells will be closer to the ideal. Figure 5.13 shows the predicted incidence of IIF for the step cooling experiments when only these data are used to optimize the parameters. It is suggested that these parameters be used to predict the behavior of chondrocytes during freezing as the step cooling experiments are less prone to error than the constant cooling experiments. The parameters have the following values for boving chondrocytes:

b $= 0.359$ $(E_a = -24.8 \text{ kcal/mol})$

$\overline{P}$ $= 13.3 \text{ N/m}^2$ $(E_a = 20.4 \text{ kcal/mol})$

τ $= .85 \text{ s}$ $(E_a = -20.4 \text{ kcal/mol})$

With measured values for the parameters of the permeability equations and the equation for IIF, it is now possible to use simulation of any freezing protocol to predict damage due to osmotic stresses. This allows modeling of the chondrocytes within the cartilage matrix which can be used to explore possible cryopreservation protocols without having to perform costly and time consuming experiments. Although the solution effects injury that accompanies slow cooling cannot be predicted from these parameters, it is usually the case that the highest cooling rate that can be achieved without intracellular ice formation will give minimal damage due to solution effects. Thus the above parameters can be used to design protocols in which cooling is maximized without leading to intracellular ice formation.

References

1. Dick, D. 1966. Cell Water. Butterworth, Inc., Washington, D.C. p. 61.

2. Diller, K. and Cravalho, E. 1970. A Cryomicroscope for the Study of Freezing and Thawing Processes in Biological Cells. *Cryobiology* **7**: 191-199.

3. Diller, K. 1979. Intracellular Freezing of Glycerolized Red Cells. *Cryobiology* **16**: 125-131.

4. Johnson, J. and Wilson, T. 1967. Osmotic Volume Changes Induced by a Permaeble Solute. *J. Theoret. Biol.* **17**: 304-311.

5. Kedem, O. and Katchalsky, A. 1958. Thermodynamic Analysis of the Permeability of Biological Membranes to Non-Electrolytes. *Biochim. et Biophys. Acta* **27**: 229-246.

6. Mazur, P. 1963. Kinetics of Water Loss from Cells at Subzero Temperatures and the Likelihood of Intracellular Freezing. *J. Gen. Physiol.* **47**: 347-369.

7. Mazur, P. 1977. The Role of Intracellular Freezing in the Death of Cells Cooled at Supraoptimal Rates. *Cryobiology* **14**: 251-272.

8. Mazur, P., Rall, W. and Leibo, S. 1984. Kinetics of Water Loss and the Likelihood of Intracellular Freezing in Mouse Ova: Influence of teh Method of

Calculating the Temperature Dependence of Water Permeability. *Cell Biophys.* **6**: 197-214.

9. Muldrew, K. and McGann, L.E. 1990. Mechanisms of Intracellular Ice Formation. *Biophys. J.* **57**: 525-532.

10. Muldrew, K. and McGann, L.E. 1993. The Osmotic Rupture Hypothesis of Intracellular Freezing Injury. Submitted to the Biophysical Journal.

11. Nelder, J. and Mead, R. 1965. A Simplex Method for Function Minimization. *Computer J.* **7**: 308-313.

12. Pegg, D. 1986. Equations for Obtaining Melting Points and Eutectic Temperatures for the Ternary System Dimethyl Sulphoxide/Sodium Chloride/Water. *Cryo-Letters* **7**: 387-394.

13. Pegg, D. 1984. Red Cell Volume in Glycerol/Sodium Chloride/Water Mixtures. *Cryobiology* **21**: 234-239.

14. Rall, W., Mazur, P. and McGrath, J. 1983. Depression of the Ice-Nucleation Temperature of Rapidly Cooled Mouse Embryos by Glycerol and Dimethyl Sulfoxide. *Biophys. J.* **41**: 1-12.

15. Toner, M., Harris, C., Hubel, A., Sterling, L., Dunn, J., Yarmush, M., Cravalho, E. and Topkins, R. 1990. Water Permeability Parameters of Isolated Hepatocytes between 0 and -12°C. *Cryobiology* **27**: 632-633.

Osmotic Shrinkage in the Presence of an Impermeant Solute

Figure 5.1
Sample measurement of osmotic shrinkage on the Coulter Counter. Each open circle represents the average of about 200 cells which pass through the orifice in 0.2 s. The suspension of isolated bovine chondrocytes was placed into a 3x isotonic salt solution at 22°C at time zero. The solid line shows the curve generated from the best fit values of Lp and Vd. The isotonic volume is determined from calibrated latex microspheres.

Osmotic Shrinkage in the Presence of a Permeant Solute
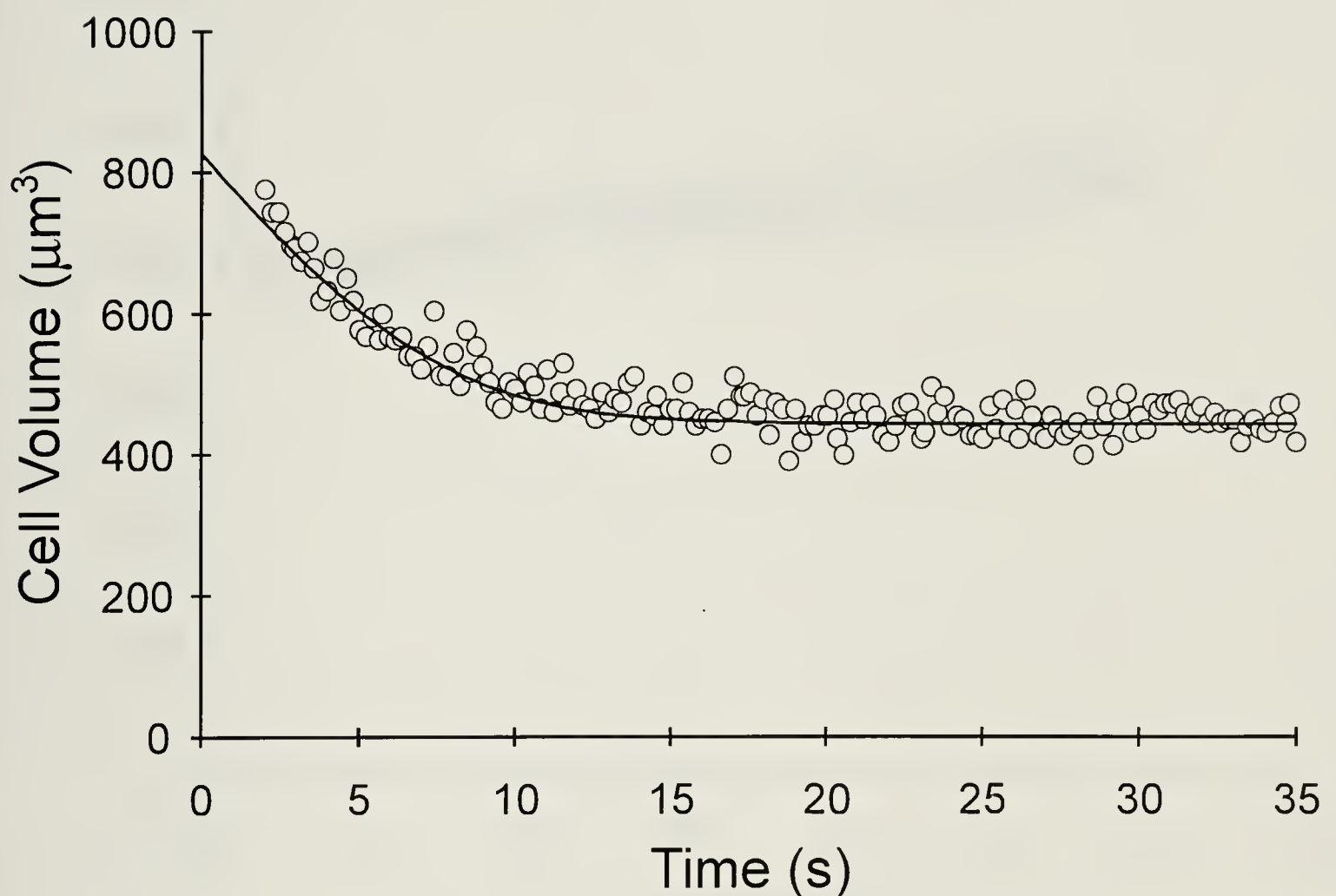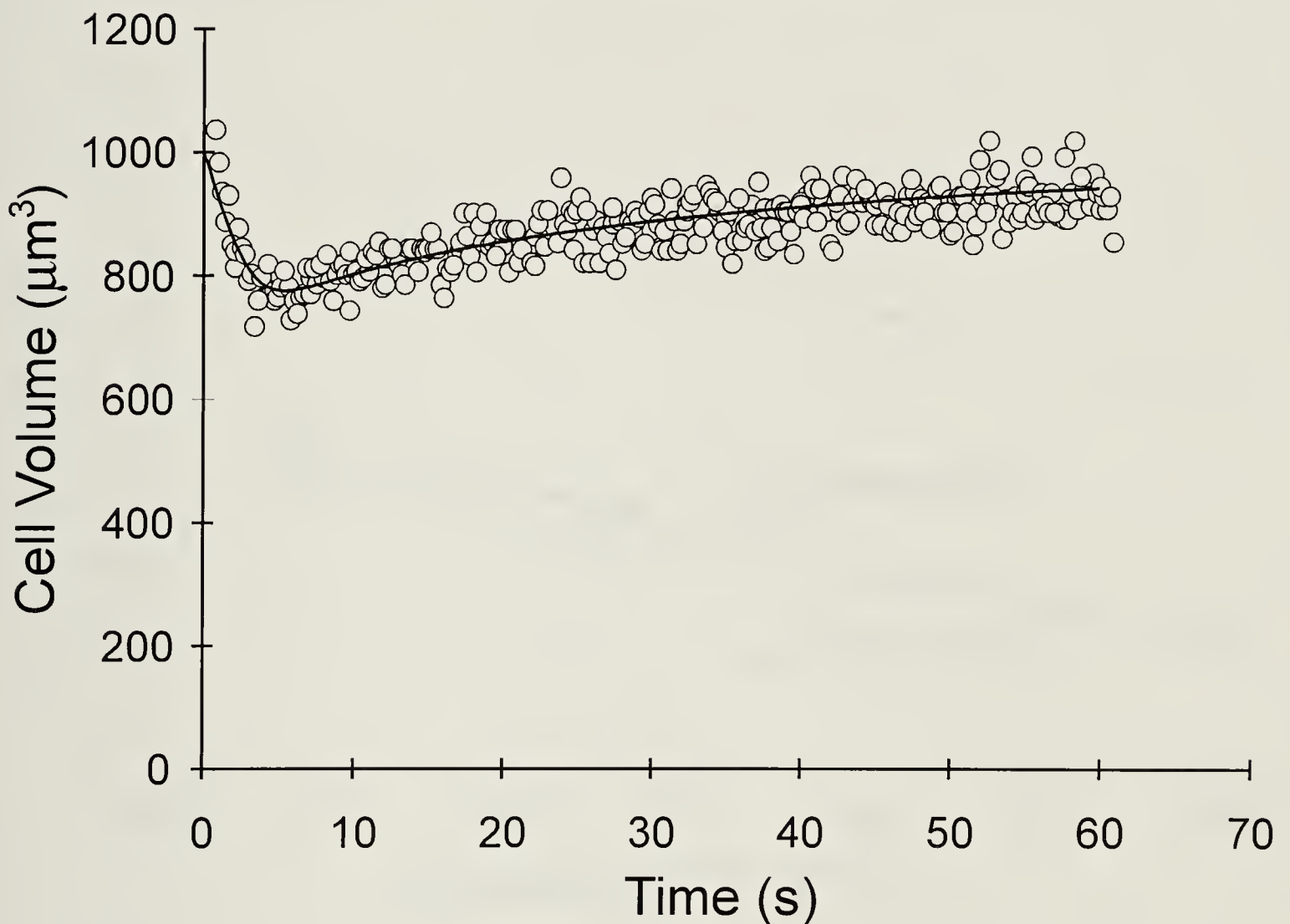

Figure 5.2
Sample measurement of osmotic shrinkage and re-swelling on the Coulter Counter. Each open circle represents the average of about 200 cells which are measured over a 0.2 s interval. The chondrocyte suspension was put into an isotonic salt solution with 1M DMSO at 22°C. The solid line shows the curve generated from the best fit values of *Lp*, *Ps*, σ, and *Vd*.

Arrhenius Plot of the Best Fit Values of the Permeability Parameters
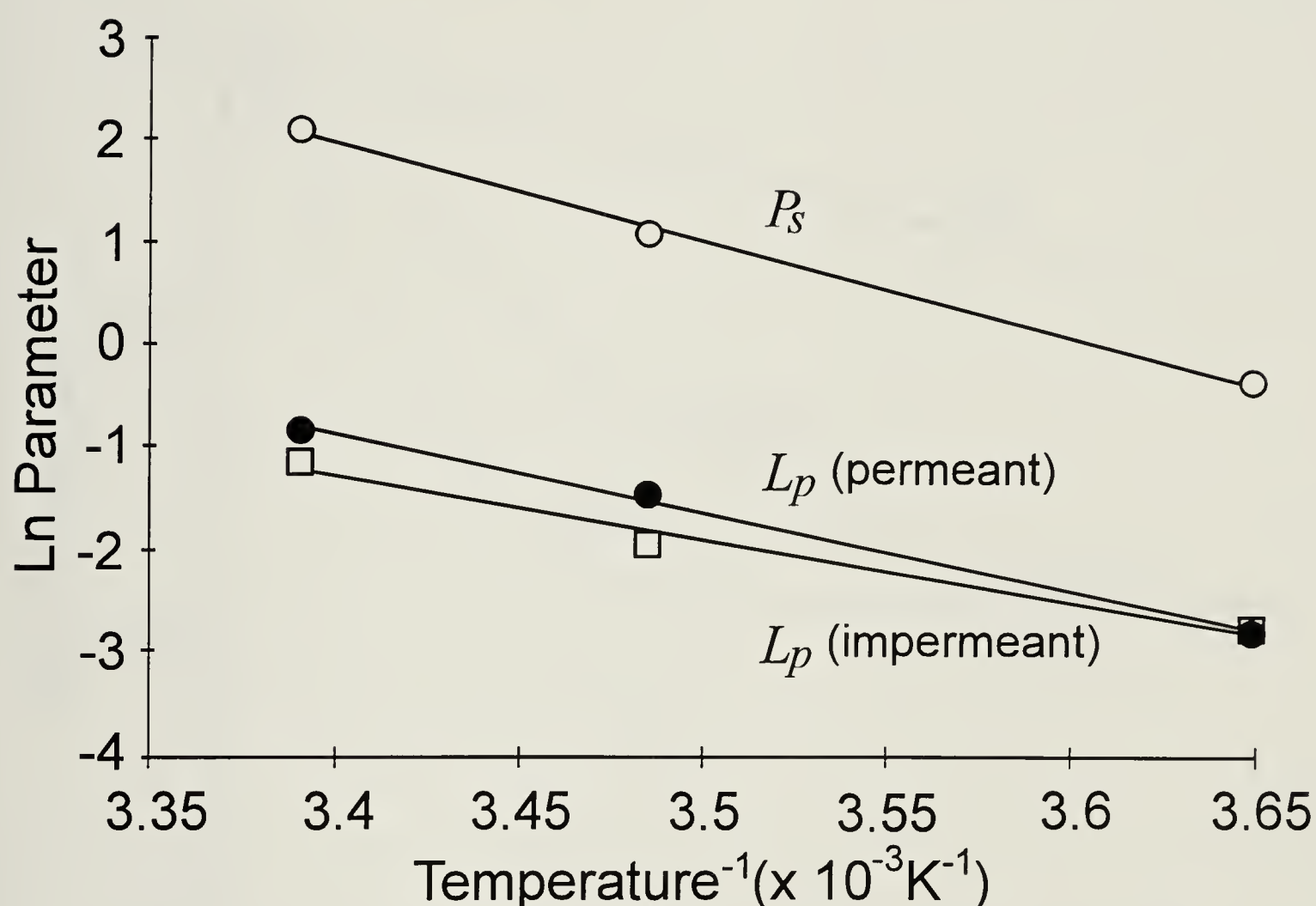
Figure 5.3
The natural logarithms of the temperature dependent parameters are plotted as functions of the inverse absolute temperature. The slopes of the regression lines can be used to derive the Arrhenius activation energies for the parameters. The open circles are for P_s which has an activation energy of 18.5 kcal/mol, the closed circles are for L_p in the absence of DMSO which has an activation energy of 14.8 kcal/mol and the open squares are for L_p in the presence of DMSO which has an activation energy of 12.2 kcal/mol. Error bars denoting the standard error are smaller than the shapes.

Figure 5.4
Calculated volumes of bovine chondrocytes when placed in a 5x isotonic salt solution at three different temperatures using the measured permeability parameters.

Concentration Dependence of Osmotic Shrinkage Due to an Impermeant Solute
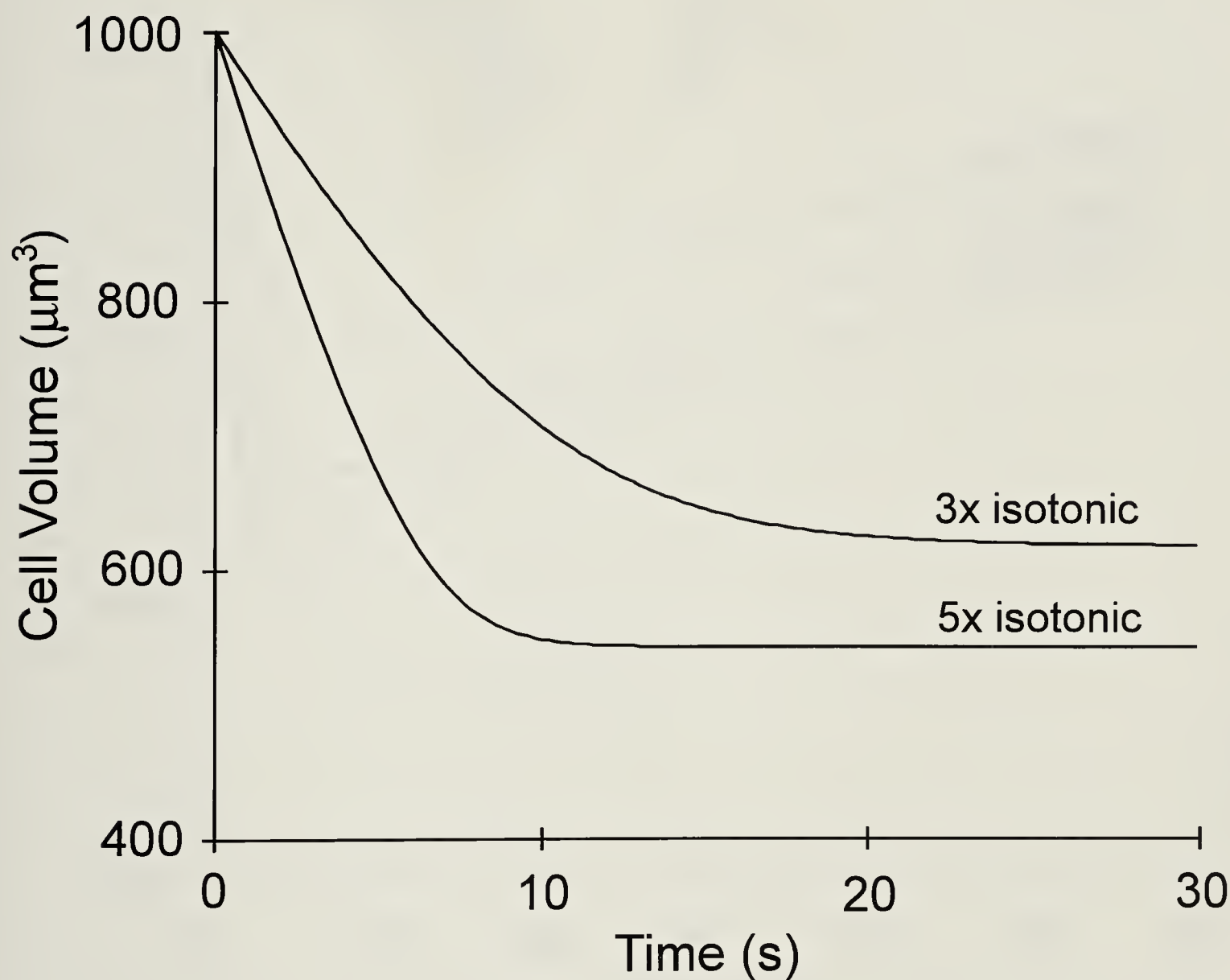
Figure 5.5
Calculated volumes of bovine chondrocytes when placed in hypertonic salt solutions at 22°C using the measured permeability parameters.

Concentration Dependence of Osmotic Volume Change Due to a Permeant Solute
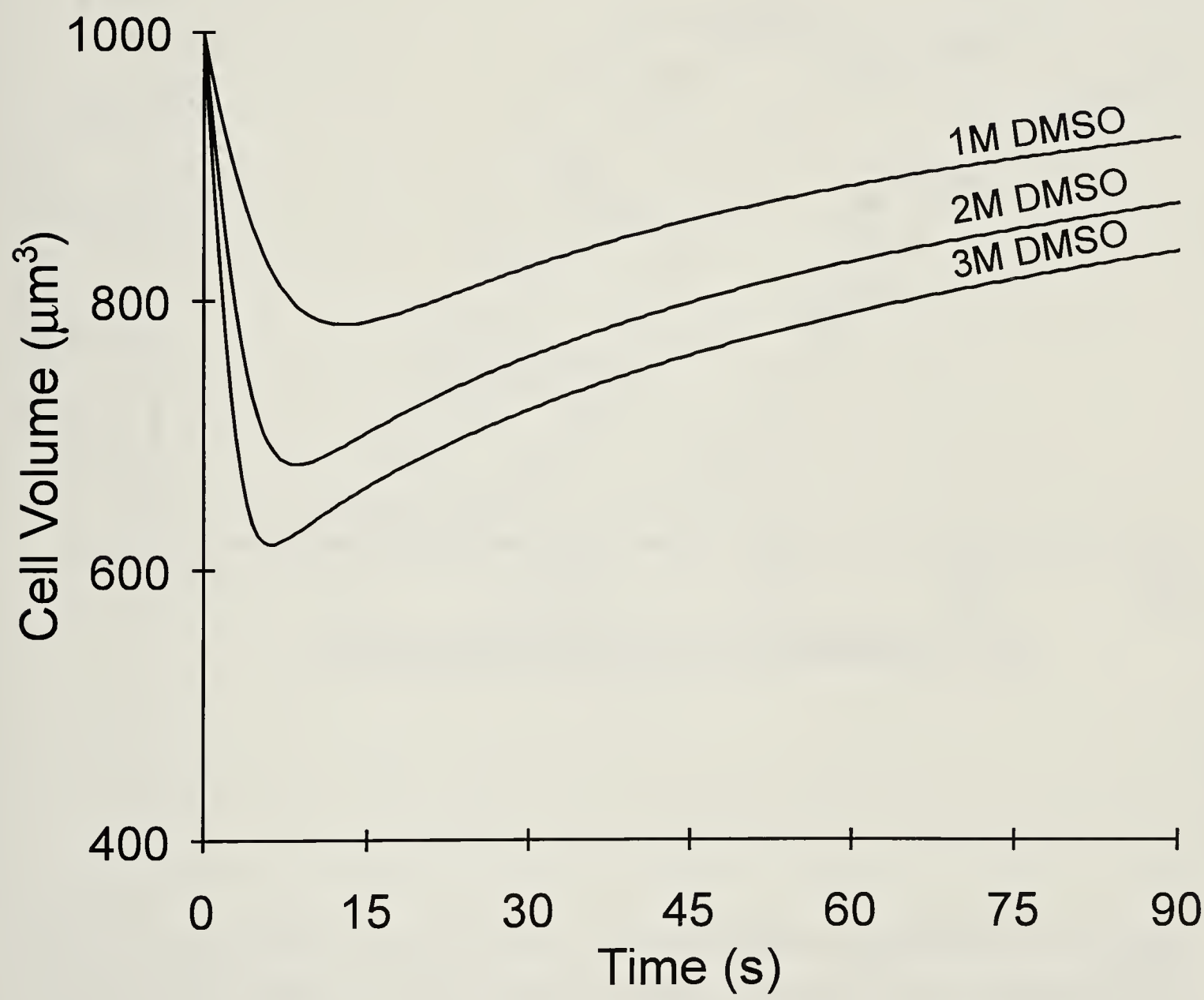
Figure 5.6
Calculated volumes of bovine chondrocytes when placed in solutions with isotonic salt and DMSO in various concentrations at 22°C using the measured permeability parameters.

Incidence of Intracellular Ice Formation upon Ice Nucleation at Supercooled Temperatures
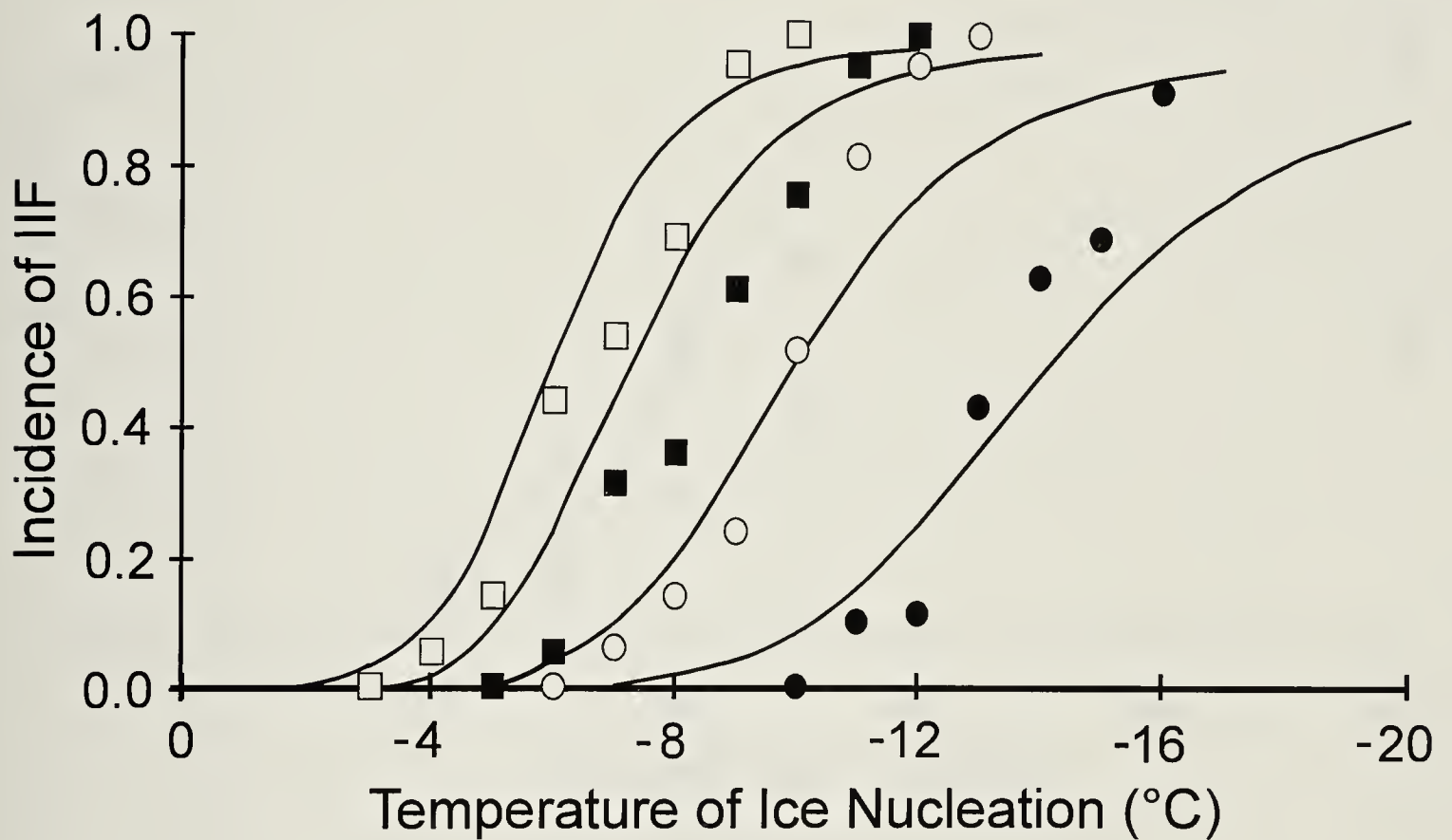
Figure 5.7

The incidence of IIF as a function of ice nucleation temperature for bovine chondrocytes cooled on the cryomicroscope. Each point represents the proportion of cells which was observed to form IIF (the minimum number of cells observed for each point was 50). The open squares represent cells suspended in isotonic media with no DMSO. The closed squares represent cells equilibrated in 0.5M DMSO before cooling. The open circles represent cells equilibrated in 1M DMSO before cooling and the closed circles represent cells equilibrated in 2M DMSO before cooling. The solid lines are the curves generated from equation 4 using the permeability equations to model water flux. The specific values of the parameters are: $b = 0.617$ ($E_a = -8.12$ kcal/mol), $\overline{\mathcal{P}} = 7.93$ N/m^2 ($E_a = 8.24$ kcal/mol) and $\tau = 0.425$ s ($E_a = -8.24$ kcal/mol).

Incidence of Intracellular Ice Formation
During Freezing at Constant Cooling Rates
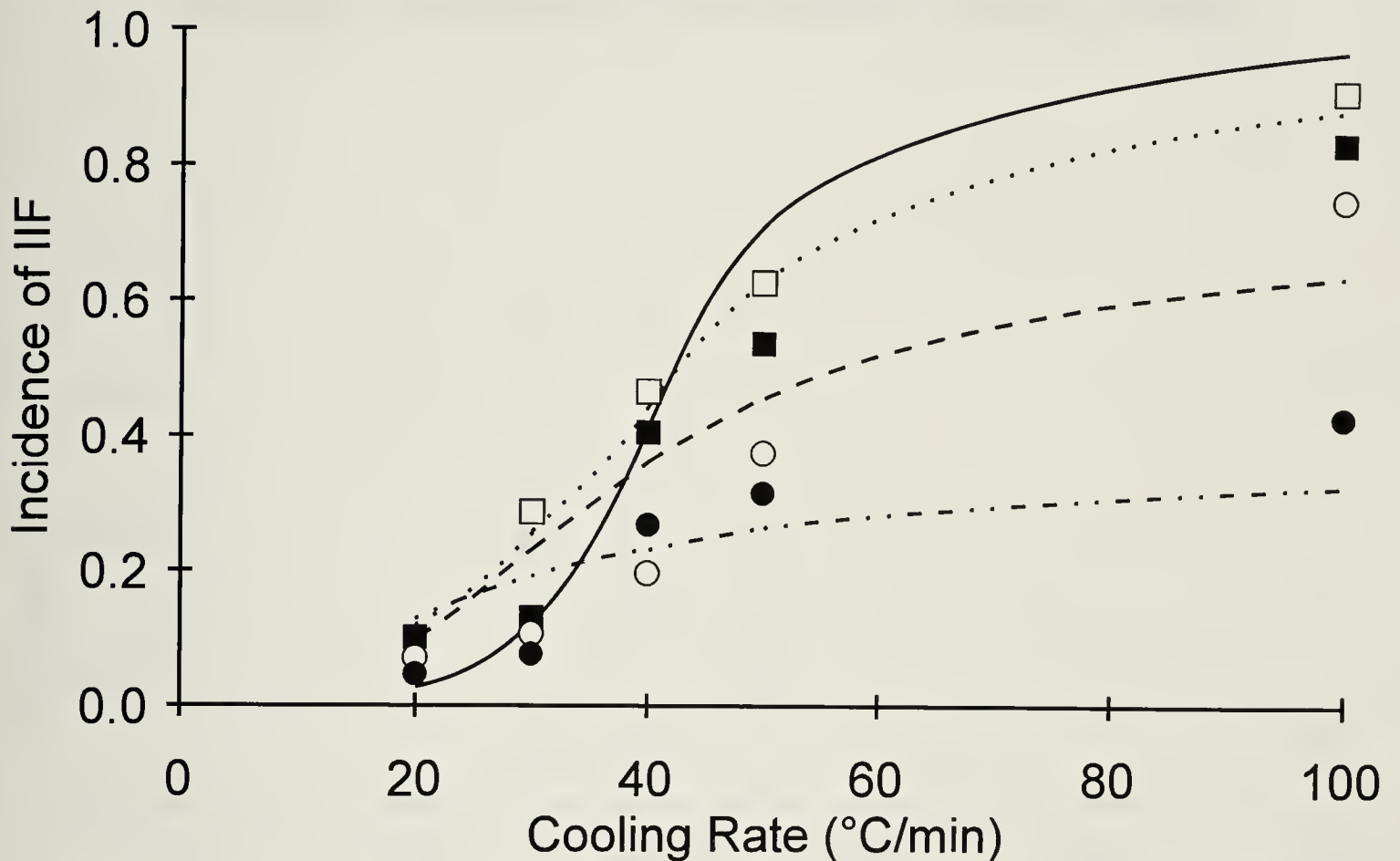
Figure 5.8

The incidence of IIF as a function of cooling rate is shown for bovine chondrocytes cooled at constant rates on the cryomicroscope. Each point represents the proportion of cells which formed IIF with a minimum number of cells per point of 50. The open squares represent cells suspended in isotonic media with no DMSO and the solid line represents the predicted incidence of IIF for this solution. The closed squares represent cells equilibrated in 0.5M DMSO before cooling and the dotted line represents the predicted incidence of IIF for this solution. The open circles represent cells equilibrated in 1M DMSO before cooling (the dashed line is the theoretical curve for 1M DMSO) and the closed circles represent cells equilibrated in 2M DMSO before cooling (the dotted and dashed line is the predicted incidence of IIF for 2M DMSO). The solid lines are the curves generated from equation 4 using the permeability equations to model water flux. The specific values of the parameters are: $b = 0.617$ ($E_a = -8.12$ kcal/mol), $\overline{\mathcal{P}} = 7.93$ N/m^2 ($E_a = 8.24$ kcal/mol) and $\tau = 0.425$ s ($E_a = -8.24$ kcal/mol).

Temperature of Intracellular Ice Formation During Freezing at Constant Cooling Rates
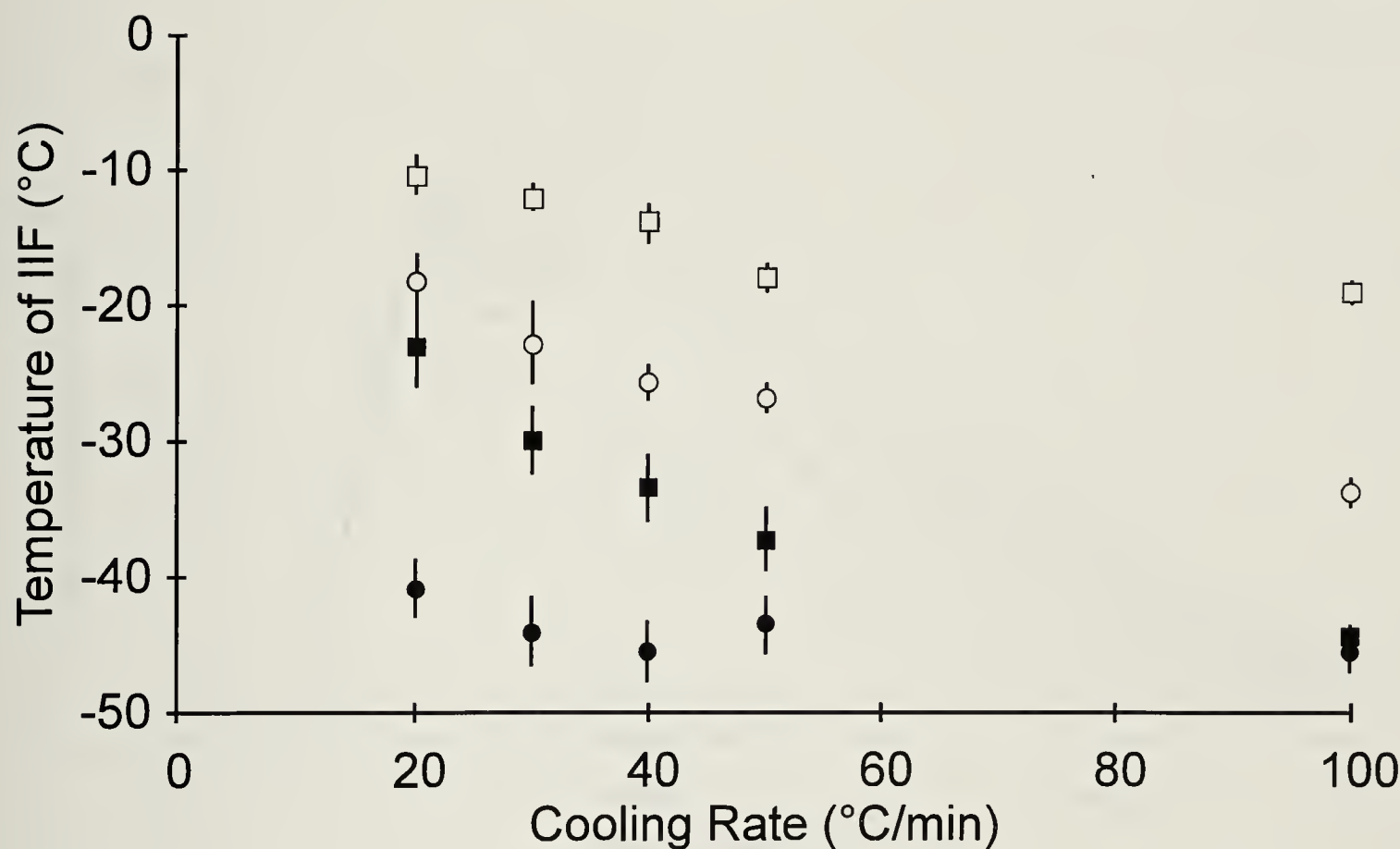
Figure 5.9
The mean temperature at which IIF occurs during constant cooling on the cryomicroscope is shown as a function of cooling rate. The open squares represent cells suspended in isotonic media with no DMSO. The open circles represent cells equilibrated in 0.5M DMSO before cooling. The closed squares represent cells equilibrated in 1M DMSO before cooling and the closed circles represent cells equilibrated in 2M DMSO before cooling. The bars represent the standard error of the mean.

Pressure Due to Water Flux During Freezing
at Constant Cooling Rates in 1M DMSO
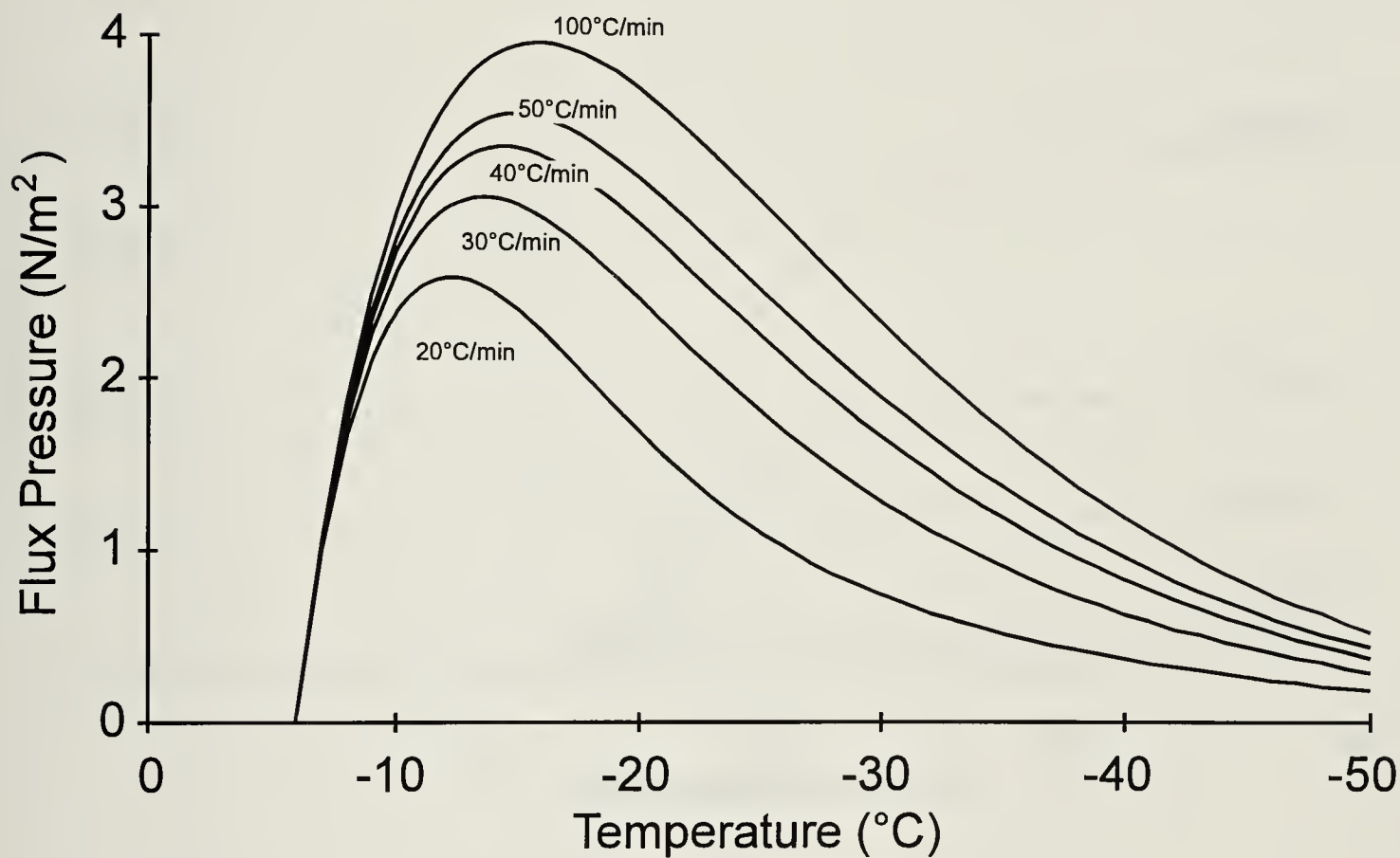
Figure 5.10
The pressure imparted on the membrane due to the friction of water flux is shown as a function of temperature during constant cooling for bovine chondrocytes equilibrated in 1M DMSO.

Probability of Intracellular Ice Formation in 1M DMSO During Freezing at Constant Cooling Rates
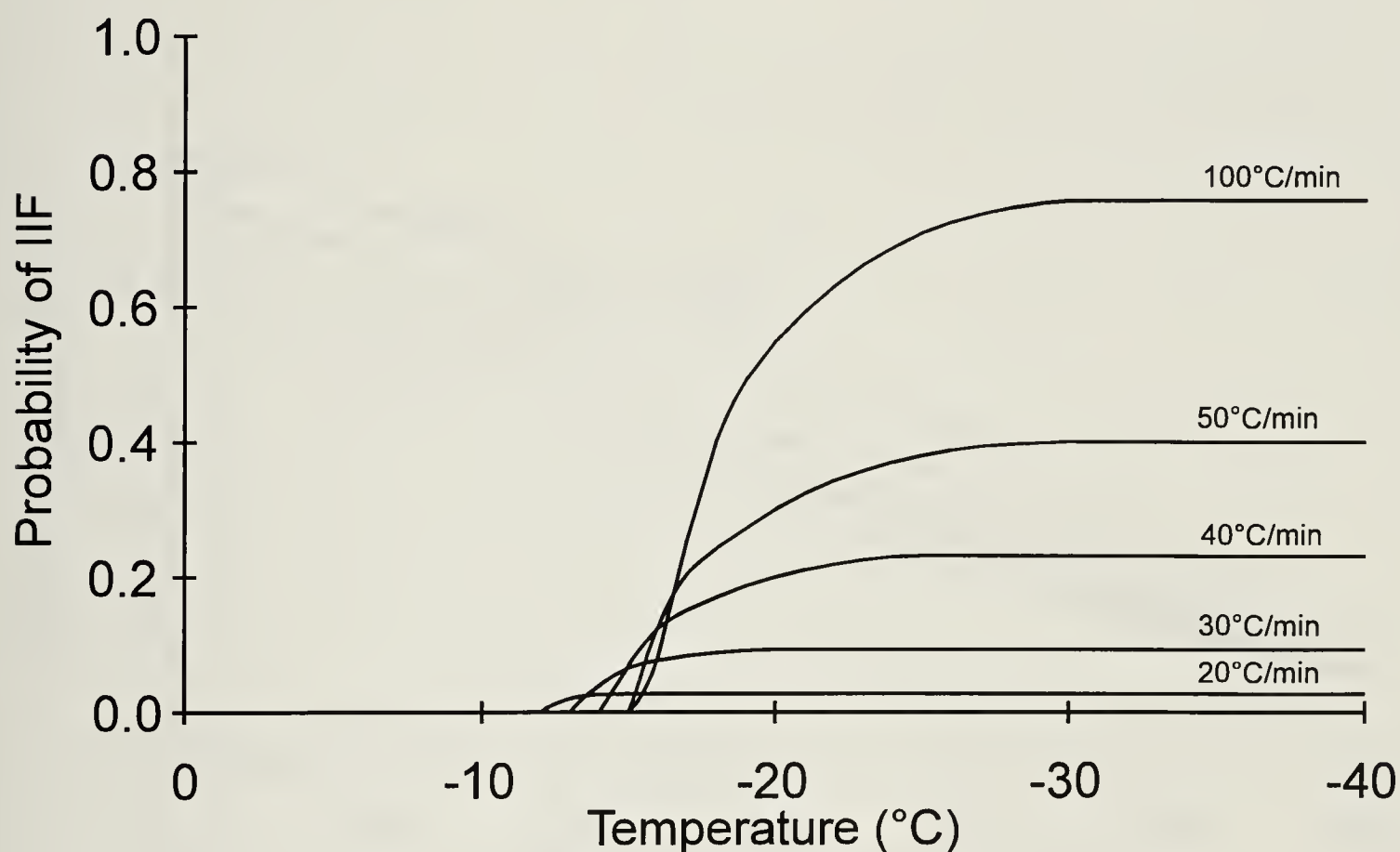
Figure 5.11
The predicted incidence of IIF is shown as a function of temperature reached during constant cooling for bovine chondrocytes equilibrated in 1M DMSO. The specific values of the parameters are: $b = 0.617$ ($E_a = -8.12$ kcal/mol), $\overline{\mathcal{P}} = 7.93$ N/m^2 ($E_a = 8.24$ kcal/mol) and $\tau = 0.425$ s ($E_a = -8.24$ kcal/mol).

Water Flux Pressure upon Ice Nucleation at Supercooled Temperatures in 1M DMSO
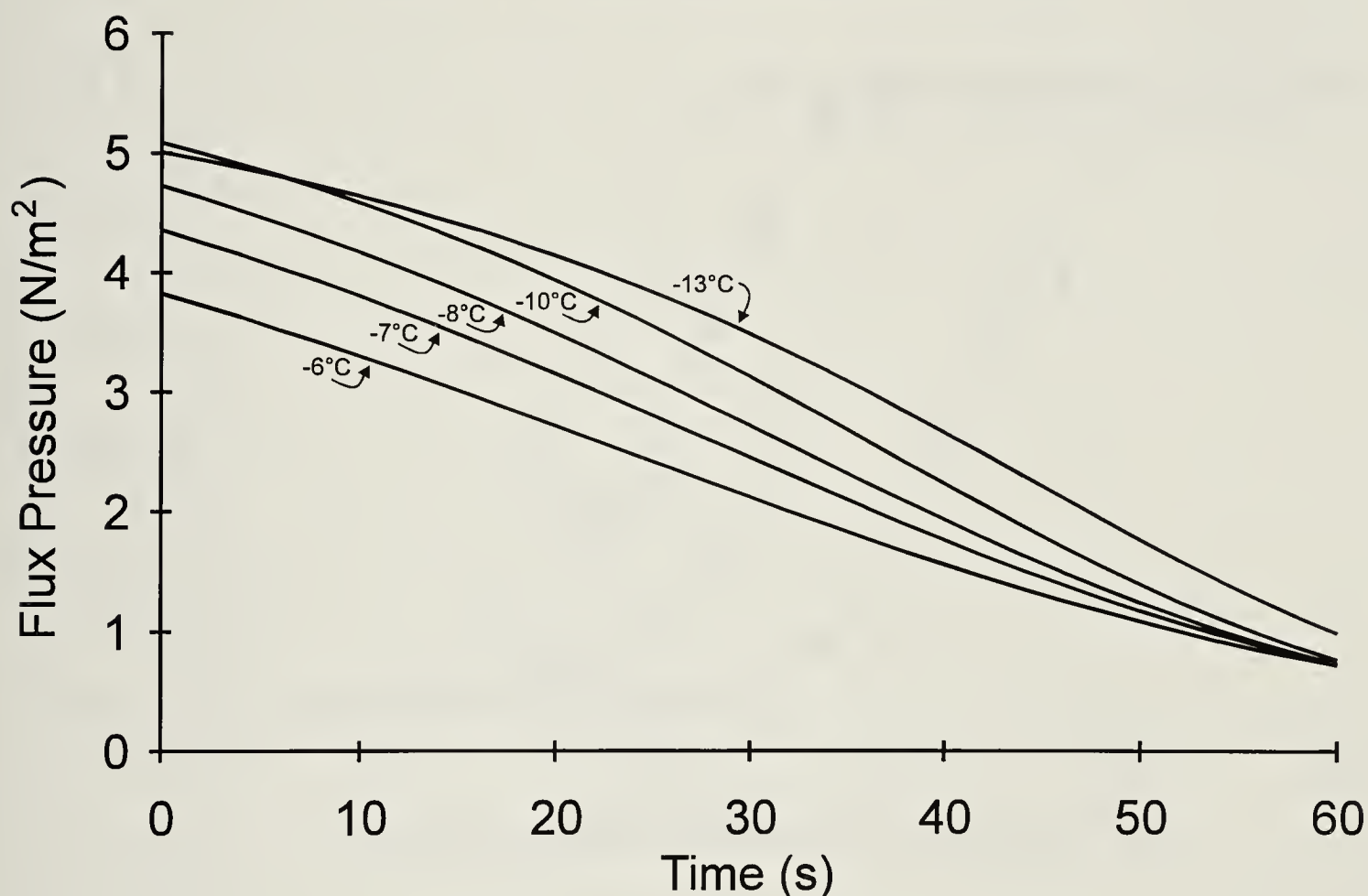
Figure 5.12
The pressure imparted on the membrane due to the friction of water flux is shown as a function of time following ice nucleation at several supercooled temperatures. The curves are for bovine chondrocytes equilibrated in 1M DMSO.

Prediction of Intracellular Ice Formation upon
Ice Nucleation at Supercooled Temperatures
Using Optimized Parameters
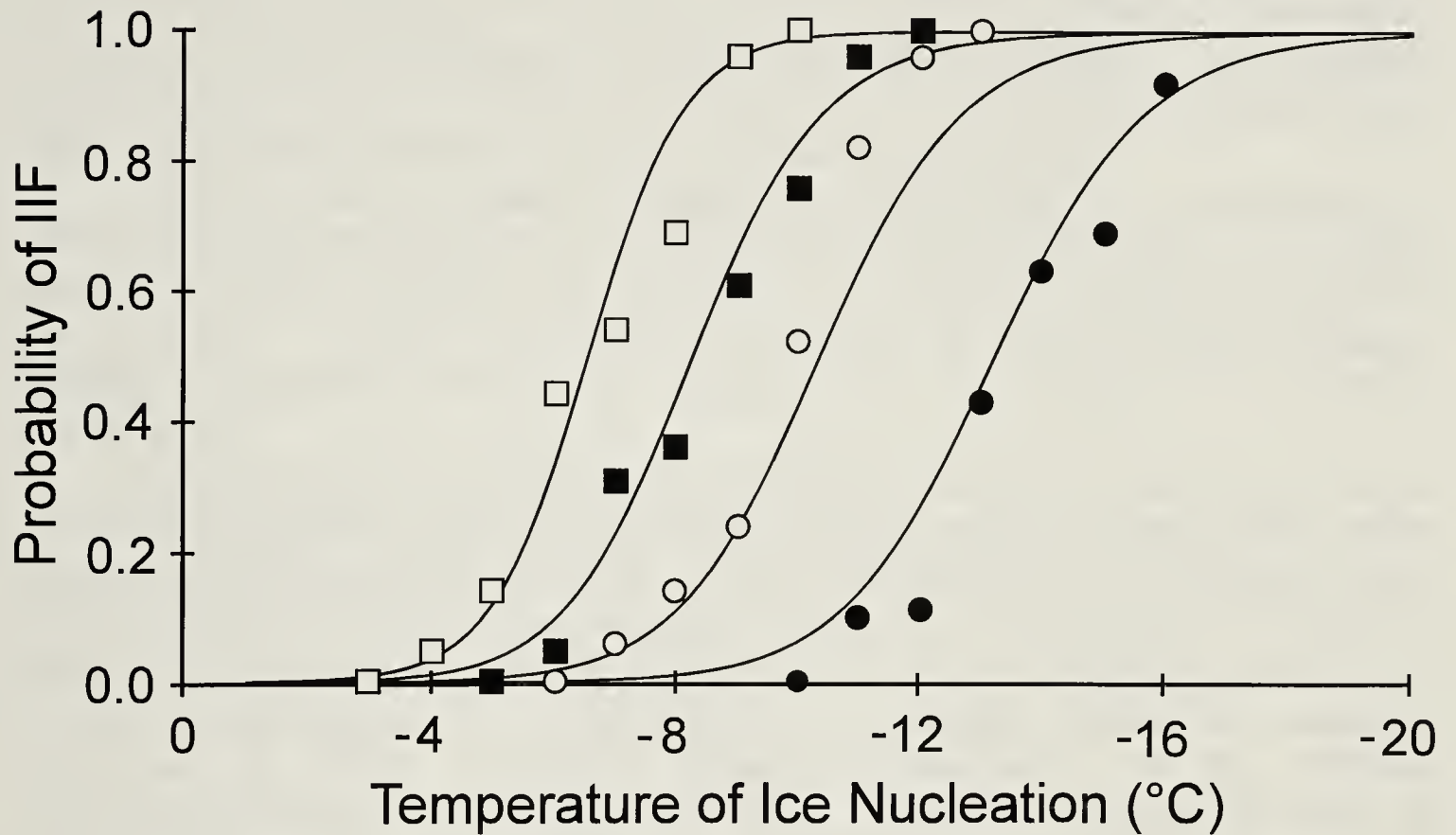
Figure 5.13
The data from figure 7 are duplicated to illustrate the predicted incidence of IIF
using just this data to fit the parameters to equation 4. The values of the
parameters used to generate these lines are: b = 0.359 (E_a = -24.8 kcal/mol), $\overline{\mathcal{P}}$
= 13.3 N/m^2 (E_a = 20.4 kcal/mol) and τ = 0.85 s (E_a = -20.4 kcal/mol).

97

Chapter 6

Permeation Kinetics of Dimethyl Sulfoxide in Articular Cartilage

Introduction

There are several instances in which biological replacement of articulating joints or focal lesions on articulating surfaces would be a superior alternative to prosthetic joints or surface reconstruction (9). In most instances, transplantation of living tissue is limited by the supply of healthy tissue for grafting. The problem of supply could be alleviated by long term tissue banking. This requires successful protocols for freezing and thawing tissue, a difficulty which has not yet been surmounted except for relatively simple biological tissues.

The cells within articular cartilage, the chondrocytes, are responsible for maintaining the biological and biomechanical properties of cartilage. It is widely believed that high viability of chondrocytes is required for long-term survival of the graft (9). Our goal is to develop techniques for cryopreserving cartilage-bearing bone grafts with minimal damage to the chondrocytes in the articular cartilage.

Recent evidence obtained in our laboratory has shown that the presence of dimethyl sulfoxide (DMSO) is beneficial to the survival of chondrocytes within cartilage during cryopreservation (8). This is not surprising, as it has been used as an effective cryoprotectant in cellular systems for decades. In order for DMSO to act as a cryoprotectant in the tissue, it must penetrate sufficiently to provide cryoprotection to chondroyctes at all depths within the cartilage. Prediction of DMSO permeation requires measurement of the diffusion coefficient of DMSO in cartilage. The use of ^{1}H-NMR to measure the influx of DMSO into tissues has been shown to be an effective technique for measuring the kinetics of uptake (2,10). In this experiment, the uptake of DMSO into the articular cartilage of porcine patellae is determined as a function of time, and these measurements used to determine the diffusion coefficient of DMSO within the cartilage matrix.

The signal produced in nuclear magnetic resonance (NMR) spectroscopy is derived from atomic nuclei with magnetic moments. The nucleus of the hydrogen atom, in its most commonly occurring isotope, is a single proton and thus has a strong magnetic moment. When a chemical species is placed in a strong magnetic field, the protons within the species will align their magnetic moment parallel to the external field (either in the direction of the field or directly opposing it). Each proton in the chemical will have a characteristic resonant frequency (depending on the immediate electronic environment, as neighboring electrons can partially shield the proton from the external field). When an external electromagnetic signal coincides with the resonant frequency, the protons can absorb energy and jump to the less stable orientation opposing the external field. When there is no applied electromagnetic field at the resonant

frequency, the protons will spontaneously revert to the more stable orientation in the direction of the external magnetic field. This process gives off electromagnetic radiation which is the NMR signal. The integral of the signal at a given frequency is a function of the number of protons with that identical electronic environment. Thus the protons of methyl groups will all contribute to the signal at a certain frequency which will be different from that produced by protons of hydroxyl groups. This principle has been applied here to determine the amounts of water and DMSO in cartilage as a function of time exposed to a solution containing a fixed concentration of DMSO at different temperatures.

Maroudas has shown that nutrients do not enter the cartilage from the vasculature in the bone (4) implying that there is a barrier to diffusion at the bone-cartilage interface. The solution to the diffusion equation for this case (a semi-infinite plane sheet) has been worked out by Crank (1) and is given in equation 1.

$$\frac{M_t}{M_\infty} = 1 - \sum_{n=0}^{\infty} \frac{8}{(2n+1)^2 \pi^2} e^{\left[\frac{-D(2n+1)^2 \pi^2 t}{4\ell^2} \right]} \tag{1}$$

M_t = amount of solute which has entered at time t
M_∞ = equilibrium solute concentration
D = diffusion coefficient
t = time
ℓ = thickness of cartilage

By fitting concentration data to this equation, the diffusion coefficient can be calculated.

Materials and Methods

Patellae were harvested from 2 month old pigs which had been used for a surgery course. The patellae were removed within 10 min of sacrifice, placed in isotonic (150 mM) phosphate buffered saline (PBS) solution, and transported to the laboratory within 20 min. The experiments were carried out at either 23.5°C or 4°C; the patellae which were to be used for the 4°C experiment were placed in a 4°C refrigerator for 30 min to allow temperature equilibration. The patellae were then placed into 3 ml of a 1M solution of DMSO in isotonic PBS (which was equilibrated to either 23.5°C or 4°C) in a 10 cm diameter petri dish with the cartilage side down so that the entire cartilage surface was submerged in the solution. The bone surface of the patella was not immersed in the DMSO solution to prevent diffusion of DMSO into the cartilage from the back. The disk of cartilage that was used for the assay was removed from near the center of the patella, so that diffusion from the sides could not have had an effect since the

distance from the edges to the center is many times greater than the maximum thickness of the cartilage. Since the cartilage surface on the patella is concave, there was almost no contact between the cartilage and the bottom of the petri dish which could have affected exposure to the solution. A piece of plastic wrap was draped over the petri dish to minimize evaporation. A 0 min control was simply dipped in the 1M DMSO solution and then swabbed with gauze; the other samples were also swabbed immediately after removing them from the DMSO solution after various exposure times. A full thickness slice of cartilage was then removed from the patella using a scalpel. This was punched with a #2 cork bore to remove a cylinder of cartilage of 5 mm diameter. The thickness of these cartilage cylinders ranged from 2.9 mm to 5.0 mm with an average of 4.1 mm. The cylinder was then placed in a plastic test tube containing 5 ml of deuterium oxide (D_2O), sealed and allowed to sit for 4 weeks at room temperature. Deuterium has no magnetic moment thus it is invisible to NMR. The principle of the experiment was to allow all the water and DMSO from the cartilage disk to diffuse out into the surrounding D_2O and then measure the amounts of water and DMSO that were present in the D_2O. The water peak from a D_2O control (measured to determine if there was contamination of the stock D_2O) was not large enough to be significant in this experiment. 1 ml of the solution was removed and placed in an NMR tube for ^{1}H-NMR analysis on a Bruker WH200 (Bruker, Carlsrhue, Germany). The absolute water and DMSO integrals from each sample were measured, allowing a comparison between samples. The DMSO integral from the 0 min control was subtracted from the sample DMSO integrals to account for residual DMSO that wasn't swabbed off efficiently (about 1% of the equilibrium concentration). The formula for determining the average concentration of DMSO within the cartilage is given in equation 2.

$$[DMSO] = \left[\frac{\dfrac{DMSO\ integral}{DMSO\ protons}}{\dfrac{H_2O\ integral}{H_2O\ protons}} \right] \cdot \frac{MW_{DMSO}}{\rho_{DMSO} \cdot 1000} + \frac{MW_{H_2O}}{\rho_{H_2O} \cdot 1000} \tag{2}$$

[DMSO]	= concentration of DMSO in sample (M)
DMSO integral	= integral of NMR signal produced by DMSO
H_2O integral	= integral of NMR signal produced by H_2O
DMSO protons	= number of protons in DMSO (=6)
H_2O protons	= number of protons in H_2O (=2)
MW_{DMSO}	= molecular weight of DMSO (= 78.1 g/mol)
MW_{H_2O}	= molecular weight of H_2O (= 18.0 g/mol)
ρ_{DMSO}	= density of DMSO (= 1.096 g/ml)
ρ_{H_2O}	= density of H_2O (= 1.0 g/ml)

The integrals of the NMR peaks are functions of the number of protons contributing to each peak. Therefore, the water peak must be divided by 2 and the DMSO peak must be divided by 6 to normalize the signals for the number of respective molecules. The mole ratio of $DMSO:H_2O$ is then multiplied by the volume of 1 mole of DMSO and the volume of 1 mole of water is added to get the concentration of DMSO in moles per liter of solution.

Results

The measured DMSO concentrations at 23°C are shown in Table 6.1. Triplicate samples were measured at each time interval up to one hour (where 5 samples were measured) and duplicate measurements were made thereafter. The data in Tables 6.1 and 6.2 clearly show that the concentration of DMSO in the cartilage reached an equilibrium value which was significantly lower than the concentration of DMSO in the bathing solution. This anomaly will be examined in detail in the discussion, however, in order to measure the kinetics of uptake, it is necessary to express the concentration of DMSO at a given time as a ratio over the equilibrium concentration of DMSO. This value is interpolated from the data in Table 6.1 to be 0.5 M which is used to normalize the data before plotting in figure 6.1. Performing a least squares fit to equation 1 for the data gathered at 23°C yields a diffusion coefficient of 1.01×10^{-5} m^2/s for DMSO in cartilage. Table 6.2 shows the measured DMSO concentrations at 4°C. The mean values are plotted in figure 6.2 following normalization to the equilibrium concentration of 0.42M. The reason for the difference in the equilibrium values will also be examined in the discussion. Fitting equation 1 to this data provides a diffusion coefficient of 1.25×10^{-5} m^2/s. The agreement between duplicate samples at both temperatures is illustrated by the very low values of the standard error of the mean as shown in the tables.

Table 6.1. DMSO concentration with time at 23°C.

time	mean [DMSO] (M)	n	std. error
5 min	0.0755	3	0.0021
10 min	0.116	3	0.0058
20 min	0.151	3	0.021
30 min	0.245	5	0.032
1 h	0.382	2	0.0045
2 h	0.414	2	0.038
3 h	0.472	2	0.031
4 h	0.438	2	0.010
5 h	0.460	2	0.008
6 h	0.488	2	0.013
8 h	0.503	2	0.012
20 h	0.477	2	0.021

Table 6.2. DMSO concentration with time at 4°C.

time	mean [DMSO] (M)	n	std. error
5 min	0.0540	3	0.014
10 min	0.102	3	0.0083
20 min	0.154	3	0.0046
30 min	0.208	3	0.044
1 h	0.271	2	0.0045
2 h	0.387	2	0.031
4 h	0.430	2	0.027
6 h	0.405	2	0.011
8 h	0.424	2	0.012
10 h	0.446	2	0.017
20 h	0.427	2	0.013

Discussion

The use of NMR to measure the diffusion of cryoprotectant is an accurate and useful technique. It allows a rapid determination of the amounts of various chemical species relative to water. In this experiment, the data thus produced for the diffusion of DMSO into articular cartilage have been used to measure a diffusion coefficient for DMSO within articular cartilage. If an analytical approach is to be used for designing protocols for cryopreserving tissues such as articular cartilage, the physico-chemical environment of the cells within the tissue must be understood during this process. Current strategies for cryopreservation of biological materials require the presence of cryoprotective compounds to reduce

injury during freezing and thawing (7). Thus it is necessary to be able to model the movement of these compounds within the tissue in order to be able to predict whether they will have a protective action.

The uptake of DMSO into articular cartilage was measured at two temperatures in order to determine the temperature dependence of the diffusion coefficient. The diffusion of DMSO in cartilage can be thought of as similar to diffusion of DMSO in water since the cartilage matrix is principally composed of water. Although the temperature dependence of diffusion of DMSO in water has not been measured, the self-diffusion coefficient of water has an Arrhenius activation energy of 4.3 kcal/mol (3) which would likely be close to that for DMSO in water. Using this activation energy to predict the difference in diffusion coefficients that were expected, the value measured at 23°C should have exceeded the value measured at 4°C by about 60%. The opposite trend was observed in which the diffusion coefficient measured at 4°C exceeded that measured at 23°C by about 24%. There is no physical basis for this result, therefore, it may be taken as a more appropriate indication of the error of the diffusion coefficients presented here than the standard errors presented in Tables 6.1 and 6.2. This error (which may be taken to be approximately +/- 50%) is most likely a result of the fact that diffusion in cartilage is assumed to follow the semi-infinite plane sheet model. This introduces a sensitive dependence on the thickness of the cartilage as the accumulation of solute against the impermeant plane at the back of the cartilage changes the concentration gradient measured as a function of depth beneath the surface. The thickness of cartilage varied widely among animals (this was not a function of depth at which the cartilage was cut as these cuts followed the bone very closely) which most likely introduced significant errors into our measurements due to the small number of replicate samples tested for each condition.

Other methodological problems also surfaced, principally as the technique of allowing the DMSO to diffuse out of the cartilage disk before measuring its concentration in the bathing medium. Ideally, the entire tissue that is to be measured should be placed into the magnet so that the internal concentration can be measured. For simplicity, however, the amount of water and DMSO that diffused back out of the cartilage was measured in this experiment. Since the amount of DMSO that diffused out of the cartilage was only about half of what would have been the equilibrium value, it is possible that some irreversible process occurs within the cartilage which prevents the substance from diffusing back out of the cartilage. Maroudas has found this to be the case for ethanol and methanol (5). The principal reason for this discrepancy, however, is probably due to the slightly acidic nature of the DMSO protons. This will result in an exchange of DMSO protons for deuterium nuclei. The rate of this exchange is expected to be very slow, although the four week incubation period that was used in this experiment is probably long enough to allow significant turnover. The differences between the equilibrium values from the 23°C experiment and the 4°C experiment are probably due to the different waiting periods that were a

consequence of scheduling difficulties for the NMR machine. Since the rate of exchange will be the same for all samples and the incubation time was also constant within each temperature group, there should be no effect on the measured diffusion coefficient (the discrepancy is dealt with here by normalizing the data to the equilibrium value) since this is strictly dependent on the kinetics of uptake. It would be useful, though, to know what the true equilibrium concentration of DMSO inside the cartilage matrix is so that modeling of the interior physico-chemical environment during freezing and thawing could be more accurate.

Maroudas has derived an equation (eq. 3) to determine the diffusion coefficient of a substance within cartilage using a tortuosity factor and the diffusion coefficient of the substance in water (6). Using an estimated diffusion coefficient for DMSO in water (the estimate is based on the molecular weight of DMSO), the diffusion coefficient predicted by Maroudas' tortuosity factor is about one half of the value that was measured in the present experiment. Given the uncertainty of the estimate of the diffusion coefficient for DMSO in water, no conclusions can be drawn as to the precision of Maroudas' equation from this data.

$$D_c = D_{H_2O} \frac{H}{\lambda^2} \tag{3}$$

D_c = diffusion coefficient in cartilage
D_{H_2O} = diffusion coefficient in water (est. at 1.0×10^{-5} cm^2/s)
H = water content of cartilage (78% [6])
λ = tortuosity factor (1.4 [6])

Figure 6.3 shows calculations of DMSO permeation into cartilage using equation 1 with the measured diffusion coefficient. The calculations were performed for five different exposure times for each of four thicknesses. The times were chosen to illustrate the kinetics of permeation over the full spectrum from a near zero concentration at the bone to the situation in which equilibrium is established. These figures can be used to design protocols for adding DMSO to articular cartilage of various thicknesses. Since the diffusion coefficient appears to be independent of temperature in the range of 4°C to 23°C, these calculations should be adequate for all protocols within this range. The permeation of DMSO into the chondrocytes, however, will be highly dependent of temperature, so any addition protocols that are carried out at low temperatures should account for this phenomenon.

The problem of determining if a cryoprotectant has been successfully added to a tissue is more difficult than for adding cryoprotectant to a cell suspension. The results of this experiment provide the necessary tools to overcome this problem for articular cartilage. The combination of the diffusion

coefficient for DMSO in cartilage and the demonstration of the relative independence of temperature on this value allows the calculation of diffusion of DMSO into cartilage at a given temperature. This is important if DMSO is to be used as a cryoprotectant as equilibration will be necessary before freezing so that the DMSO can act throughout the tissue. It should be noted that the permeability of the chondrocytes is strongly temperature dependent and so even though the concentration of DMSO in the matrix will be independent of temperature, the concentration of DMSO within the chondrocytes will be greatly slowed at lower temperatures. This must be taken into account when designing protocols for the cryopreservation of cartilage.

References

1. Crank, J. 1975. The Mathematics of Diffusion, 2nd ed. Oxford University Press, New York. pp. 46-49.

2. Fuller, B., Busza, A. and Proctor, E. 1989. Studies on Cryoprotectant Equilibration in the Intact Rat Liver Using Nuclear Magnetic Resonance Spectroscopy: A Noninvasive Method to Assess Distribution of Dimethyl Sulfoxide in Tissues. *Cryobiology* **26**:112-118.

3. House, C.R. 1974. Water Transport in Cells and Tissues. Edward Arnold, Ltd. London, England. pp. 20-21.

4. Maroudas, A., Bullough, P., Swanson, S. and Freeman, M. 1968. The Permeability of Articular Cartilage. *Journal of Bone and Joint Surgery* **50B**:166-177.

5. Maroudas, A. 1970. Distribution and Diffusion of Solutes in Articular Cartilage. *Biophys. J.* **10**:365-379.

6. Maroudas, A. 1979. Physico-chemical Properties of Articular Cartilage, in *Adult Articular Cartilage*, 2nd ed. Pitman Medical. pp. 131-170.

7. Mazur, P. 1984. Freezing of Living cells: Mechanisms and Implications. *Am. J. Physiol.* **247**, C125-C142.

8. Muldrew, K., Novak, K., Hurtig, M., Schachar, N. and McGann, L. 1992. Localization of Cellular Injury in Articular Cartilage During Cryopreservation. *Cryobiology* **29**:704-705.

9. Schachar, N. and McGann, L. 1991. Cryopreservation of Articular Cartilage, in *Bone and Cartilage Allografts: Biology and Clinical Applications*, Friedlaender and Goldberg, editors, American Academy of Orthopaedic Surgeons. pp. 211-230.

10. Taylor, M. and Busza, A. 1992. A Convenient, Non-invasive Method for Measuring the Kinetics of Permeation of Dimethyl Sulphoxide into Isolated Corneas Using NMR Spectroscopy. *Cryo-Letters* **13**:273-282.

Kinetics of DMSO Uptake in Porcine Cartilage at 23°C
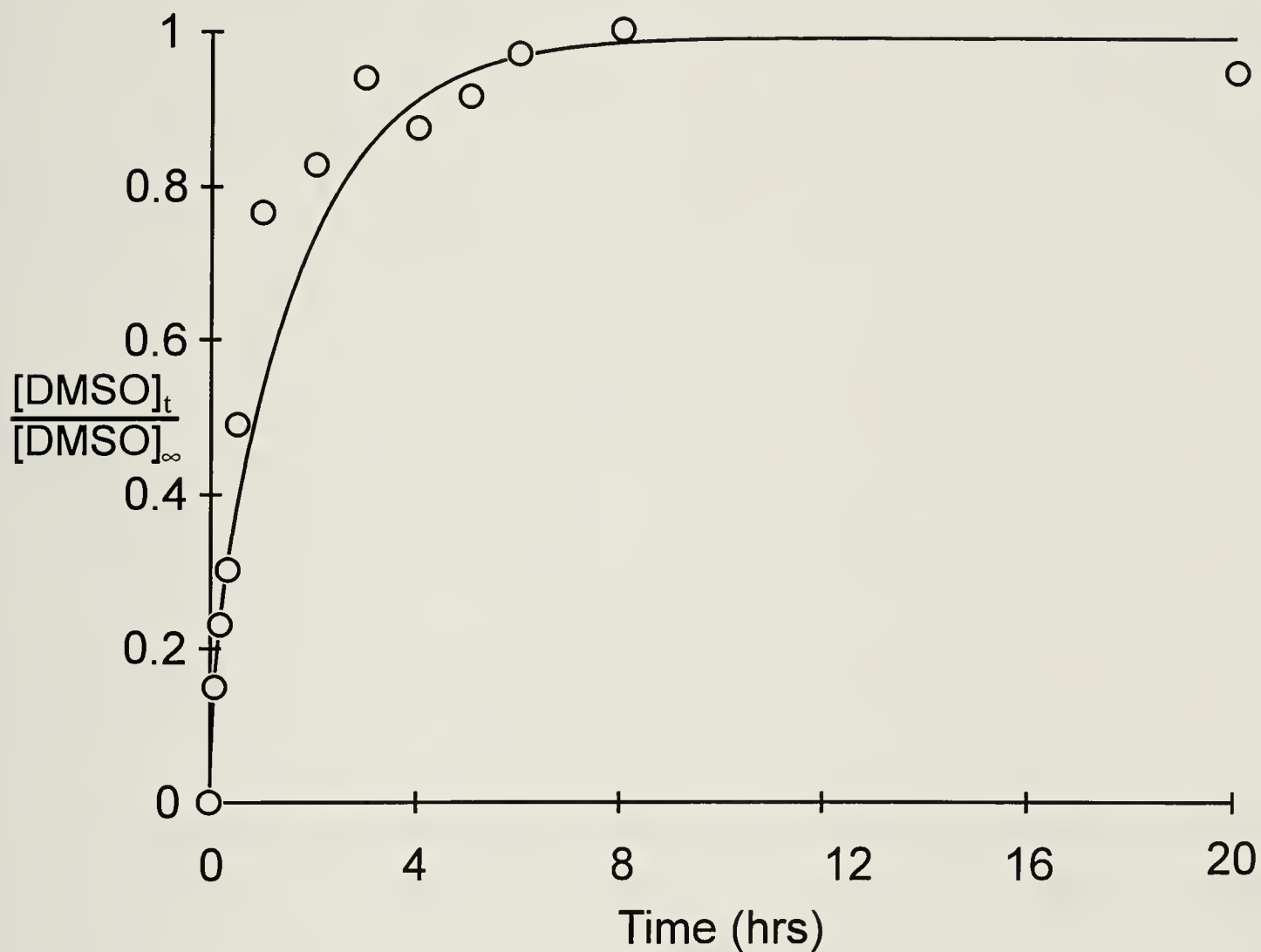
Figure 6.1.
The uptake of DMSO into Porcine articular cartilage (average thickness = 4.1 mm) is shown at intervals up to 20 hrs at a temperature of 23°C. The solid line is the least squares fit of equation 1 which yields a diffusion coefficient of 1.01×10^{-5} m^2/s. The data has been normalized by assuming an equilibrium concentration within the cartilage of 0.5 M DMSO.
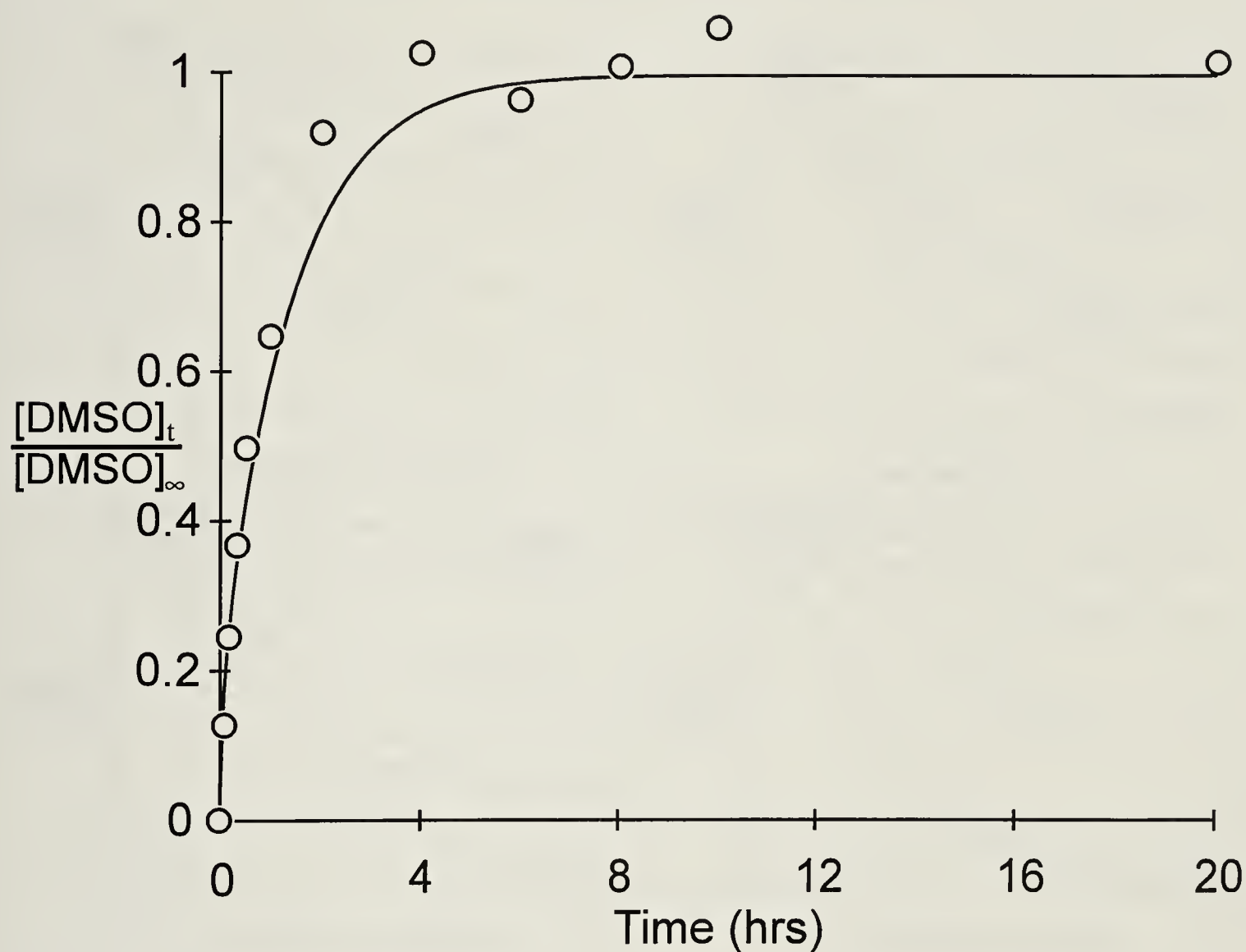
Figure 6.2.
The uptake of DMSO into Porcine articular cartilage (average thickness = 4.1 mm) is shown at intervals up to 20 hrs at a temperature of 4°C. The solid line is the least squares fit of equation 1 which yields a diffusion coefficient of 1.25×10^{-5} m^2/s. The data has been normalized by assuming an equilibrium concentration within the cartilage of 0.42 M.

Calculation of DMSO Concentration Profile
For Various Thicknesses of Articular Cartilage
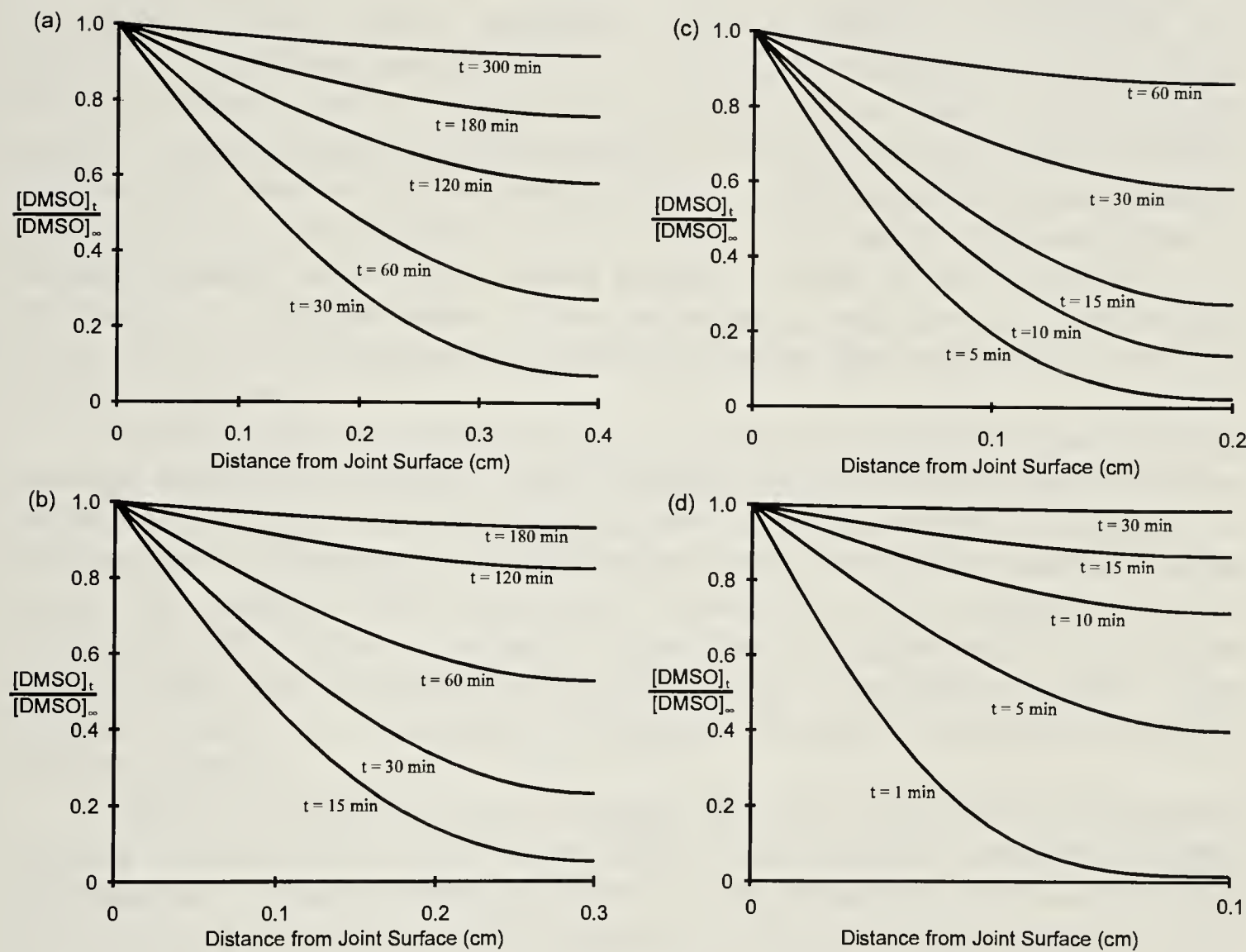
Figure 6.3.
Predictions of the concentration profile of DMSO within articular cartilage of various thicknesses are shown as a function of time of exposure. Thicknesses of 1 mm (a), 2mm (b), 3mm (c) and 4mm (d) are shown as they represent the range of thickness usually encountered in human articular cartilage. The abscissa represents the cross-section of the cartilage matrix with the joint surface at 0 and the bone interface at the furthest point to the right. The simulations are for diffusion at 23°C.

Chapter 7

<u>Localization of Freezing Injury in Articular Cartilage</u>*

Introduction

Surgical treatment of traumatic injuries, arthritis, osteonecrosis or metaphyseal bone tumors frequently requires biologic reconstruction and resurfacing of articular surfaces (10), creating a clinical need for cryopreserved articular cartilage both for biologic joint replacement as well as repair of focal lesions. In centers where joint transplantation using bone and cartilage allografts is carried out, this is a preferred method (12, 10), although a gap exists between the demand and the supply of suitable tissue. Successful cryopreservation of cartilage-bearing bone grafts would enable a bank of donor tissue to be maintained for transplantation. The advantages of long term banking are that the tissue can be screened for infectious diseases and matched for size and surface congruency.

Current techniques of freezing and thawing bone with articular cartilage surfaces are widely believed to result in lethal injury to chondrocytes within the cartilage. It is likely that appreciable survival of chondrocytes is necessary for the long-term maintenance of the articular surface given the relatively large volume of cartilage matrix that each chondrocyte must maintain and the apparently limited ability of cartilage to repair itself or regenerate (1). Early work demonstrating the possibility of cryopreserving chondrocytes isolated from articular cartilage (11,13) has lead us to pursue the goal of cryopreserving intact articular cartilage.

Work in our laboratory has previously focused on the basic cryobiology of isolated chondrocytes (7,8,9). In this study, intact articular cartilage has been subjected to a graded freezing process in the presence and absence of a cryoprotectant to determine the response of the chondrocytes *in situ* to the stresses of freezing and thawing. The graded freezing technique has been used with many cellular systems (5,6) to elucidate the conditions under which slow freezing injury (often referred to as solution effects injury) and rapid freezing injury (usually associated with intracellular freezing) occur. The technique involves cooling cells slowly and removing paired samples at specified temperatures: one sample is then warmed while the other is plunged into liquid nitrogen.

Articular cartilage has three morphologically distinct layers, as shown in figure 7.1, which are parallel to the articular surface (1). The superficial layer consists of the outermost 5-10% lying just below the articular surface. The cells are slightly flattened and more densely packed than in the other layers. In the

---

* A version of this chapter has been submitted for publication. Muldrew, Hurtig, Novak, Shachar & McGann 1993. *Cryobiology*.

110

middle is the intermediate layer in which the cells are spherical and evenly spaced and appear to follow the arched paths of the collagen fibers. The intermediate layer consists of about 40-50% of the tissue. The deep layer consists of the 40-50% of the cartilage that is adjacent to the bone. The cells are spherical and arranged in columns which are perpendicular to the bone-cartilage interface. Using a vibratome to section the tissue after freezing and thawing, we were able to correlate cell recovery with position in the tissue.

The purpose of these experiments is to determine the conditions under which chondrocytes are injured during freezing and thawing of intact cartilage. The nature of the injury and the location of this injury will allow us to assess current practices in clinical cryopreservation of cartilage as well as suggesting strategies for improving these practices.

Materials and Methods

Fresh ovine femoral condyles were obtained from a slaughterhouse and osteochondral dowels (10 mm in length) were extracted using a multi-directional gimbaled aiming device mounted on a vice (which allows the target bone specimen to be held tightly with four adjustable screws). The coring bit (10mm inside diameter) is directed through the aiming device such that it will cut perpendicular to the articular surface of the bone. This apparatus is very precise and rigid, allowing removal of a core without damage to the core or the surrounding articular surface. It has been adapted and customized based on parts from the Concept Allograft Kit (Concept Inc., Largo, Florida, USA). The dowels thus obtained were immediately placed in an isotonic solution (150 mmol/l) of phosphate buffered saline (PBS). Before freezing, some of the dowels were equilibrated in 10% (wt/wt) dimethyl sulfoxide (DMSO) in isotonic PBS for 30 min at 23°C. All plugs were frozen in 10 ml plastic test tubes with either 2 ml of isotonic PBS or 2 ml of 10% DMSO/isotonic PBS. The test tubes were cooled at 1°C/min in a programmable alcohol bath (ice formation was seeded by inserting a copper wire that had been cooled in liquid nitrogen into the sample; this was done at -2°C for the isotonic PBS and at -5°C for the 10% DMSO/isotonic PBS). Pairs of tubes were removed from the alcohol bath at -5, -10, -15, -20, -25, -30 and -40°C: one was placed in a 37°C water bath and warmed immediately, while the other was plunged in liquid nitrogen, stored for a minimum of 1 hour (to allow temperature equilibration) and then warmed in a 37°C water bath. Each condition was performed in triplicate. After warming, the plugs were sliced on a TPI Vibratome 1000 (TPI, inc., St. Louis, Missouri): 70 µm thick serial sections were cut perpendicular to the articular surface, extending to the bone. The full thickness cartilage was then removed from the bone with a scalpel and assayed for freeze-thaw injury. The plasma membrane is the primary site of freeze-thaw injury in most cellular systems (4), so paravital staining was used to indicate whether the procedure had violated the integrity of the membrane. Several 70 µm slices were mounted on a microscope slide with

fluorescein diacetate (FDA - 10 µM) and ethidium bromide (EB - 10 µM) and incubated in the dark at 37°C for 10 min. The samples were then viewed on a Zeiss fluorescent microscope using ultraviolet illumination (440-480 nm). The images were saved on VHS video tape for later analysis.

The images on the video tape were digitized using a TARGA+ board (Truevision, Indianapolis, Indiana) installed in an IBM personal computer and a custom program was used to allow the operator to divide the image into the superficial, intermediate and deep layers and then count the cells in each layer that stained green (FDA) or orange (EB). Since the number of cells that were counted varied widely among samples, a weighting function, based on the number of cells in each sample, was used to determine the mean value of recovery and the standard error of the mean.

Results

Figure 7.2 shows the overall recovery of chondrocytes, irrespective of position in the matrix, for the four conditions. The pattern that emerges is very similar to cellular systems (5) in which there is a decline in recovery with decreasing temperature (the temperature in this case refers to the minimum temperature reached during slow cooling) in the group that is directly warmed, which is significantly lessened by the presence of DMSO. The groups that are plunged in liquid nitrogen gradually increase in recovery with decreasing temperature (the temperature reached before plunging). The two types of injury (the solution effects injury that occurs during slow cooling and the rapid cooling injury that occurs during plunging) are additive, so the recovery of the group that is plunged in liquid nitrogen does not exceed the recovery of the group that is warmed. The presence of DMSO has little effect on recovery in the plunged group.

For samples cooled without cryoprotectant, figure 7.3 shows chondrocyte recovery as a function of position in the tissue and the minimum temperature reached before warming. The recovery in the superficial layer and the deep layer are similar while there is almost no recovery in the intermediate layer below -5°C. In the group plunged into liquid nitrogen, figure 7.4 shows that, again, the superficial and deep layers exhibit similar recoveries while the intermediate layer shows almost no recovery under any conditions.

For samples equilibrated with 10% DMSO, figure 7.5 shows recovery as a function of position for the group that was warmed directly but equilibrated with DMSO. Again, the pattern of similar results in the superficial and deep layers but much lower recovery in the intermediate layer is repeated. In this case, however, there is some recovery in the intermediate layer whereas without DMSO there was virtually none. Figure 7.6 shows recovery versus position for the group with DMSO that was plunged in liquid nitrogen. In this group, the deep layer shows some recovery at the higher temperatures (where rapid freezing injury is greatest), and then at the lower temperatures, the superficial and deep

layers show similar recoveries. The intermediate layer shows the poorest recovery throughout.

Fresh, untreated controls showed FDA positive staining of 90% and unfrozen controls exposed to 10% DMSO for 30 min. showed 97% FDA positive staining (the 7% difference is due to variation between donors). The recoveries of the experimental groups that were not exposed to DMSO are expressed as percent of fresh control and the groups that were exposed to DMSO are expressed as percent of DMSO control.

Discussion

The data in figure 7.2 demonstrate that at least two types of freezing injury are acting on the chondrocytes within the cartilage: one associated with slow cooling and one associated with rapid cooling. This situation is similar to the results obtained with the graded freezing technique applied to isolated cells in suspension (5). The cartilage matrix thus acts like a physiological solution during freezing (this is not unreasonable as the matrix is over 80% water (3)). This result is significant since it allows modeling of the physico-chemical events that occur during freezing within the matrix. This may be crucial in understanding the position-dependent nature of injury that is observed, the simplest explanation of which is that the chondrocytes in the intermediate layer are distinguished from those in the deep or superficial layers by being more susceptible to freeze-thaw injury. This hypothesis can only be accepted if the stresses that the chondrocytes face are not maximized in the intermediate zone. Modeling of solvent and solute movements within the matrix would indicate whether conditions in the intermediate layer are more damaging than in the other layers.

There are several physical variables which vary with position in the tissue during the freezing and thawing procedure. A primary variable is the kinetics of DMSO permeation. Insufficient permeation would provide cryoprotection to the superficial layer, with recovery expected to decrease with distance into the tissue. The observation of cryoprotection of chondrocytes in the deep zone indicates that an exposure of 30 min. at 23°C was sufficient for adequate DMSO permeation. Differential rates of cooling could also cause injury to be localized. Because of the thermal mass of a tissue, the rate of cooling will not be uniform throughout the tissue; the center will lose heat more slowly than the edges. If the cooling rates were significantly different between the superficial layer and the deep layer, then the injury to the respective cell populations could also differ significantly. The combination of these factors could explain the localization of injury in the intermediate zone in the following manner: if the cooling rate of the deep zone was optimal so that high recovery was obtained in this zone and the penetration of DMSO into the cartilage was restricted to the superficial zone to give high recovery in this area, then the intermediate zone would show the poorest recovery. Such combinations of physico-chemical events within a tissue

can have complex interactions which can only be appreciated by modeling or direct measurement.

Indirect evidence supports the hypothesis that the chondrocytes of the intermediate layer are more susceptible to injury than those of the other two layers (hence the localization of injury has a biological and not a biophysical cause). If the physico-chemical conditions are the principal variables responsible for the observed differences, then the thickness of the cartilage should be an important determinant of chondrocyte recovery. The variation in thickness of articular cartilage among donors differed by as much as a factor of five in samples where injury was specific to the intermediate layer. Thus the conditions in the deep layer of a sample in which the cartilage is 1 mm thick may be similar to those in the superficial or intermediate layers of a sample in which the cartilage is 5 mm thick. Since the sensitivity of the intermediate layer does not appear to correlate with the thickness of the cartilage, it seems likely that the sensitivity is a result of differences in the cells themselves or their environment in the intermediate layer. Maroudas (14) has investigated the chemical composition of the morphological zones of articular cartilage and found the following depth dependent variations: the water content of the superficial zone is highest with a steady decrease with increasing depth below the joint surface; the collagen content decreases sharply in going from the superficial zone to the intermediate zone and continues decreasing gradually to the deep zone; and proteoglycan content gradually increases with increasing depth below the joint surface, reaching its highest levels in the deep zone.

There is currently a clinical need for focal reconstruction of joint surfaces as, for instance, in osteochondritis dissecans in juveniles (2). The results of this study show that banking of osteochondral dowels with high recovery of chondrocytes within the cartilage is possible and this could be used as a source of material for allografts. Since the recovery of chondrocytes has considerable variability between donors, we recommend that clinical application based on the techniques described here should use two dowels from the same donor, one as a quality control, to ensure a high recovery in the material to be transplanted. Although the results of this study have shown this to be a technique which could now be put into clinical use, efforts should be made to improve the efficiency of the technique as no attempt at optimization has yet been made. Given the expense of harvesting and the difficulty in obtaining human tissue, this goal should be pursued without delay.

References

1. Fulkerson, J., Edwards, C. and Chrisman, O. 1987. Articular Cartilage. *In* "The Scientific Basis of Orthopaedics" (Albright and Brand, editors), pp. 347-371. Appleton & Lange, Norwalk, Connecticut.

2. Garret, J. 1986. Treatment of Osteochondral Defects of the Distal Femur with Fresh Osteochondral Allografts: a Preliminary Report. *Arthroscopy* **2**: 222-226.

3. Maroudas, A. 1979. Physico-chemical Properties of Articular Cartilage, *In* "Adult Articular Cartilage", 2nd ed. pp. 131-170. Pitman Medical.

4. Mazur, P. 1984. Freezing of Living cells: Mechanisms and Implications. *Am. J. Physiol.* **247**: C125-C142.

5. McGann, L. 1979. Optimal Temperature Ranges for Control of Cooling Rate. *Cryobiology* **16**: 211-216.

6. McGann, L. 1978. Differing Actions of Penetrating and Nonpenetrating Cryoprotective Agents. *Cryobiology* **15**: 382-390.

7. McGann, L., Stevenson, M., Muldrew, K. and Schachar, N. 1988. Kinetics of Osmotic Water Movement in Chondrocytes Isolated from Articular Cartilage and Applications to Cryopreservation. *J. Orthop. Res.* **6**: 109-115.

8. McGann, L., Muldrew, K. and Schachar, N. 1990. Freezing Injury in Isolated Chondrocytes During Rapid Cooling; in Proceedings of the 24th annual meeting of the Canadian Orthopaedic Research Society.

9. McGann, L., Mcallister, D., Muldrew, K. and Schachar, N. 1988. Permeability of Isolated Chondrocytes to Dimethyl Sulfoxide; in Proceedings of the 22nd annual meeting of the Canadian Orthopaedic Research Society.

10. Schachar, N. and McGann, L. 1991. Cryopreservation of Articular Cartilage, *In* "Bone and Cartilage Allografts: Biology and Clinical Applications" (Friedlaender and Goldberg, editors), pp. 211-230. American Academy of Orthopaedic Surgeons, Park Ridge, Illinois.

11. Smith, A. 1965. Survival of Frozen Chondrocytes Isolated from Cartilage of Adult Mammals. *Nature* **205**: 782-784.

12. Stauffer, R. 1991. Problems with Using Metallic Implants for Replacement of Bony Defects, *In* "Bone and Cartilage Allografts: Biology and Clinical Applications" (Friedlaender and Goldberg, editors), pp. 295-299. American Academy of Orthopaedic Surgeons, Park Ridge, Illinois.

13. Tomford, W., Duff, P. and Mankin, H. 1985. Experimental Freeze-Preservation of Chondrocytes. *Clin. Orthop.* **197**: 11-14.

14. Venn, M. and Maroudas, A. 1977. Chemical Composition and Swelling of Normal and Osteoarthrotic Femoral Head Cartilage. II. Chemical Composition. *Annals of the Rheumatic Diseases* **36**: 121-129.

Morphology of Articular Cartilage

Superficial Zone

Intermediate Zone

Deep Zone

Tidemark

Calcified Zone
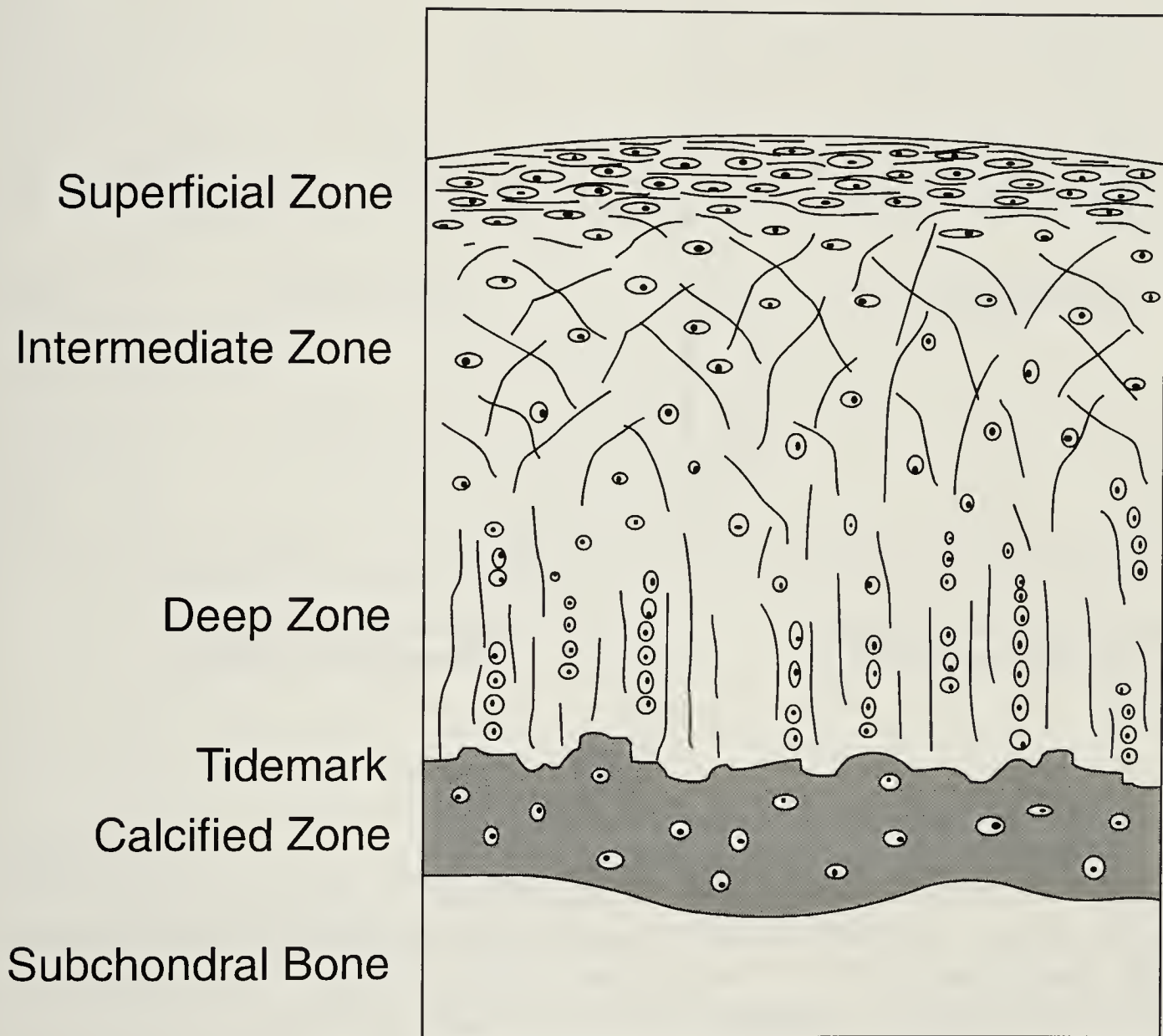
Subchondral Bone

Figure 7.1.
This schematic representation of a cross-section of articular cartilage illustrates the distinct morphological zones which were used to localize the injury of freezing and thawing. The shape and distribution of the chondrocytes as well as the alignment of the collagen fibers differs in each of the three zones of non-calcified cartilage.
(Adapted from ref. 1)

Recovery of Chondrocytes Following Graded Freezing
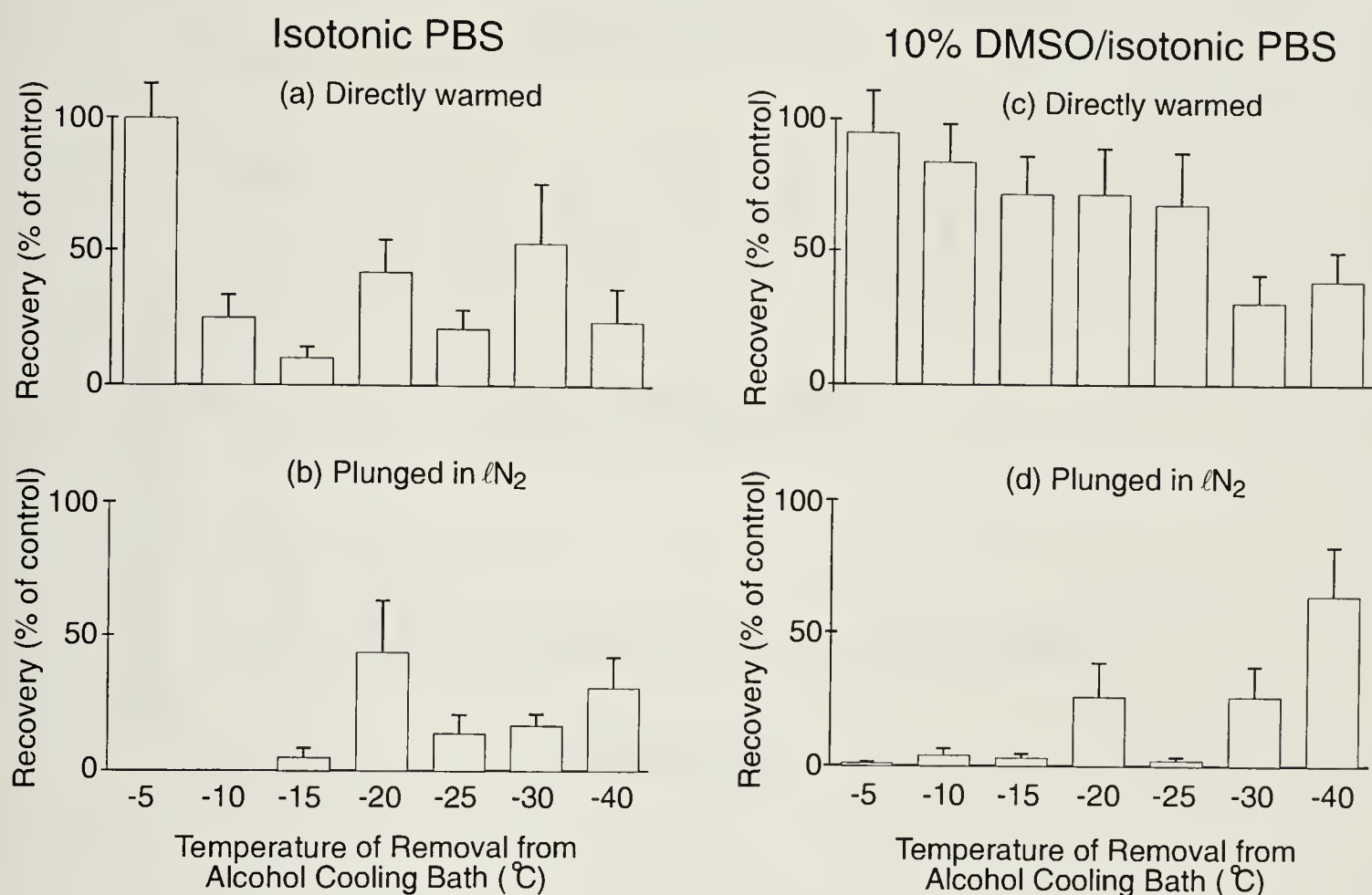
Figure 7.2.
The percent recovery of chondrocytes is shown as a function of temperature reached during 1°C/min cooling for each of four conditions: (a) the cartilage is suspended in an isotonic solution and placed in a 37°C water bath after the minimum temperature is reached; (b) the cartilage is suspended in isotonic media but upon reaching the minimum temperature, the sample is placed in liquid nitrogen for 1-3 hours before thawing in a 37°C water bath; (c) the cartilage is suspended in isotonic media with 10% w/w DMSO added and thawed in a 37° C water bath upon reaching the minimum temperature; (d) the cartilage is suspended in isotonic media with 10% w/w DMSO added and is placed in liquid nitrogen for 1-3 hours after reaching the minimum temperature during slow cooling before thawing in a 37°C water bath. The error bars denote the standard error of the mean weighted for sample size (n = 3).

Localization of Injury Following Direct Warming Without Cryoprotectant
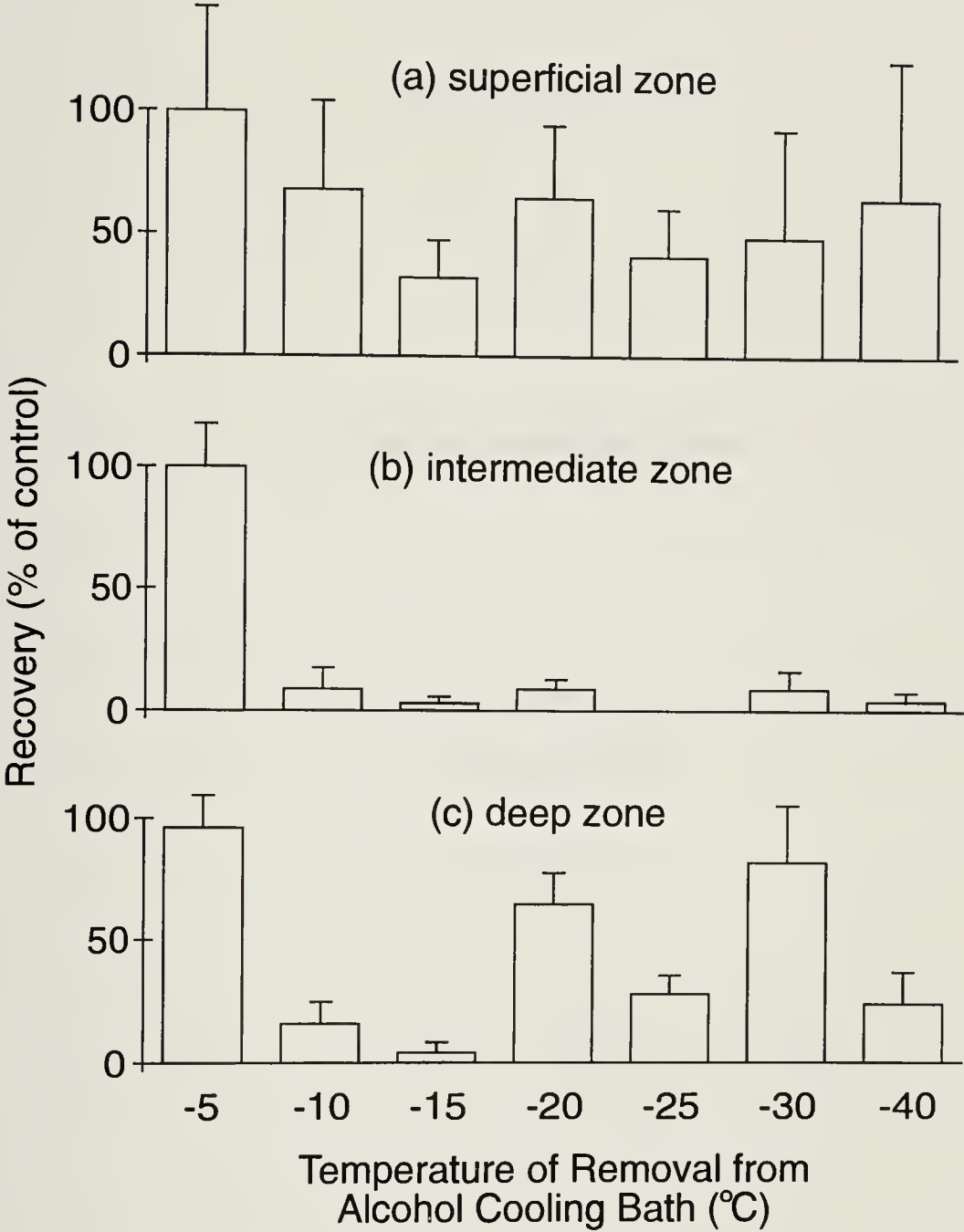
Figure 7.3.

The percent recovery of chondrocytes, *in situ*, suspended in isotonic media and warmed in a 37°C water bath directly after reaching the minimum temperature during cooling at 1°C/min is shown as a function of the minimum temperature reached for each morphological region of cartilage. (a) shows the recovery of the superficial zone, (b) shows the recovery of the intermediate zone and (c) shows the recovery of the deep zone. The error bars denote the standard error of the mean weighted for sample size (n = 3).

Localization of Injury Following Plunging in Liquid Nitrogen Without Cryoprotectant

Figure 7.4.
The percent recovery of chondrocytes, *in situ*, suspended in isotonic media and then plunged in liquid nitrogen (and held there for 1-3 hours) after reaching the minimum temperature during cooling at 1°C/min, after which they were warmed in a 37°C water bath is shown as a function of the minimum temperature reached for each morphological region of cartilage. (a) shows the recovery of the superficial zone, (b) shows the recovery of the intermediate zone and (c) shows the recovery of the deep zone. The error bars denote the standard error of the mean weighted for sample size (n = 3).

Localization of Injury Following Direct Warming With Cryoprotectant

(a) superficial zone

(b) intermediate zone

(c) deep zone

Recovery (% of control)

Temperature of Removal from Alcohol Cooling Bath (°C)
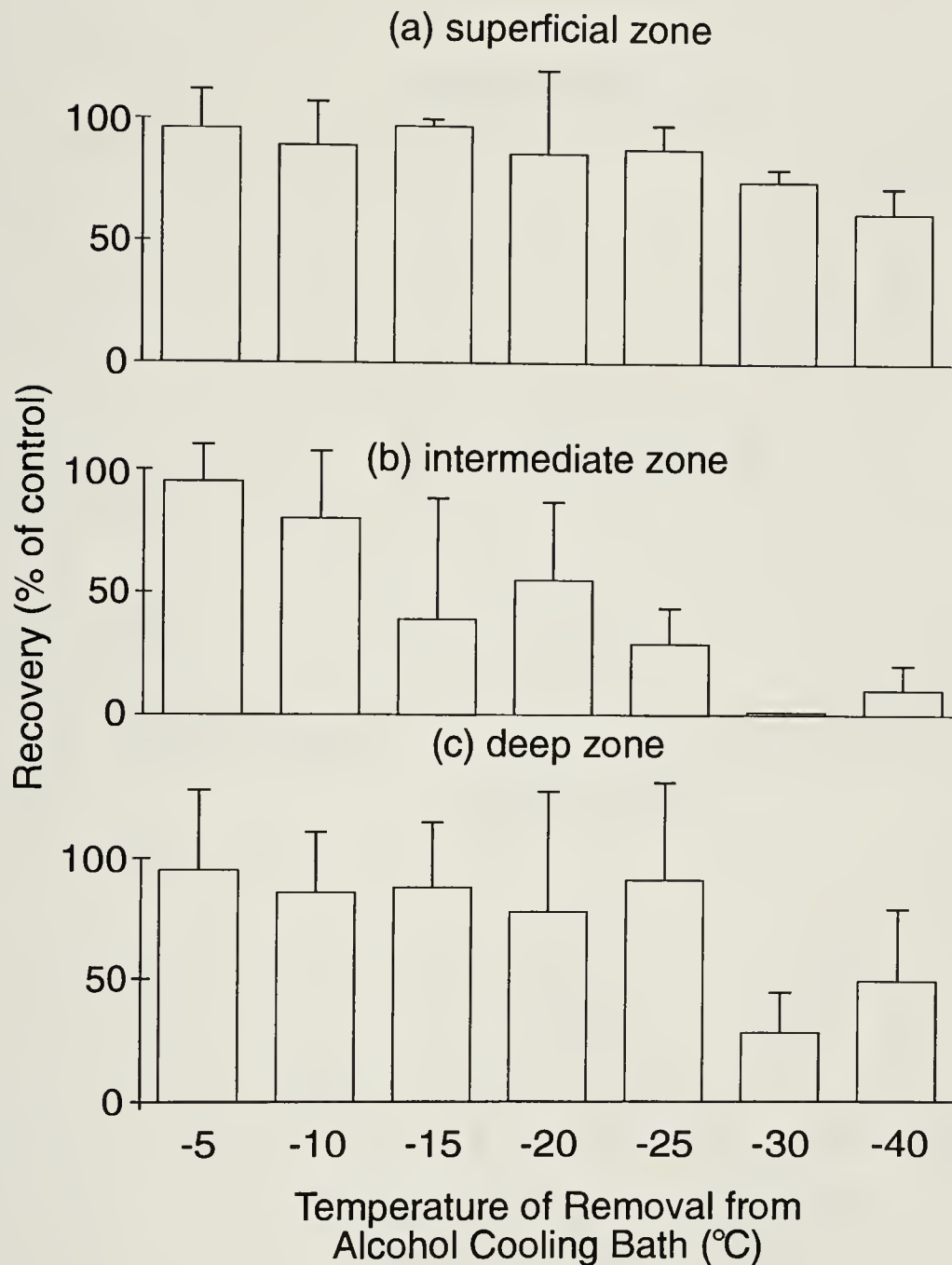
Figure 7.5.
The percent recovery of chondrocytes, *in situ*, suspended in isotonic media with 10% w/w DMSO added and warmed in a 37°C water bath directly after reaching the minimum temperature during cooling at 1°C/min is shown as a function of the minimum temperature reached for each morphological region of cartilage. (a) shows the recovery of the superficial zone, (b) shows the recovery of the intermediate zone and (c) shows the recovery of the deep zone. The error bars denote the standard error of the mean weighted for sample size (n = 3).

Localization of Injury Following Plunging
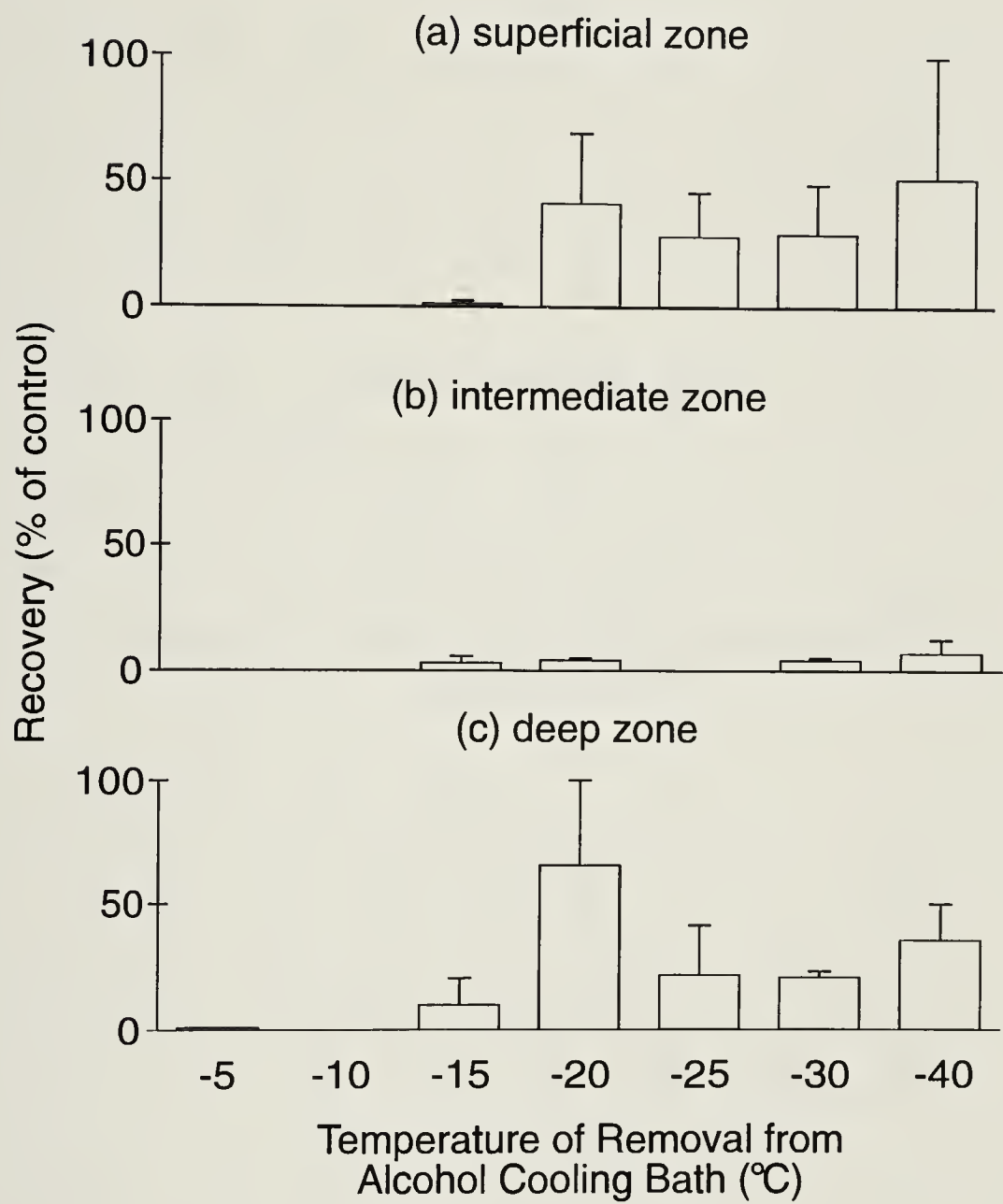in Liquid Nitrogen With Cryoprotectant
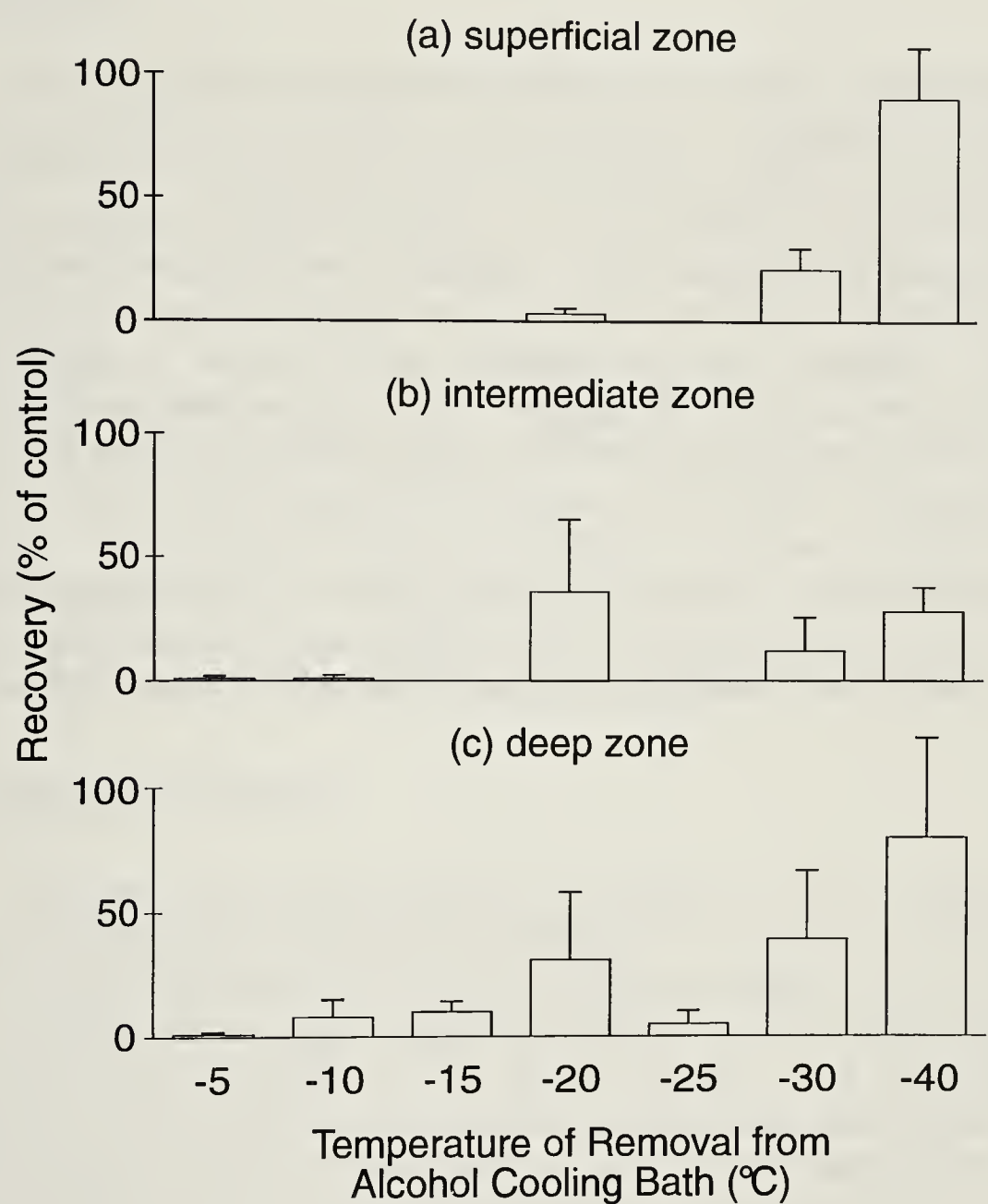
Figure 7.6.
The percent recovery of chondrocytes, *in situ*, suspended in isotonic media with 10% w/w DMSO added and then plunged in liquid nitrogen (and held there for 1-3 hours) after reaching the minimum temperature during cooling at 1°C/min, after which they were warmed in a 37°C water bath is shown as a function of the minimum temperature reached for each morphological region of cartilage. (a) shows the recovery of the superficial zone, (b) shows the recovery of the intermediate zone and (c) shows the recovery of the deep zone. The error bars denote the standard error of the mean weighted for sample size (n = 3).

Chapter 8

Simulation of Optimal Cryopreservation Protocol for Articular Cartilage

Introduction

We are now in a position to apply the osmotic rupture hypothesis to the problem of finding an optimal cryopreservation strategy for articular cartilage. The diffusion of a cryoprotectant (in this case DMSO) into the cartilage matrix and the resulting osmotic stresses can be modeled as can the osmotic stresses that will be present during freezing. The magnitude of these stresses can be used with the osmotic rupture hypothesis to predict damage. Thus, we can use a computer to search for a protocol that will minimize the injury due to cryoprotectant addition and rapid freezing. Since the osmotic rupture hypothesis cannot be used to predict solution effects injury (slow cooling injury), it would seem to be a trivial problem: the slower the cooling, the higher the predicted recovery. It was demonstrated in chapter 7, however, that the solution effects injury is appreciable at a cooling rate of 1°C/min. The optimization, then, is to find the quickest way of going from the freezing point to storage temperatures so that the time spent in high concentrations of solutes is minimized.

Assumptions of Model

Several assumptions need to be made for any implementation of this model. The following have been developed to provide a protocol which could be used in a clinical situation for human articular cartilage. The cartilage is taken to be 3 mm thick. The cryoprotectant that will be used is DMSO which should have a minimum concentration in the tissue of 1M. It is assumed that thermal gradients do not exist in the cartilage -- this is only reasonable for the case of osteochondral dowels, in which the mass of bone underlying the cartilage is not large enough to serve as a heat reservoir at slow cooling rates. The cartilage matrix is assumed to behave as a physiological solution which can be described, during freezing, by the equations developed by Pegg (1) for the ternary solution DMSO, NaCl, H_2O. A corollary of this assumption is the conjecture that ice forms within the cartilage at the same temperature as it forms in the external solution. Since the results presented in chapter 4 suggest that there may be some error associated with modeling concentrated DMSO solutions, the parameters which are used in the osmotic rupture equation are taken solely from the constant cooling experiments of chapter 5. These data reflect the actual response of the chondrocytes to constant cooling in the presence of DMSO and should, therefore, provide the most suitable basis for this simulation. The population of chondrocytes in articular cartilage (and their local chemical

environments) are presumed to be homogeneous. The evidence from chapter 7 indicates that this may well be false, however, this evidence only suggests a position dependent sensitivity to solution effects injury; the response to rapid cooling may not show similar results. The final assumption is that negligible injury occurs once the tissue has reached -80°C.

Optimization Approach

The approach that will be taken is to follow seven representative cells (each one taken from a particular depth in the cartilage) through the cryopreservation protocol, using the permeability and osmotic rupture parameters that were measured for isolated chondrocytes to predict the magnitude of injury for a particular protocol. The outermost cell is assumed to be 100 μm below the surface, and the rest are distributed at 500 μm intervals to the cartilage-bone interface. The addition of DMSO is modeled using the diffusion coefficient for DMSO in the matrix that was measured in chapter 6 and is done in a single addition step. A maximum of 60 min was allowed for DMSO equilibration to reduce the possibility of chemical toxicity. The DMSO concentration for each of the seven cells at the end of this time period was used in the cryopreservation simulation. To keep the protocol as simple as possible (so that it may be used clinically), the freezing procedure was limited to two steps with constant cooling rates in each step. The two cooling rates as well as the transition temperature are the parameters that were optimized by the computer simulation. An upper limit of 100°C/min was set on the cooling rates as it is unlikely that faster rates could be achieved without specialized equipment.

Criteria for Success

The program minimizes the maximum probability of rupture for each of the seven representative cells during both cooling rates while also minimizing the total time spent cooling to -80°C. The function that was used to relate these two parameters was to sum the squares of the maximum levels of injury and then multiply this value by the total time taken during cooling. The resulting value was minimized by the program by altering the two cooling rates and the transition temperature. The complete source code to the program that was used is listed in appendix 2; the interested reader may use this to see exactly how the model was implemented or to explore the model with different assumptions or criteria.

Results

It was found that the cartilage had to be placed in at least a 2M solution of DMSO in order to achieve a concentration of at least 1M at the cartilage-bone interface. Modeling the water flux upon plunging in 2M DMSO showed that the damage for the cell 100 μm below the surface was less than 10% and this fell to

less that 5% for the cell that was 500 μm below the surface. The concentration profiles for each cell as a function of time are shown in figure 8.1. The concentrations of DMSO for each of the cells at 60 min were used in the simulation of the freezing response in the simulation. The protocol that the program converged on was an initial cooling rate of 2.6°C/min to -24.4°C, followed by a cooling rate of 98.4°C/min to the final temperature of -80°C. Table 8.1 shows the predicted levels of damage that were encountered with this protocol.

Table 8.1 Predictions of Maximum Injury for Cartilage Cross-Section Cryopreserved with an Optimal Protocol.

Depth of Cell Below Surface (mm)	Damage During Initial Cooling Rate (%)	Damage During Final Cooling Rate (%)
0.1	4.9	2.6
0.5	5.1	2.6
1.0	5.5	2.6
1.5	5.8	2.6
2.0	6.1	2.6
2.5	6.3	2.6
3.0	6.4	2.6

Discussion

This result suggests a protocol for the successful cryopreservation of articular cartilage. The suggested protocol must be considered as a product of a specific model, however. This model has limitations due to the several assumptions that were made in producing it (any model has to have simplifying assumptions -- a physical system is always its own best simulation), and these should be understood by anyone who wishes to implement this protocol. The results of chapter 7 have shown that cartilage may not be as homogeneous as was assumed by the model employed in this chapter. These differences seem to be manifested only as solution effects injury, so the approach of minimizing the time spent at high solute concentrations may cancel any effect that these differences may have introduced. However, if there are real differences in the structure of the chondrocytes in the different morphological regions of the tissue, then there may also be differences in the permeability properties as well as the properties which determine sensitivity to membrane rupture. This question is worth addressing, perhaps to improve the efficiency of cryopreservation, but mainly to increase the knowledge of the biology of articular cartilage.

Admittedly, the tissue model used in this study is very simple. The principal benefits (in terms of the technology of cryopreservation) of the osmotic rupture hypothesis are felt to lie with its application to more complicated tissues, and perhaps, eventually, whole organs. The articular cartilage model provides a

scaffold upon which to build such applications. The permeability parameters of the constituent cells must be measured as well as the parameters which describe osmotic injury, the behavior of the intercellular space must have a mathematical description -- both during freezing and during addition of cryoprotective agents and the architecture of the tissue must be accounted for. These measurements allow one to model the injury response of the constituent cells which then allows optimization on selected criteria. In some tissues, it may be desirable to kill certain cells (to reduce immunogenicity following transplantation), a criterion which can be simply implemented in this scheme. Cryopreservation protocols which strive for vitrification -- solidification without the formation of ice crystals -- can also be optimized using this theory. The addition of high concentrations of cryoprotectants (necessary to achieve vitrification) can be modeled so that an index of injury is obtained for specific addition protocols. The technique also allows one to determine if true vitrification is actually necessary -- rapid cooling in high concentrations of cryoprotectants may not lead to damaging osmotic stresses under some conditions. Thus the principal result of this chapter is not simply a protocol for cryopreserving articular cartilage, but a program of how to find successful cryopreservation protocols for any organized tissue.

References

1. Pegg, D. 1986. Equations for Obtaining Melting Points and Eutectic Temperatures for the Ternary System Dimethyl Sulphoxide/Sodium Chloride/Water. *Cryo-Letters* **7**: 387-394.

DMSO Concentration Profiles for 7 Representative Cells in Articular Cartilage

depth below
surface

0.1 mm

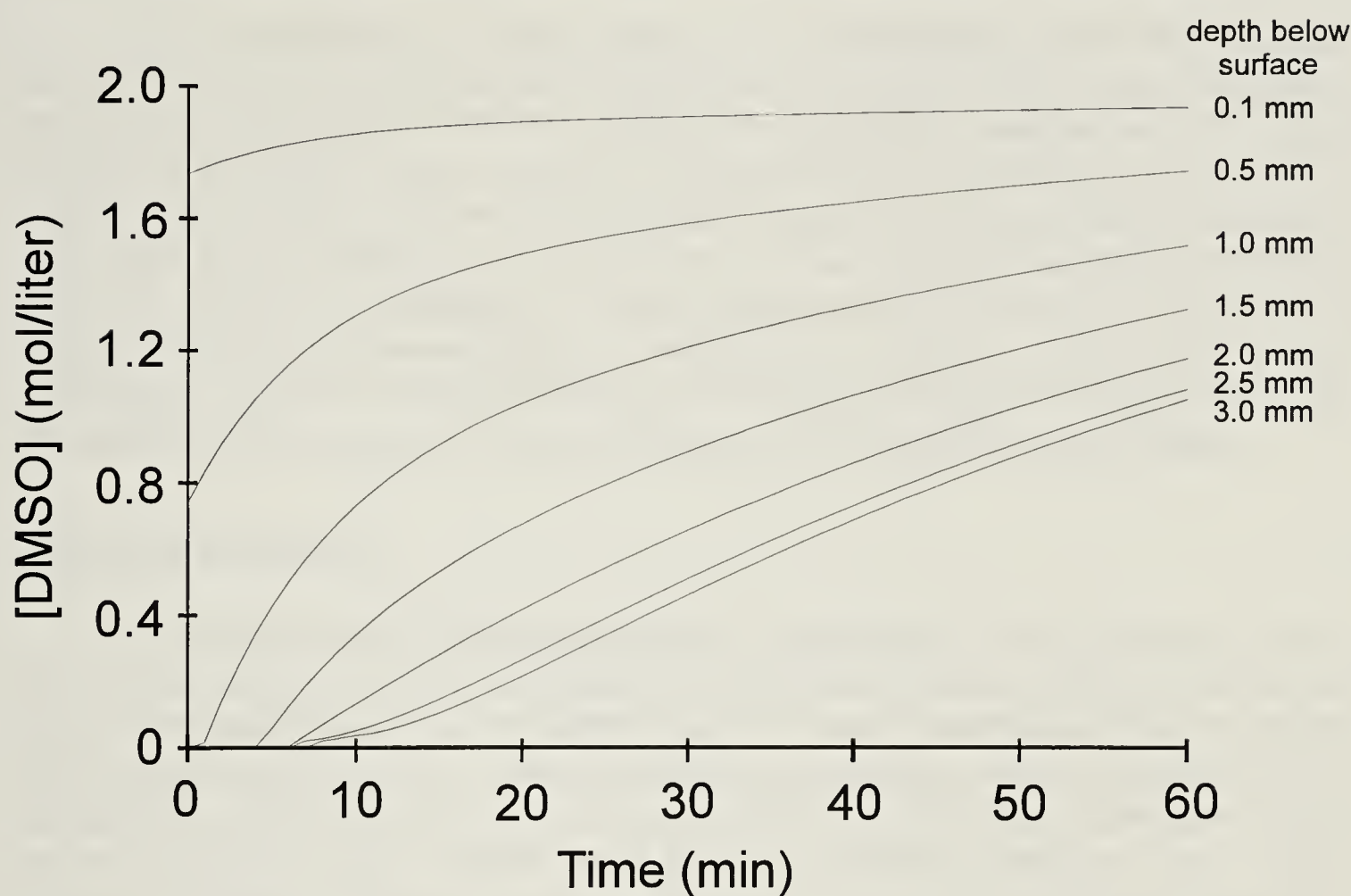0.5 mm

1.0 mm

1.5 mm

2.0 mm
2.5 mm
3.0 mm

Figure 8.1.
The concentration of DMSO is shown as a function of time following immersion in a solution of 2M DMSO. The seven profiles represent discrete depths within the cartilage in the direction perpendicular to the joint surface.

Chapter 9

General Discussion and Conclusions

Review of Thesis Objectives

The hypothesis that was stated in the introduction was the principal assumption of the osmotic rupture hypothesis: that water moving due to osmotic pressure gradients can lead to a rupture in the plasma membrane. The initial portion of the thesis was devoted to developing this hypothesis into a robust mathematical theory and testing this theory against the experimental evidence. The other major objective of the thesis was to use articular cartilage as a model tissue to develop a technique of using mathematical modeling to optimize a protocol for the cryopreservation of mammalian tissues. To do this, it was necessary to perform measurements on cartilage and chondrocytes so that the parameters which are used in the equations could be applied to this tissue.

Summary of Results

The initial result of the mathematical development of the osmotic rupture hypothesis was a means of calculating the physical pressure that is exerted on the plasma membrane due to water flux of a given magnitude. The pressure generated from the level of water flux that is associated with the occurrence of intracellular ice formation was then compared to the hydrostatic pressure that is required to rupture lipid bilayers and it was found that the pressure due to water flux was sufficient to cause a rupture. Following this, the equation which predicts the probability of rupture as a function of water flux was applied to data describing the conditions under which IIF can occur. The equation was able to describe the phenomena associated with IIF with a remarkable accuracy.

The implementation of the theory requires modeling of the osmotic responses of cells during freezing. Thus the principal assumption used in this practice (the extrapolation of permeability parameters, measured at above freezing temperatures, to sub-freezing temperatures using an Arrhenius relation) was also tested. Although the extrapolation to very low temperatures was not tested directly, the challenge to this assumption (3) was based on the idea that the presence of ice caused a dramatic alteration of the properties of the plasma membrane. This idea was shown to be incorrect for the cells used in the test, thus the basis of the challenge can be discounted.

In order to establish this theory as the most rigorously tested hypothesis of the genesis of intracellular ice, it was used to predict the occurrence of IIF during sinusoidal cooling protocols. In this experiment, the cells were taken down to a set temperature and then the temperature was cycled sinusoidally. Under these conditions, the cell behaves as a damped oscillator, the thermal cycling allowing the uncoupling of the water flux and the degree of supercooling

by introducing a phase shift. The osmotic rupture equation was able to describe, exactly, the incidence and phase angle of IIF for the case with no DMSO. With 1M DMSO, the phase angle of IIF was predicted exactly, however the incidence of IIF was overestimated by the theory. The nature of this discrepancy remains unresolved, although there is no question that some of the assumptions that were used to model the osmotic responses of cells in high concentrations of DMSO were unjustified. Until such time as the description of these solutions is improved, the source of the discrepancy must remain undecided.

In order to apply the theory to the search for an optimal protocol for the cryopreservation of articular cartilage, the behavior of the cells and the solution within the cartilage matrix had to be determined. This involved measurements of the permeability of the chondrocytes to water and to DMSO which allowed the relevant parameters to be determined. The conditions under which IIF formed in chondrocytes was also investigated, so that this information could be combined with modeling of the water flux to estimate the parameters which are used in the osmotic rupture equation. The diffusion coefficient for DMSO in cartilage matrix was measured to allow modeling of the kinetics of DMSO uptake, which, in turn, could be used to model the degree of osmotic injury that accompanied the addition of DMSO. The freezing behavior of chondrocytes within the cartilage matrix was then investigated to provide support for the assumption that the solution in the matrix behaves similarly to physiological solutions. The patterns of rapid freezing injury and solution effects injury which were obtained were very similar to results on cellular suspensions, thereby justifying the model of freezing injury in cartilage. Thus, the mathematical model of the osmotic responses of articular cartilage was used in a computer program to find an optimized protocol for cryopreservation.

Significance for Cryobiology

The results of this study suggest that cryopreservation of articular cartilage can be carried out with greater that 90% recovery, which is probably sufficient to maintain the biomechanical properties of the cartilage following transplantation (1,2). This result, although a dramatic example of the power that is obtained by combining mathematical modeling with a theoretical basis on which to predict injury, is not the most significant portion of this body of work. As was stated in the introductory chapter, it was never intended that this thesis should provide the final word on the cryopreservation of articular cartilage, but rather, show how the osmotic rupture hypothesis can be used to optimize cryopreservation protocols for organized tissues, an area that sorely needs fresh approaches. The method advocated in this thesis is one of building a foundation of knowledge of the constituent parts and then applying this knowledge to the problem of understanding the whole. The tools to do this consist of the ability to model osmotic responses at low temperatures and a theoretical basis on which to translate these responses into meaningful information. As well as providing a

useful tool for improving the technology of cryopreservation, computer simulation can be used to explore the behavior of the models and thereby suggest fruitful avenues of experimental research. It is hoped that the ideas presented herein will stimulate both the search for improved cryopreservation protocols and the understanding of the behavior of living things at low temperatures.

References

1. McPherson, R., Hurtig, M., Novak, K., Muldrew, K., McGann, L. and Schachar, N. 1993. Creep Behavior of Osteochondral Grafts in Sheep. Transactions of the 39th Annual Meeting of the Orthopaedic Research Society. p. 227.

2. Muldrew, K., Novak, K., Hurtig, M., Schachar, N. and McGann, L. 1993. Cryopreservation of Articular Cartilage Using *in vitro* and *in vivo* Assays. Transactions of the 39th Annual Meeting of the Orthopaedic Research Society. p. 275.

3. Toner, M., Harris, C., Hubel, A., Sterling, L., Dunn, J., Yarmush, M., Cravalho, E. and Tompkins, R. 1990. Water Permeability Parameters of Isolated Hepatocytes between 0 and -12°C. *Cryobiology* **27**:632-633.

Appendix I

General Derivation of Einstein's Diffusion Equation

The following thought experiment (after Levitt, [chapter 2, ref. 16]) illustrates Einstein's idea for his diffusion equation in an entirely general manner. If one has a beaker of water containing a small amount of a tracer which is identical to water except that the tracer is under the action of a force in the direction of the bottom of the beaker (*eg.* the tracer could be D_2O in a gravitational field), the tracer will be distributed in the beaker according to the Boltzmann distribution at equilibrium (see figure A1.1a):

$$C(x) = C_i \cdot e^{\frac{Fx}{kT}}$$

$C(x)$	= Concentration distribution function
C_i	= Initial concentration
F	= Force acting on tracer
x	= Distance from the bottom of the beaker
k	= Boltzmann's constant
T	= Absolute temperature

Since the natural tendency of the tracer is to diffuse down the concentration gradient, the equilibrium situation can be thought of as a balance between the drift flux, caused by the force, and the diffusive flux:

$$J_D = -J_F$$

J_D	= Diffusive flux
J_F	= Drift flux

The diffusive flux is given by:

$$J_D = -D\frac{dC}{dx}$$

D	= Diffusion coefficient for the tracer

The drift flux is due to the applied force, therefore, it is given by:

$$J_F = C \cdot \bar{v}$$

$\bar{v}$	= Drift velocity of tracer

The force is equal to the product of the drift velocity and a frictional coefficient:

$$F = f \cdot \bar{v}$$

f = coefficient of friction for the tracer moving through the fluid

Therefore, the drift flux is given by:

$$J_F = \frac{CF}{f}$$

Combining the relations for the drift flux and the diffusive flux gives:

$$-D\frac{dC}{dx} = -C_i \cdot e^{\frac{Fx}{kT}} \cdot \frac{F}{f}$$

Solving this equation yields the Einstein relation:

$$D = \frac{kT}{f}$$

If we imagine a membrane being placed into this beaker at equilibrium (see figure A1.1b), normal to the direction of the force, then it follows that the same distribution will exist across this membrane. Therefore, the same relation will hold for water traversing the membrane. If the water molecules only interact with membrane lipids inside the membrane (there are no water-water interactions), then the diffusion coefficient (D) will be for water diffusion in a lipid environment (where the lipids are those of the membrane in question).

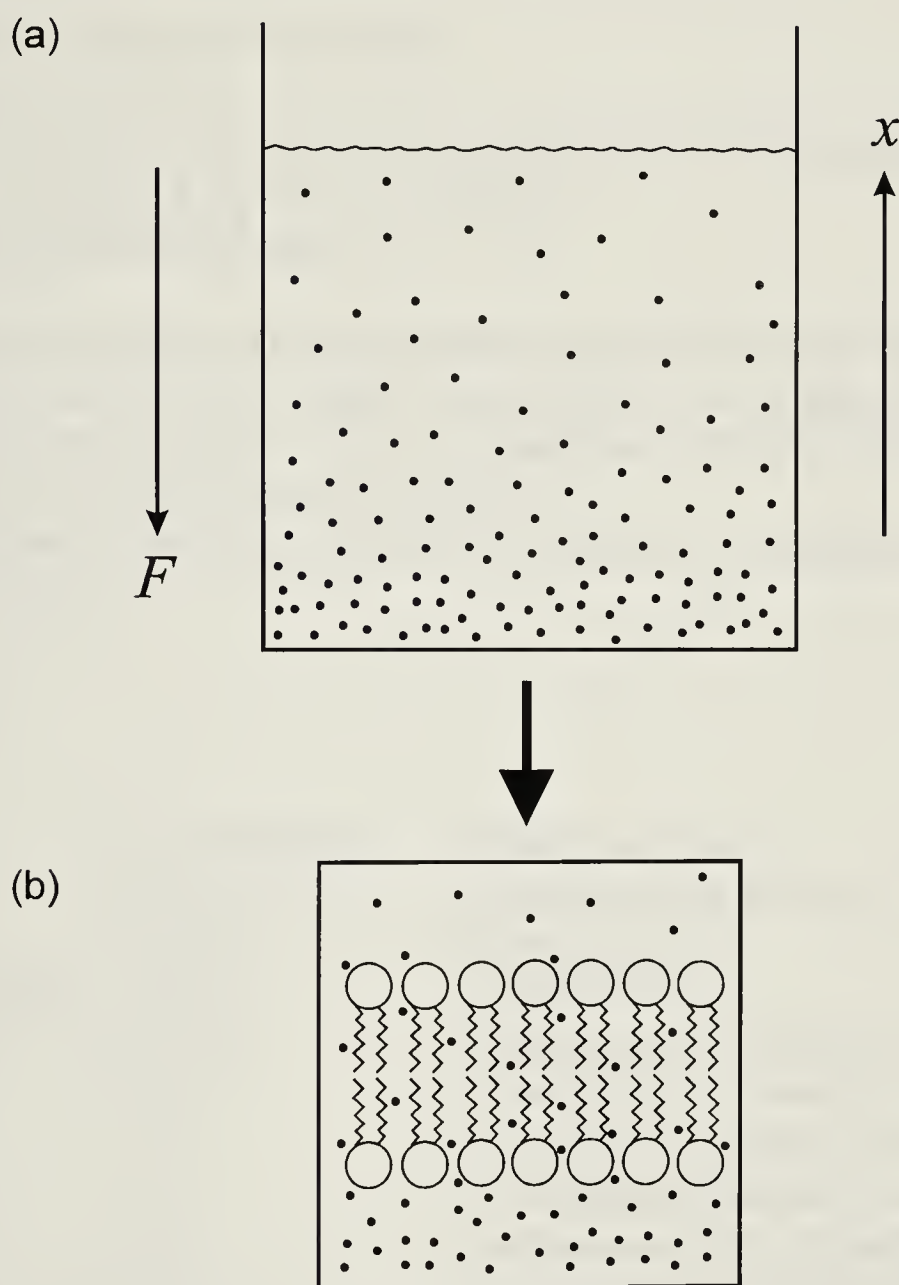# Thought Experiment to Illustrate the Derivation of Einstein's Diffusion Equation

Figure A1.1.
The equilibrium distribution of a tracer which is under a force not felt by the solvent is a Boltzmann distribution as illustrated in (a). If we consider a molecular membrane placed into this distribution at equilibrium, shown in (b), then the same distribution will exist across the width of the membrane.

Appendix II

Source Code for the Program to Find the Optimal Freezing Protocol for Articular Cartilage

program Cartilage_Optimization;

```
{ Program to find optimal freezing protocol for Articular cartilage }
{ Ver. 1.0, June 16, 1993, Ken Muldrew }
{ Written for Borland Pascal, ver. 7.0 }

{ The freezing protocol is optimized to produce the least damage in the }
{ least amount of time for seven representative cells (taken from various }
{ depths in the cartilage).  Injury is predicted using the osmotic rupture }
{ hypothesis of rapid freezing damage. }
{ The reader's integrity being above question, no copyright is reserved in }
{ any country. }
```

uses crt;

const

incrt	= 0.001666667;	*{ time increment }*
R	= 0.082*1e15;	*{ universal gas constant - um3*atm/mol*K }*
T0	= 273.16;	*{ 0 degrees C }*
FinalTemp	= -80.0;	*{ cool to -80 C }*
b	= 0.381;	*{ parameter for osmotic rupture equation }*
P50	= 8.80;	*{ parameter for osmotic rupture equation }*
b_Ea	= -10.1;	*{ Arrhenius activation energy of b - kcal/mol }*
P_Ea	= 8.5;	*{ Arrhenius activation energy of b - kcal/mol }*
L_Tg	= -3.0;	*{ reference temp. for osmotic rupture parms }*
tau	= 0.08;	*{ parameter for osmotic rupture equation }*
Vo	= 1000;	*{ isotonic volume of bovine chons - um3 }*
Vd	= 0.43 * Vo;	*{ osmotically inactive volume of bovine chons }*
sigma	= 0.95;	*{ reflection coefficient for DMSO in chons }*
Lpg	= 0.146;	*{ hydraulic conductivity for bovine chons }*
LpEa	= 12.2;	*{ Arrhenius activation energy for Lp - kcal/mol }*
Psg	= 2.7;	*{ DMSO permeability for bovine chons }*
PsEa	= 18.5;	*{ Arrhenius activation energy for Ps - kcal/mol }*
Tg	= 14.0;	*{ reference temp. for permeability parms }*

var
  i : integer;
  MeltingPoint,Co,Cf,Tc,A,t,Lp,S,So,Sf,V,Ps : extended;

```pascal
  DMSOconc, T1, CR1, CR2, CoolingRate, DegreeCount : extended;
  MaxProb : array[1..7,1..2] of extended;
  ch : char;

function Arrhenius(Parm,Ea,T,Tg : extended) : extended;
{ find the value of a parameter at a given temperature }
  const R = 0.00199; { gas constant - kcal/mol*K }
  begin
    Arrhenius := Parm * exp(Ea/R*(1/(273+Tg)-1/(273+T)));
  end;

function Eutectic : extended;
{Returns an estimate of the eutectic temp for DMSO/0.15M NaCl/H2O}
  begin
    Eutectic := -65.471 * DMSOconc / (0.86954 + DMSOconc) - 21.2;
  end;

function NaCl(T : extended) : extended;
{Returns osmolarity of NaCl in soln at a given temperature for a solution}
{containing DMSO and 0.15M NaCl.  DMSOconc is in mol/lit}
  var a,b : extended;
  begin
    if DMSOconc < 0.001 then
      begin
        if (T <= 0) and (T >=-21.2) then
          NaCl := (-0.5519709 * T) + (-0.0051394 * T * T)
        else if (T < 0) then NaCl := 8.99
        else NaCl := 0.3;
      end
    else
      begin
        a := 2.5572/DMSOconc - 0.10861/(DMSOconc*DMSOconc);
        b := 50.7421*DMSOconc/(0.072205 + DMSOconc) - 65.0;
        if (T <= 0) and (T >= Eutectic) then
          NaCl := a * T / (b + T)
        else if (T > 0) then NaCl := 0.3
        else NaCl := NaCl(Eutectic);
      end;
  end;

function DMSO(T : extended) : extended;
{returns molarity of DMSO in soln at a given temperature}
  var a,b : extended;
  begin
    if (T <= 0) and (T >= Eutectic) then
```

```pascal
    begin
      a := 8.48052*DMSOconc/(0.092943+DMSOconc);
      b := 50.7421*DMSOconc/(0.072205 + DMSOconc) - 65.0;
      DMSO := a * T / (b + T);
    end
  else if (T > 0) then DMSO := DMSOconc
  else DMSO := DMSO(Eutectic);
 end;


function MeltPoint : extended;
{ returns the melting point of a DMSO/0.15M NaCl/H20 soln }
  var T : extended;
  begin
    if DMSOconc > 0.001 then
      begin
        T := 0.0;
        repeat
          T := T - 0.01;
        until DMSO(T) >= DMSOconc;
        MeltPoint := T;
      end
    else MeltPoint := -0.5;
  end;


function Pressure(T,Flux : extended) : extended;
{ returns the pressure exerted on the membrane due to water flux }
  const
    k = 1.38e-23;     { Boltzmann's constant }
    delta_x = 5.0e-9; { width of the hydrophobic region the plasma membrane }
    H2Ovol = 3.0e-11; { volume of one water molecule }
  var
    Dw : extended;    { diffusion coeff. for water in liquid hydrocarbon }
  begin
    flux := flux / -60.0; { convert to seconds }
    Dw := Arrhenius(4.56e-9,3.35,T,30);
    Pressure := k * (T+T0) * (Flux / H2Ovol) * delta_x /
             (A * 1e-12 * Dw);
  end;


function Logistic(T,P : extended) : extended;
{ a two parameter logistic equation - integral of the binomial distribution }
  var
    bb, PP50 : extended;
  begin
    bb := Arrhenius(b,b_Ea,T,L_Tg);
```

```pascal
    PP50 := Arrhenius(P50,P_Ea,T,L_Tg);
    Logistic := 1/(1 + exp(-1*bb*(P - PP50)));
  end;

procedure CalcInjury(cell, i : integer; flux, T : extended);
{ Calculate the probability of IIF at some temperature and flux level }
{ The time constant, tau, is small and thus ignored for slow cooling }
  var
    Prob_IIF, P : extended;
  begin
    P := Pressure (T,flux);
    Prob_IIF := Logistic(T,P);
    if Prob_IIF > MaxProb[cell,i] then MaxProb[cell,i] := Prob_IIF;
  end;

function CalcArea(V : extended) : extended;
{ calculates the surface area of a sphere }
  var radius : extended;
  begin
    radius := exp(ln(3 * V / (4 * Pi)) / 3); { cube root }
    CalcArea := 4 * Pi * radius * radius;
  end;

procedure CalcVol(cell : integer);
{ Solves the Johnson & Wilson equations numerically to calculate the }
{ movement of water and DMSO across the membrane. }
  var
    DegreeCount, i, j, count : integer;
    Flux, time : extended;

    { dV_dt and dS_dt are the J & W differential equations }
    function dV_dt(V,S : extended) : extended;
      begin
        dV_dt := Lp * A * R * (Tc+T0) * ((Co*(Vo-Vd) + (sigma * S))/V -
             (sigma * Sf) - Cf);
      end;

    function dS_dt(V,S : extended) : extended;
      begin
        dS_dt := (Ps * A * (Sf - S/V) + (1-sigma) * 0.5 * (Sf+S/V) * flux);
      end;

  begin
    case cell of
      1 : DMSOconc := 1.96;  { Distribution of DMSO in tissue }
```

137

```
  2 : DMSOconc := 1.76;  { cell 1 is 0.1 mm below the surface }
  3 : DMSOconc := 1.54;  { cell 7 is 3 mm (at the bone interface) }
  4 : DMSOconc := 1.34;
  5 : DMSOconc := 1.18;
  6 : DMSOconc := 1.10;
  7 : DMSOconc := 1.06;
end; {case}
Co := 0.3/1e15;              { initial NaCl }
Cf := Co;                    { final   NaCl }
Sf := DMSOconc/1e15;         { final   DMSO inside }
S := Sf*(Vo-Vd);             { initial DMSO inside }
V := Vo - Vd;                { osmotically active water volume }
A := CalcArea(Vo);           { assume that the cell is a sphere }
t := 0.0; flux := 0.0;
for i := 1 to 2 do MaxProb[cell,i] := 0.0;
MeltingPoint := MeltPoint;
Tc := MeltingPoint - 0.1; { start just below the m.p. }
DegreeCount := round(60.0 / CR1 / (60.0 * incrt));
time := (T1 - Tc) / CR1;
if time < 0 then time := -1 * time;
t := 0.0;
count := 0;
while t <= time do          { cool from m.p. to T1 }
  begin
    inc(count);
    Tc := Tc - (CR1 * Incrt);              { decrement the temperature }
    Lp := Arrhenius(Lpg,LpEa,Tc,Tg);   { get the parameters at Tc }
    Ps := Arrhenius(Psg,PsEa,Tc,Tg);
    Cf := NaCl(Tc)/1e15;                   { get the solute concentrations }
    Sf := DMSO(Tc)/1e15;
    flux := dV_dt(V,S);                    { water flux }
    V := V + Incrt * flux;                 { volume change }
    S := S + Incrt * dS_dt(V,S);           { solute change }
    if count = DegreeCount then            { report at 1 degree C intervals }
      begin CalcInjury(cell,1,flux,Tc); count := 0; end;
    t := t + incrt;                        { increment the time }
  end;
DegreeCount := round(60.0 / CR2 / (60.0 * incrt));
time := (FinalTemp - Tc) / CR2;
if time < 0 then time := -1 * time;
t := 0.0;
count := 0;
while t <= time do          { cool from T1 to FinalTemp }
  begin
    inc(count);
```

```pascal
        Tc := Tc - (CR2 * Incrt);
        Lp := Arrhenius(Lpg,LpEa,Tc,Tg);
        Ps := Arrhenius(Psg,PsEa,Tc,Tg);
        Cf := NaCl(Tc)/1e15;
        Sf := DMSO(Tc)/1e15;
        flux := dV_dt(V,S);
        V := V + Incrt * flux;
        S := S + Incrt * dS_dt(V,S);
        if count = DegreeCount then
          begin CalcInjury(cell,2,flux,Tc); count := 0; end;
        t := t + incrt;
      end;
  end;


procedure Optimize;
{ This is the simplex routine for optimizing the parameters }
{ Code is based on the implementation given in the following reference: }
{ Caceci, M. and Cacheris, W.  Fitting Curves to Data.  Byte Magazine }
{ May, 1984, pp. 340-362. }
{ The simplex algorithm converges on a minimum by superimposing }
{ vertices on the surface formed by the response of a function using trial }
{parameters.  A process of reflection, expansion, contraction or shrinkage }
{ of the vertices is used to converge on the minimum of this surface. }
const
  m = 3;                { number of parameters to fit }
  n = m+1;              { number of vertices in the simplex }
  alfa = 1.0;           { reflection coefficient }
  beta = 0.5;           { contraction coefficient }
  gamma = 2.0;          { expansion coefficient }
  ErrLevel = 1e-4;      { acceptable errors }
  Max_Iter = 100;       { maximum number of iterations }
  root2 = 1.414214;


type
  vector = array[1..n] of extended;
  index = byte;


var
  done : boolean;
  i,j : index;
  h,l : array[1..n] of index;
  n_iter : integer;
  next, center, mean, error, maxerr, p, q, step : vector;
  errsum : extended;
  simp : array[1..n] of vector;
```

```pascal
  str, fname : string;

procedure Initialize;
 { initialize the simplex }
 var i,j : index;
 begin
   for i := 1 to n do
     for j := 1 to n do simp[i,j] := 0.0;
   simp[1,1] := -15.0;        { T1 - initial guesses }
   simp[1,2] := 5.0;          { CR1 }
   simp[1,3] := 20.0;         { CR2 }
   for i := 1 to m do step[i] := (simp[1,i] / 5.0);
   for i := 1 to n do maxerr[i] := ErrLevel;
 end;


procedure sum_of_residuals(var x : vector);
{ find the sum of squared errors for a given set of parameters }
{ This routine calls the function which provides the response surface }
{ parameters passed in x[1..4], error returned in x[5] }
 var
   i : index;
   time1, time2 : extended;
 begin
   T1 := x[1];          { temperature  #1 }
   CR1 := x[2];         { Cooling Rate #1 }
   CR2 := x[3];         { Cooling Rate #2 }
   if ((T1 < (MeltingPoint-0.1)) and (T1 > FinalTemp)
     and (CR1 > 0.0) and (CR1 < 100) and (CR2 > 0.0) and (CR2 < 100)) then
     begin
       for i := 1 to 7 do CalcVol(i);                    { use 7 positions in cartilage }
       time1 := abs(T1 - MeltingPoint) / CR1;    { time at CR1 }
       time2 := abs(FinalTemp - T1) / CR2;       { time at CR2 }
       x[n] := 0.0;
       for i := 1 to 7 do
         { square the probabilities of rupture and multiply by time }
         x[n] := x[n] + (MaxProb[i,1] * MaxProb[i,1] +
           MaxProb[i,2] * MaxProb[i,2]) * (time1 + time2);
     end
   else x[n] := 10000.0;    { these values are not allowed }
   errsum := x[n];
 end;

procedure new_vertex;
{ swap trial vertex for worst vertex }
 var i : index;
```

```
    begin
      for i := 1 to n do simp[h[n],i] := next[i];
    end;

procedure order;
{ find the highest and lowest values for each parameter in simplex }
  var i,j : index;
  begin
    for j := 1 to n do
      begin
        for i := 1 to n do
          begin
            if simp[i,j] < simp[l[j],j] then l[j] := i;
            if simp[i,j] > simp[h[j],j] then h[j] := i;
          end;
      end;
  end;


begin  {Optimize }
  Initialize;
  sum_of_residuals(simp[1]);        { find error of initial guesses }
  for i := 1 to m do
    begin
      p[i] := step[i] * (sqrt(n) + m - 1) / (m * root2);
      q[i] := step[i] * (sqrt(n) - 1) / (m * root2);
    end;
  for i := 2 to n do    { fill the simplex }
    begin
      for j := 1 to m do simp[i,j] := simp[1,j] + q[j];
      simp[i,i - 1] := simp[1,i - 1] + p[i - 1];
      sum_of_residuals(simp[i]);     { find errors }
    end;
  for i := 1 to n do
    begin
      l[i] := 1;
      h[i] := 1;
    end;
  order;                 { find the best and worst vertices }
  n_iter := 0;
  repeat                 { begin the search for the optimal parameters }
    done := true;
    inc(n_iter);
    for i := 1 to n do center[i] := 0.0;
    for i := 1 to n do
      if i <> h[n] then
```

141

```
    for j := 1 to m do
      center[j] := center[j] + simp[i,j];
for i := 1 to m do { reflect the worst vertex }
  begin
    center[i] := center[i] / m;
    next[i] := (1.0 + alfa) * center[i] - alfa * simp[h[n],i];
  end;
sum_of_residuals(next);
if next[n] <= simp[l[n],n] then    { if reflected vertex is better than }
  begin                            { the best then swap it for the worst }
    new_vertex;
    for i := 1 to m do              { try extending the reflected vertex }
      next[i] := gamma * simp[h[n],i] + (1.0 - gamma) * center[i];
    sum_of_residuals(next);
    if next[n] <= simp[l[n],n] then new_vertex; { if the extended vertex }
  end     { is better than the best then swap it for the reflected vertex }
else
  begin
    if next[n] <= simp[h[n],n] then   { if the reflected vertex is better }
      new_vertex           { than the worst then swap it for the worst }
    else
      begin
        for i := 1 to m do    { contract the worst vertex }
          next[i] := beta * simp[h[n],i] + (1.0 - beta) * center[i];
        sum_of_residuals(next);
        if next[n] <= simp[h[n],n] then     { if the contracted vertex is }
          new_vertex    { better than the worst then swap it for the worst }
        else
          begin
            for i := 1 to n do
              begin
                for j := 1 to m do      { shrink all but the best vertex }
                  simp[i,j] := (simp[i,j] + simp[l[n],j]) * beta;
                sum_of_residuals(simp[i]);
              end;
          end;
      end;
  end;
order;                { find the new best and worst vertices }
for j := 1 to n do
  begin
    error[j] := (simp[h[j],j] - simp[l[j],j]) / simp[h[j],j];
    if done then
      if error[j] > maxerr[j] then done := false;
  end;
```

```pascal
      write(n_iter,' : ');  { progress report }
      writeln(T1:6:3,' ',CR1:6:3,' ',CR2:6:3,' ',errsum:6:3);
    until (done or (n_iter = max_iter));
    for i := 1 to n do    { find the average values of final simplex }
      begin
        mean[i] := 0.0;
        for j := 1 to n do
          mean[i] := mean[i] + simp[j,i];
        mean[i] := mean[i] / n;
      end;
    writeln('The final simplex is : ');
    for i := 1 to n do writeln(mean[i]:6:3,' '); writeln;
    for i := 1 to 7 do writeln(MaxProb[i,1]:5:3,' ',MaxProb[i,2]:5:3);
  end;

begin  { main }
  writeln('Optimizing . . . ');
  Optimize;
  ch := readkey;
end.
```